Chair of Process Technology and Industrial Environmental Protection

Master's Thesis

Advances of materials for ion-selective membranes for extraction of Lithium ions out of saline water

Silvia Raggam, BSc

February 2021

MONTANUNIVERSITÄT LEOBEN
www.unileoben.ac.at

EIDESSTATTLICHE ERKLÄRUNG

Ich erkläre an Eides statt, dass ich diese Arbeit selbständig verfasst, andere als die angegebenen Quellen und Hilfsmittel nicht benutzt, und mich auch sonst keiner unerlaubten Hilfsmittel bedient habe.

Ich erkläre, dass ich die Richtlinien des Senats der Montanuniversität Leoben zu "Gute wissenschaftliche Praxis" gelesen, verstanden und befolgt habe.

Weiters erkläre ich, dass die elektronische und gedruckte Version der eingereichten wissenschaftlichen Abschlussarbeit formal und inhaltlich identisch sind.

Datum 31.01.2021

Unterschrift Verfasser/in
Silvia Raggam

Vorgelegt von:

Silvia Raggam

01335278

Betreuer/Gutachter:

Dr. Amir Razmjou Chaharmahali, University of New South Wales, Australia

Univ.-Prof. Dipl.-Ing. Dr.-Ing Markus Lehner, University of Leoben, Austria

Munirah Izzah Binti Mohammad, BE (Hons), PhD candidate at UNSECO Centre for Membrane Science and Technology, University of New South Wales, Australia

ACKNOWLEDGEMENTS

I highly acknowledge all of my supervisors. Dr. Amir Razmjou Chacharmahali for enabling the more than interesting experience in a field of research and a university structure totally new and fascinating to me. Also, when I decided to abruptly stop experimental work due to Covid-19 hitting the world and left the country, he was always supporting me and giving advices remotely. I am more than grateful for this constructive teamwork. A special thanks goes to Munirah Izzah Binti Mohammad, BE who guided my way throughout all the experimental work showing me new analyzation methods and helped me with every question I had. Even though they might have been trivial she always had answers that were on point and broadened my limit of understanding in topics that are not that trivial. She created an atmosphere of learning and researching in which I really enjoyed working. I am also grateful for all the support that Univ.-Prof. Dipl.-Ing. Dr.-Ing Markus Lehner gave me through his communication that was always straight forward and encouraging. Also, I thank him for his unrestricted will to help me with financial support from University of Leoben throughout my time in Australia.

Special thanks also go to my friends Bernd Schulz, MSc who encouraged me to ask for a research internship at UNSW through which this work evolved and helped me with the organization of it and Matthias Schebeck, MSc who helped me throughout all my studies and gave me advice on the final version of my thesis.

Last but not least, I want to thank my family who supported me throughout all my studies emotionally and financially.

Kurzfassung

Ionen-selektive Membranen für Trennung von Lithium-Ionen aus salzhaltigen Gewässern

Fortschritte der Materialien und Anwendungssysteme

Das Element Lithium spielt nicht nur in Produkten, die wir tag täglich verwenden, eine wichtige Rolle, sondern auch als Speicher für Energie, die azyklisch anfällt, was der Fall ist für die meisten erneuerbaren Energieformen. Dadurch, dass der konventionelle Abbau aus dem Primärrohstoff eine unzumutbare Last für die Umwelt darstellt und es noch keine industrielle Möglichkeit gibt Lithium-Ionen aus Sekundärrohstoffen zu extrahieren, besteht eine große Nachfrage nach eine ökonomisch und ökologisch nachhaltige Möglichkeit zur Extraktion von Lithium. Membranprozesse, die eine wichtige Rolle im Ionenaustausch jeder lebenden Zelle spielen, könnten die Lösung für einen umweltfreundlichen und kostensparenden Extraktionsprozess für Lithium sowohl aus primärer als auch sekundärer Quelle sein. Diese Arbeit zeigt verschiedene mögliche Membranmaterialien auf und spezialisiert sich folgend auf Metall-organische Verbindungen (MOF), welche eine sehr geordnete Porenstruktur mit geringer Größenverteilung aufweisen. Zusätzlich können diese Poren funktionalisiert werden, weshalb gerade diese Strukturen ein sehr interessantes Material für Lithiumionen-selektive Membranen darstellen. Der Ansatz dieser Arbeit beinhaltet das Wachstum einer ZIF-8 Schicht auf der kommerziell erhältlichen NF90 Membran gefolgt vom Wachstum einer ZIF-L Schicht. Daraus resultiert eine asymmetrische Porenstruktur, die für das Trennungsverhalten der Membran entscheidend ist. Die Ergebnisse dieser Membran beinhalten Selektivitäten von 1.52 für K^+/Li^+ und 1.09 für Na^+/Li^+. Diese Arbeit gibt einen Einblick in die Performance von verschiedenen Membranmaterialen für die Extraktion von Lithium aus salzhaltigen Wässern.

Abstract

Advances of materials for ion selective membranes for extraction of Lithium-ions out of saline water

Lithium plays a vital role not only in products used in daily life but also as an indispensable element for storage of acyclic occurring energy resources which is the case for a big part of renewable energies. Conventional primary resource extraction methods posing tremendous burdens on the environment and no industrially used process for lithium ions from secondary resources lead to a need for a both, economically and ecologically, sustainable method of Lithium extraction. Membrane processes playing a huge role for ion exchange in every living cell, could be the key to an environmentally friendly and cost-saving lithium extraction method from primary and secondary resources. This work represents different approaches regarding the material of membranes and focuses on metal organic frameworks (MOF) which have extremely ordered pores with a small pore size distribution. Additionally, those pores can be tuned and therefore represent a highly interesting material for a lithium-ion selective membrane. In this research, a layer of ZIF-8 was built on commercial membrane NF90 support by an easy fabrication method followed by a layer of ZIF-L. This results in an asymmetric pore structure which is crucial for enhancement of separation properties. Selectivity ratios of 1.52 and 1.09 were obtained for K^+/Li^+ and Na^+/Li^+, respectively. This work thus gives insight into the performance of different membrane materials for lithium-ion extraction out of saline water.

Table of Content

Page

1 Background and Introduction

One of the most geopolitically discussed topics of my generation is climate change, what leads to it and what can be done to slow it down to prevent natural catastrophes. Thinking of emissions leading to climate change a topic that might come to our minds quickly is fossil fuel driven vehicles. One approach to this problem is E-mobility which is getting more commercial in recent years and is mostly achieved by Lithium-ion batteries. However, Lithium-ion batteries (LIBs) are not only used in electrically driven vehicles but play a tremendous role in short-time energy storage due to a vast need for different applications. As storage of solar energy or for excess energy of other renewable sources, just to name two of them. Only thinking about human life and activity is not bond to daytime which is when solar energy is available, makes clear that short-term energy storages are highly needed.

This leads to a higher demand in Lithium sources to supply the production of batteries. There are several research approaches of secondary resource production from LIBs, incorporating hydrometallurgical [1] and pyrometallurgic [1], [2] processes. However, none of these are industrially practiced in big scale yet as they consist of a high number of process steps and exhibit low lithium selectivity.

Therefore, the amount of Lithium coming from recycling cannot meet the entire demand for this element which was 45 k tons in 2017 and is foreseen to be 95k tons in 2025 with up to 65% of it only for Lithium-ion batteries. [3] Looking at these numbers, sustainable methods in primary and secondary resource extraction are highly needed.

Today, Lithium is mostly extracted from natural resources, especially minerals and brines whose occurrence ratio of Lithium is 38 to 62, respectively. [4] Also, sea water plays a role as natural source with a Lithium content of around 0.18ppm [5] resulting in large amounts worldwide. However, due to low concentration this source is not yet used commercially.

Among minerals the ones with the highest share of Lithium are pegmatites, especially spodumene and petalite, whose mineral deposit Lithium content is around 0.5-2%. Largest amounts of those ores are in Australia, Brazil, Canada, China, Surinam and Zimbabwe with significant production of ore concentrates in Australia, Canada, Portugal, Russia and Zimbabwe. This concentration can be done via two processes – acidic and alkaline, depending on the type of mineral. The acidic process also varies with the used feed; however, the basic principle consists of an acidic treatment followed by degradation through roasting and water leaching. The used acid is H_2SO_4 and roasting for the degradation of Lithium silicates is done at presence of sodium and calcium compounds and temperatures of 250-400°C whereas higher temperatures up to 1000°C lead to higher yields up to >90%. The alkaline process consists of a pre-treatment, which can be gypsum roast, followed by grounding and calcinating with limestone at 825-1050°C. The calcine is afterwards milled and treated with water to lithium-hydroxide which can be then transformed to lithium chloride or lithium carbonate. [1] These methods need highly concentrated acids as well as high temperatures. Next to the

complexity of these processes and sometimes the hardly accessible locations of the mineral resources [6] those properties make clear that different extraction methods are key for the future demand of Lithium.

Conventional extraction out of brine is based on solar evaporation followed by refining. The brine is concentrated in a pond via solar evaporation over a year where sodium, potassium and magnesium chlorides crystallise. For removal of magnesium hydroxide in the process circular moved lime milk is added. After a filtration and washing step a calcium-lithium-salt solution remains which is concentrated in its Lithium content through circular moved Lithium carbonate. The formed calcium carbonate is filtered, and the Lithium salt solution is further concentrated through evaporation, precipitation with Na_2CO_3 and another filter and washing process resulting in high concentrated Lithium carbonate. Although the costs for conventional extraction out of brine are 30-50% less than extraction out of minerals, the main problems of this process are the long duration of a process circle and the low recovery efficiency. Additionally, which might be the most problematic issue, this process poses a tremendous burden on the environment due to several factors, for example the enormous water consumption and waste generation. [1] Resuming, this also asks for alternative methods to extract Lithium out of brine.

Alternatives incorporate adsorption, precipitation and ion-exchange processes. Adsorption is mainly performed by inorganic ion exchange materials that show high selectivity towards Lithium. Precipitation uses various co-precipitating agents depending on the saline water feed for example aluminium salts for geothermal water. Often high amounts of bivalent ions have to be separated in a pre-treatment. Ion exchange is mainly performed by an adsorption and a stripping/elution process and can be done using various materials. [1] Adsorption and ion-exchange materials are often processed into membranes as they exhibit good mechanical stability which is important for scale up purposes. Not only membranes consisting out of adsorption and ion exchange materials are suitable for selective extraction of Lithium, but also membranes exhibiting nanochannels are a hot topic of recent research for this application and will be discussed in detail in this work. Stable nanochannels themselves can be fabricated by different materials incorporating the material observed in this work, namely metal organic frameworks. Metal-organic frameworks (MOFs) are nanoporous materials with a homogenously structured ultra-high porosity. Their structural diversity (induced by different concentrations of ligands and metal ions) and different functionalities (e.g., thermal stability) draw attention on them for a wide variety of separation and sensing applications.

2 Motivation and Objectives

One part to slow down climate change represents the field of transition of energy sources meaning reducing fossil fuel use and enhancing production of renewable energies. A huge natural and renewable energy source is the sun. Its energy can be obtained and used during the day; however, energy is also needed during night-time which leads to a demand of storage opportunities. Also, other products that are needed in every day's life like laptops or mobile phones need short-term energy storages. Lithium exhibiting a high energy and power density (Figure 1) renders it to THE opportunity for high efficiency batteries that can be used for short-term energy storage (Figure 2).

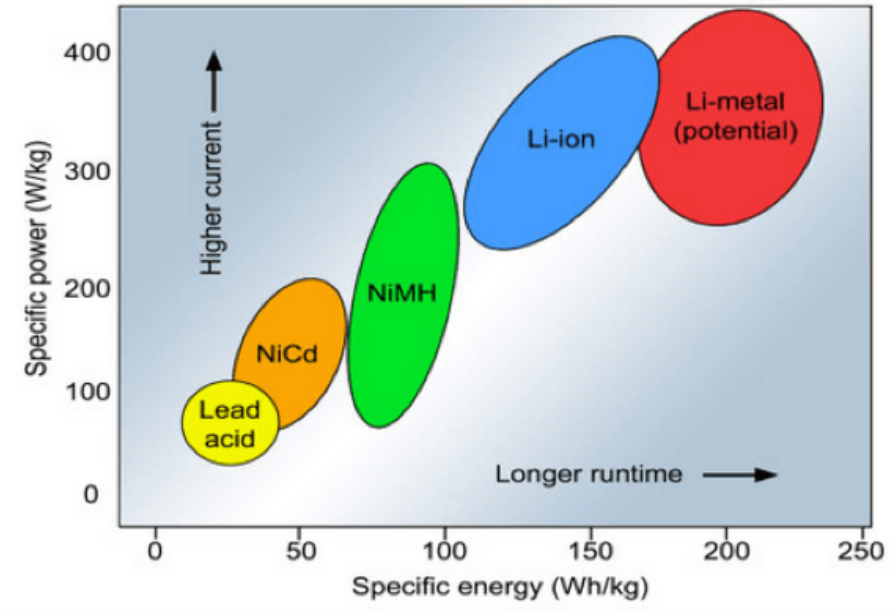

Figure 1: comparison of energy storage materials [7]

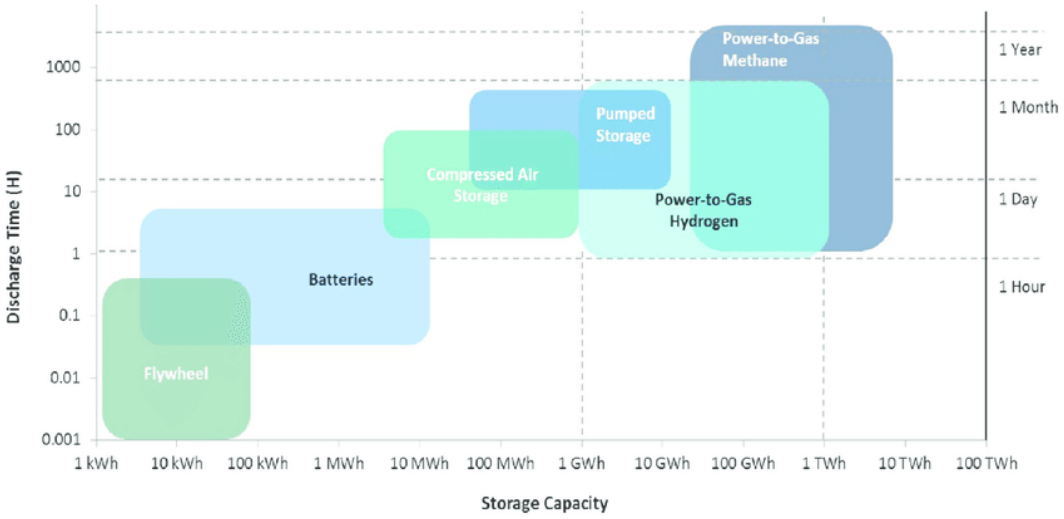

Figure 2: comparison of energy storage systems [8]

Therefore, Lithium is an extremely important element for a more sustainable future. As mentioned before, Lithium from secondary resources cannot satisfy future demand for this material which leads to a need in sustainable methods for extraction of it from primary resources. Conventional methods used at the moment are in need of a vast amount of hard chemicals, high temperatures and complex processes. Membrane processes, which also play a vital role in biological life, however, are simple to operate and are mostly done at room temperature. Chemicals are only in need for fouling control which can be also done mechanically. This led to the idea of using a membrane process to extract Lithium out of saline water which represent the more substantial resource of Lithium. Saline waters, however, exhibit other monovalent ions with nearly the same size as Lithium rendering the membrane for this process a highly sophisticated material. In this work several approaches for this material will be discussed followed by analysation of one specific membrane set up using metal organic frameworks.

3 Fundamentals (Literature Review)

In recent years a lot of different approaches to solve the challenge of extracting Lithium ions out of sea or brine water rather than getting it from the ore were researched. This is due to a big demand in industries, for example, the renewable energy sector and the small occurrences in minerals. Different approaches, especially in membrane processes, will be discussed in the following. Starting from different membrane types until the approach this work was following. After that, possible ways of explanation for the principles of movement in this type of membrane will be written about. Also, the techniques for characterization and performance tests of the researched membrane will be explained.

3.1 Membranes for monovalent – multivalent ion separation

Most commonly, processes based on membranes were investigated to selectively extract Lithium ions from different types of saline waters. A lot of successful research has been done in separating monovalent ions (sodium ions (Na^+), potassium ions (K^+) and lithium ions (Li^+)) from bivalent ones such as magnesium ions (Mg^{2+}) and calcium ions (Ca^{2+})). Ge et al. published a review on monovalent cation perm-selective membranes that hinder the passing of multivalent ions. [9] Broadly speaking, those membranes consist out of a hydrophobic polymer matrix, fixed ion exchange groups and counter ions that can move inside and out. The authors sum up that there are three approaches to explain the perm-selectivity of these membranes: 1) sieving due to the pore size, 2) due to different electrostatic repulsions of mono- and multivalent ions or 3) due to differences in the free energy of dehydration-hydration processes. There has been a lot of research in trying to take advantage of these effects. Li et al., for example, fabricated a nanofiltration (NF) membrane with a positively charged skin layer by interfacial polymerization. They modified it by EDTA to enhance the separation performance. This compound is able to build complexes with bivalent ions such as Mg^{2+} and therefore improves the selectivity of monovalent ions over bivalent ions. The as-prepared membrane resulted a selectivity factor of $S_{Li,Mg}$ =9.2 at a flux of $6 Lm^{-2}h^{-1}$. [10] The skin layer of the membrane is positively charged to fully exploit the Donnan effect. This effect explains the aspiration of a charge equilibrium on both sides of the membrane. Because of its size and the binding EDTA, Magnesium ions cannot pass the membrane, therefore a selective Lithium flux is enhanced. Also, bivalent cations are more repulsed from a positively charged membrane than monovalent ones. In addition, Zhang et al. took advantage of this effect and produced a positively charged membrane using a capillary ultrafiltration membrane as substrate. Using this membrane, they reached rejections of 96.9% for $MgCl_2$ and 20.3% for LiCl which results in a perm-selectivity of 25.7. [11] For brines with high Mg^{2+}/Li^+ ratios or high concentrations of other multivalent ions, such membranes can be the key for pre-treatment processes.

To achieve solutions containing only Lithium ions, other materials for membranes need to be investigated. Those membranes are highly sophisticated considering their ability to separate ions that have the same charge and nearly the same size. At the moment, such membranes are not used yet industrially and in big scale. However, there is an urgent need of a Li-ion

separation process out of brine, considering the highly rising demand for Li-ion batteries and the highest concentrations of Lithium present in sea water. Therefore, different approaches to this problem regarding the membrane material and the system it is used in are researched at the moment. Materials for Lithium-selective membranes differ in structure and operating principle. Most recent researched materials to my knowledge can be categorized in ion-exchange membranes, liquid membranes with carrier-mediated transport and nanochannel structures. In the following, advantages and disadvantages of membranes in these three sectors will be assessed and discussed.

3.2 Ion-exchange Membranes

In the field of ion-exchange membranes a broadly researched structure is the Lithium-ion-sieve (LIS) which is normally used in powder form. However, due to poor performance of this powder such as low permeability and high energy consumption in industrial applications, other forming processes were researched. These include granulation, foaming, membrane and fibre forming. Ion sieves consist either of manganese oxides or titanium oxides, which can form stable frameworks “around” the target ions. Even when these ions are stripped, the matrix properties need to be consistent. In that way vacant sites are generated that have the perfect size to only fit the target ions or smaller ones. This makes the compounds very selective adsorbers. The fact that Lithium has the smallest ion radius of all metal ions eliminates a problem with interfering ions. [12] The working principle of the ‘LIS-effect’ consists of an adsorption and a stripping/desorption step (Figure 3). At first, Lithium ions that were responsible for the appropriate cavity size in the oxides are stripped by a solution containing hydrogen (e.g., HCl). In that way hydrogen replaces Lithium in its sites and a Lithium-rich solution is obtained. The hydrogen containing oxide LIS(H) is then exposed to a Lithium-containing solution like brine or sea water. Lithium ions are adsorbed by the oxide and replace the hydrogen which leaves the solution Lithium-deprived. To receive the Lithium inside the LIS it will be undertaken a stripping process with a hydrogen-containing solution resulting in a Lithium-rich solution. The systems LIS are used in include adsorption columns and electrochemical methods. These configurations result in very high selectivities and good capacities of around 9-10 mg Li^+ / g LIS [13], [14], [15] up to 18.6 mg Li^+ / g LIS at optimum temperature of 30°C [16] and higher when electrical potential was applied [17], [18]. However, systems using these materials also suffer from big challenges. Regarding manganese oxides, dissolution of the matrix can lead to severe water pollution causing problems in industrial applications. For titanium oxides this problem plays a smaller role because of a very high titanium-oxygen bond energy leading to a very stable structure. Their biggest challenge lies in the functionality at electrochemical applications. [12] Another problem of LIS is the Lithium purity (~33%) when there are high concentrations of sodium in the brine or sea water. [19] Overall, the fact that the adsorption/desorption process underlying these systems is not continuous could cause problems in the feasibility of large-scale applications. Thus, negative aspects of membranes underlying an adsorption/desorption process are that there is always a limit of capacity after which the membrane has to be immersed in a different solution resulting in two part-steps of the process which makes it more depended on sophisticated application systems. A positive

aspect, however, is that the vacant sites are well defined for the target ions so that a well-advanced system can reach high selectivities even without a big pre-treatment.

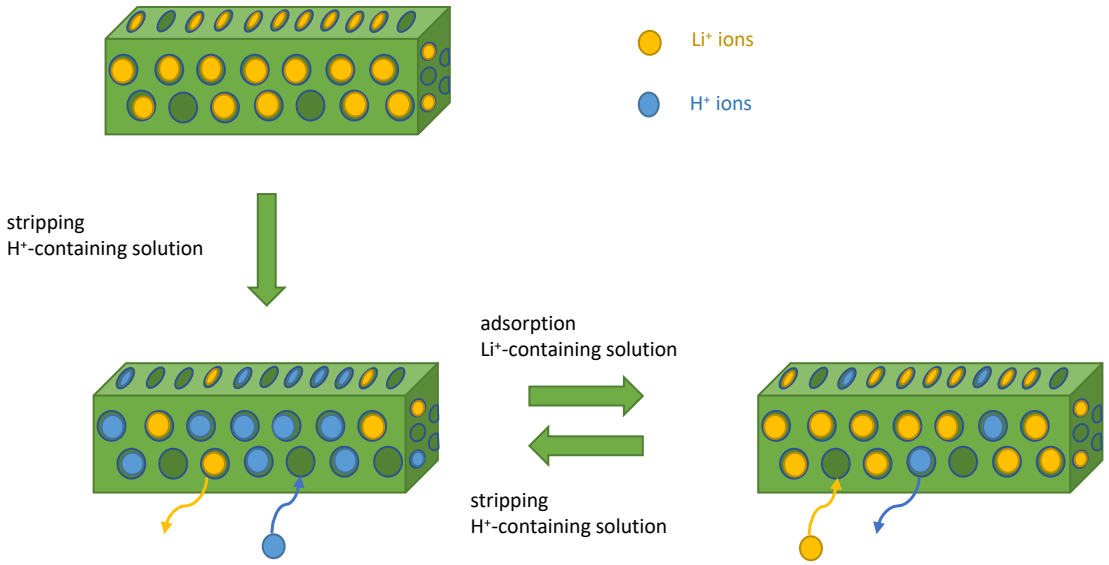

Figure 3: Working principle of Lithium ion sieves - 'LIS effect', own image leaned on [12]

Another recently studied structure of ion exchange membranes are ion imprinted membranes (IIMs). Like in preparation of LIS, vacant sites which are perfectly matching the target ions dimensions are achieved due to a preassembly with template ions. First, these ions, ligands and functional monomers form ternary complexes which become polymers when crosslinkers are added. It is crucial that the bonds between ligands and monomers are saturated and covalent to assure the vacant sites stability. The polymer is then rinsed with an eluent which dissolves out the template ions by protonation leaving behind the vacant sites. (Figure 4)

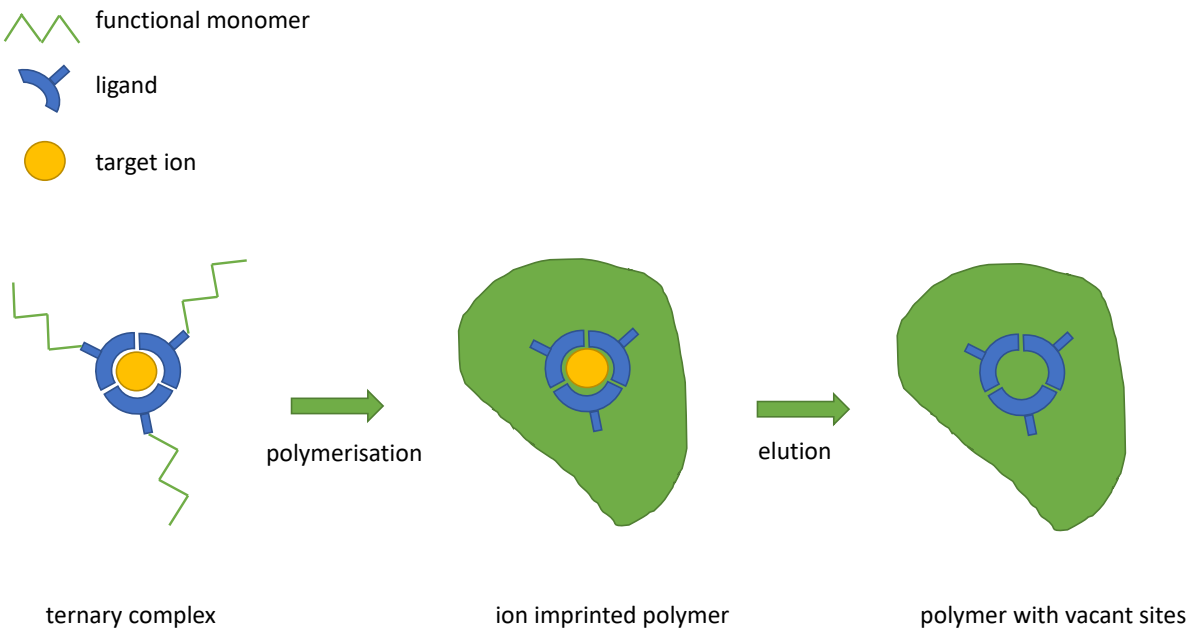

Figure 4: fabrication of ion imprinted polymers, own image leaned on [20]

To receive vacant sites for alkali metal ions, ligands like ring-like crown ethers and cup-like calixarene are combined with conventional functional monomers like methacrylic acid. Membranes can then be fabricated either by grinding the ion imprinted polymer and filling it into the middle of two membranes (filled membranes), or mixing the grounded polymer with a casting solution and then fabricate the membrane through phase inversion, or mixing it with a dispersed phase and fabricate a membrane by precipitation or in situ polymerization, or by a layer of ion imprinted polymer on a substrate membrane using in situ polymerization. Membranes fabricated by the latter method are called composite membranes and are the most promising due to their ability of variation of parameters in the synthesis and hence their achievement of different properties like heat resistance or chemical stability. Ion imprinted membranes working principle follows either the solution-diffusion model or the “gate” model. (Figure 5) The solution-diffusion model says that all ions can enter the membrane, target ions are attracted by the vacant sites and will be “trapped” there while other ions will pass the membrane easily. This results in a retarded permeation and selectivity is achieved by different permeabilities of different ions. Using this model, the separation process is limited when all vacant sites are full and no more adsorption by target ions is possible. The “gate” model, however, says that due to the higher attraction of target ions to the vacant sites in the membrane these ions will move easily and thus faster enter and diffuse through it. [20] Piletsky et al. [21] describes this as an internal driving force which is due to the interaction between recognition sites and target ion. Investigations of ion imprinted membranes for alkali ion separation using crown ether as the ligand result in selectivity coefficients of $a_{Li/Na}$= 1.85, $a_{Li/K}$= 2.07 [22] and $a_{Li/Mg}$= 4.42 [23], using calixarene result in selectivity separation factors of $a_{Li/Na}$= 72.05 and $a_{Li/K}$= 93.35 [24]. Absolute advantages of ion imprinted membranes are the simple assembly and the ability of reproduction which leads to lower capital costs and the stability

during the separation process and also after recovery which leads to lower operational costs. [20] A disadvantage might be smaller selectivity factors in comparison to other structures.

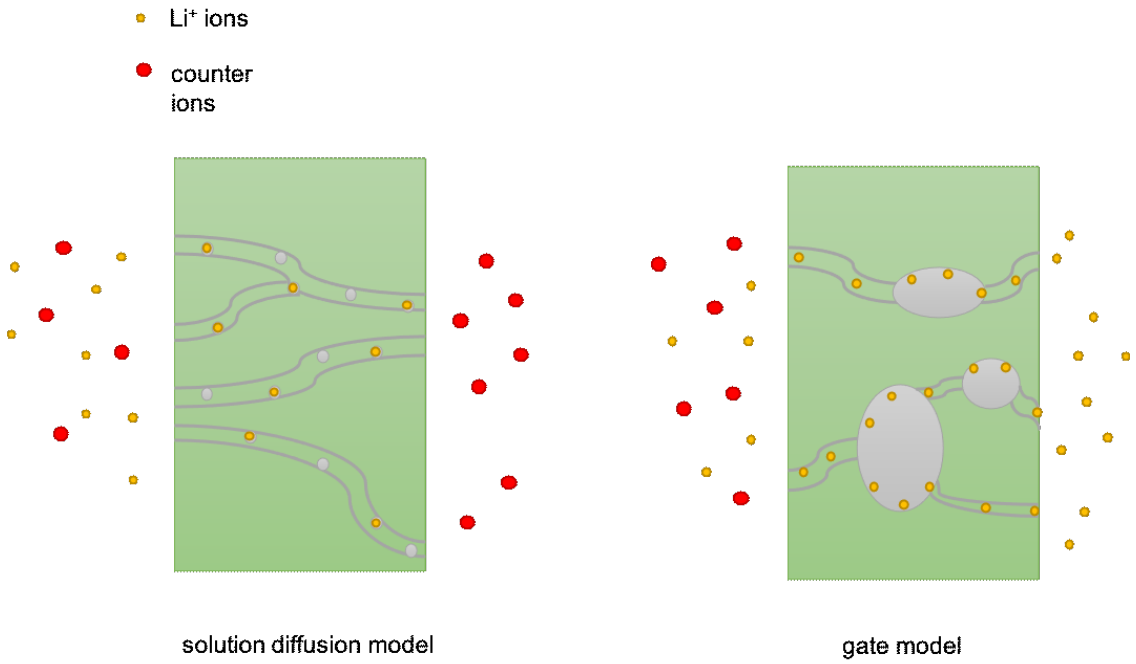

Figure 5: movement principles in ion imprinted membranes, own image leaned on [20]

The following table shows a performance comparison of ion exchange membranes.

Table 1: properties of different ion exchange materials

Material	Group	Capacity [mg/g]	Initial concentration [mg/l]	Aspects to consider	Source
H_2TiO_3	LIS	~ 0.1-13	~ 0.2-8	pH cannot be too low	[13]
		94.5	7000		
HMO/Al_2O_3 composite	LIS	~ 8.3-9	30	Too much Al_2O_3 leads to Mn dissolution	[14]
HMO/polyacrylonitrile composite nanofibres	LIS	10.3	35	Mn leaching (<3%)	[15]

Polyacrylamide/MnO_2 composite	LIS	~ 7	~ 13.6	Dissolution of Mn^{2+}	[16]
$LiMn_2O_4$	LIS	~ 22	145.8	Separation performance drops after cycles	[17]
$Li_{1-x}Ni_{1/3}Co_{1/3}Mn_{1/}3O2/Ag$	LIS	23	208.2		[18]
Multilayered IIM containing crown ethers	IIM	21.55	50	Capacity declines after 5 cycles	[22]
IMM containing crown ethers	IIM	27.1	200	Capacity loss of ~ 2% after each cycle	[23]
Mesoporous films containing calix[4]arene	IIM	~ 16	50	Adsorption equilibrium only after 4h	[24]

The capacity describes how many milligrams of lithium ions are inserted per gram of LIS or IIM powder. The initial concentration gives the lithium concentration in the feed source which also contains counter ions either in higher or the same concentration. Despite the high adsorption capacities of some materials, ion exchange membranes have some negative aspects. First, the whole process depends on two separated steps, the adsorption and desorption step. Due to that, more sophisticated plants are needed which also wear faster because of the use of HCl during the desorption step. The time to reach the equilibrium where all sites are filled with Lithium ions is long (four hours at [24]) which leads to long process times. For small initial concentrations of lithium, the H_2TiO_3 gives the best capacities (see Figure 6). As can be expected, the higher the initial concentration in the bulk, the higher the measured capacity of the material due to an overflow of target ions. Depending on the feed concentration, different materials can be reasonable for extracting Lithium ions using an ion exchange method. Looking at the higher capacity of IIM with crown ether at an initial concentration of 50 mg/L over IIM with calixarene leads to the conclusion that this material would be more successful. However, there are much higher selectivity factors at IIM with calixarene. The trade-off between those two factors should always be highly considered.

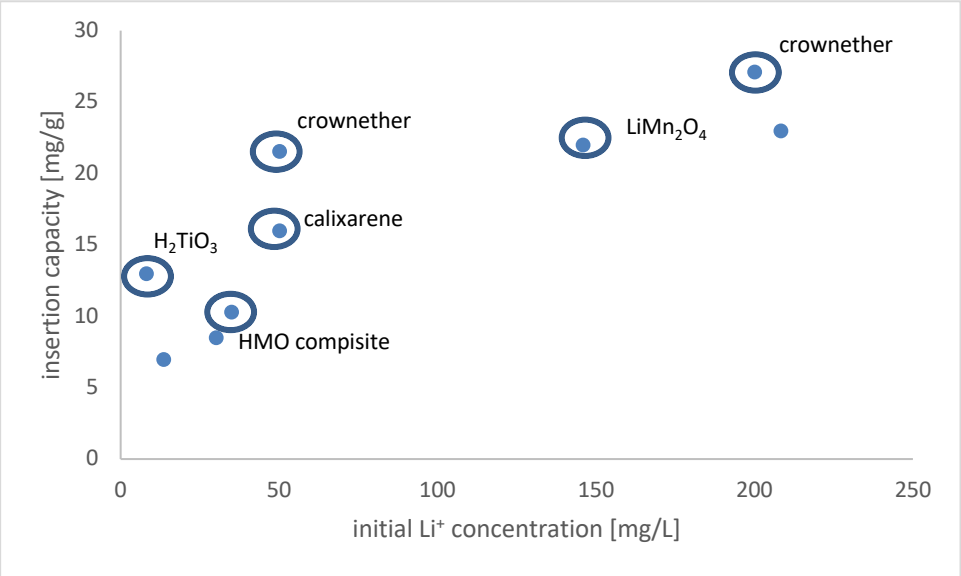

Figure 6: capacities of different ion exchange materials depending on the source concentration

3.3 Liquid Membranes

A different method to selectively extract Lithium from brine waters is by using synthesized ionophores resulting in a carrier-mediated transport. These synthetic carriers are able to bind target ions and ‘carry’ them to the other side of the membrane. Often, they are inserted in supported liquid membranes which consist of a microporous, polymeric matrix filled with a liquid, organic phase. [25] The ionophores are part of the organic phase which extracts the Lithium ions out of the solution. After a specific time, the organic phase is back extracted in acidic solutions. These extraction/back-extraction processes are well comparable to the adsorption/desorption process of Lithium-ion sieves or the “solution-diffusion” model of ion imprinted membranes. Research on Lithium-selective ionophores include crown ethers, metallomacrocycles and hemi-spherands. [26] To overcome the challenge of low lithium capacities of mononucleating systems Gohil et al. [26] investigated a multinucleating fluorogenic macrocyclic ionophore which can bind two Lithium ions at the same time. Although this configuration can lead up to a loading capacity of 27.06% (moles of extracted Lithium ions/moles of ionophores) at presence of other ions, it shows no capacity at low concentrations which might be the main challenge to address in further research. Yilmaz et al. observed that also at some ion-selective electrode (ISE) membranes complexes of target ions and ionophores of different stoichiometries exist and suggested to strongly include this effect when designing new ionophores or trying out new ionophore-to-ionic site ratios. They mark that those complexes could include target ions but also interfering ones which lowers the membranes selectivity. Experiments with multiple ionophore-to-ionic site ratios should be done to find the right composition and overcome this problem. [27]

As can be interpreted from above, crown ethers play a big role in selectively adsorbing Lithium ions. They are used in ion-exchange membranes such as ion imprinted membranes but also in liquid membranes as ionophores. Crown ethers possess dipoles where the oxygen atoms

are negatively polarized. Positively charged ions undergo an ion-dipole interaction with them. Researchers take advantage of this effect and a lot of novelties have been published recently. Tas et al. [28] , for example, blended a crown ether containing poly(arylene ether ketone) (CPAEK) with sulfonated poly(ether ether ketone) (SPEEK) to receive a hydrophilic, ion-selective membrane. The Lithium and Potassium fluxes through the membrane are determined by the SO_3^- sites of the SPEEK and the complex formation between the ions and dibenzo-18-crown-6. The selectivity of around 14 (K^+/Li^+) is only maintained in the initial state of 25 minutes which can be explained by the lack of free complexation sites after that. Although dibenzo-18-crown-6 forms stronger complexes with K^+ than with Li^+, the K^+ flux through the membrane is higher which results in a selectivity towards Potassium. Other researchers found similar challenges. Kazemabad et al. [19] investigated a new polyelectrolyte multilayer membrane (PEMM) where the polycation consisted out of polyethyleneimine (PEI) with embedded 15-crown-5 crown ether. Polyelectrolytes are polymers with electrolyte groups which dissociate in water and make the polymer positively or negatively charged. (PEI, for example, receives hydrogen ions when immersed in water and gets positively charged). The authors wanted to create a membrane that binds alkali-metal ions with the less affinity to Lithium to get a Lithium rich permeate. They researched its stability and selectivity towards Lithium ions in presence of Potassium ions. They found out using the crown ether modified membrane in a filtration experiment gives selectivity numbers below one over the first ninety minutes approximating one afterwards. This means that the membrane shows selectivity only in the first ninety minutes. After that, they explain that all the crown ether sites are saturated, and no more ions can be adsorbed. To their surprise the permeate was potassium-rich meaning that the crown ether rather built complexes with Lithium. They believe that the good selectivity in the first period of time is because crown ether forms complexes with two potassium ions resulting in big complexes which is hindered because of the little space in the branched structure of PEI. With Lithium, however, it forms 1:1 complexes which fit in the structure. Although after these 90 minutes the selectivity is low in comparison to before, the Lithium permeability factor is 1.5 times higher than that of Potassium. The authors explain that this is due to a higher intrinsic mobility of Lithium in the membrane. The authors suggest taking other crown ethers in consideration by using different precursors to receive Lithium in the permeate rather than the retentate.

3.4 Nanochannel structures

Another approach to selectively receive Lithium ions from brine is to create channels with different properties to only let target ions through. Gong et al. [29], for example, simulated a microchannel system with an electric field barrier that should hold back K^+ and Mg^{2+} resulting in a Lithium and Sodium-rich permeate. This would be optimal for the application at brines with high Mg^{2+}/Li^+ ratio. According to them, the co-existence of Sodium in the permeate (after passing the microchannel) does not pose a big problem due to the easy separation of precipitated Li_2CO_3 when the permeated solution reacts with Sodium carbonate. The simulated system consists out of two microchannels with positively charged walls connected through an anion exchange membrane. (Figure 7)

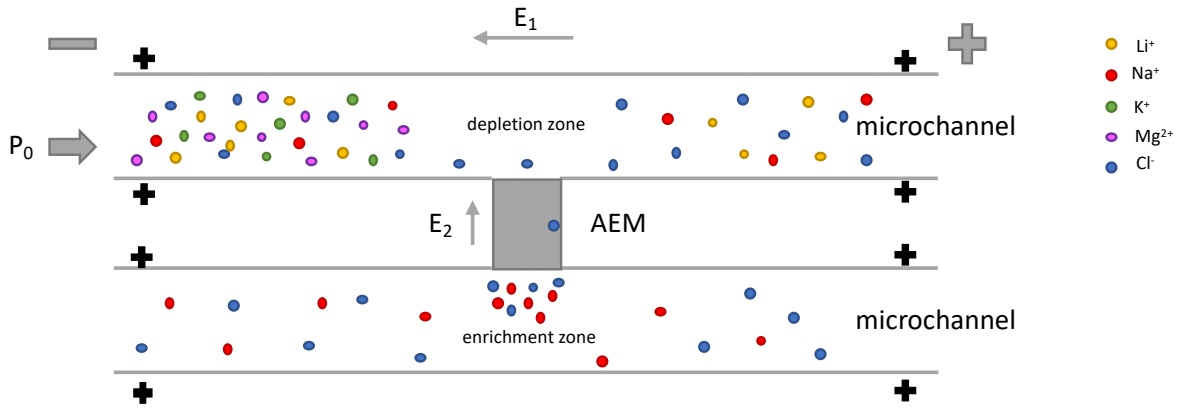

Figure 7: simulated microchannel system; own image leaned on [29]

The ion flow in the upper microchannel is created on one hand by an external pressure P_0 and on the other hand by an electric field E_1 pointing in the opposite direction of the fluid flow enhancing the electroosmotic flow. Another electric field is applied in the Anion exchange membrane. It points upwards to attract anions that are near the positively charged microchannel wall. Due to this electric field an ion depletion zone arises near the membrane in the upper microchannel creating an ion concentration polarization (ICP) environment. The field exerts electrophoretic forces on cations in the channel which results in an ion movement relative to the fluid flow. Thus, the ion movement is determined by the rightward fluid drag force and the leftward electrophoretic force. For ions with different properties (size, valence etc..) the balance between those two forces is different which results in a selective flow (when the optimal external pressure and electric field forces are applied.) The equilibrium is at a point where the ions are focused. For Li^+, having the lowest electrophoretic mobility, this point is near the highest value of E_2 and for Na^+ it is farer to the left in the microchannel. The electrophoretic mobility of K^+ and Mg^{2+} is so high that they are not focused at all and therefore move further back. The maximum electric field strength determines the energy barrier ions have to overcome to pass through the microchannel. Another mechanism the ion movement is dependent on is the neutrality condition. To get sharp peaks of target ion concentration near the electric field it is important that there are enough Cl^- ions to have equal charge densities. In order to maintain this equality in charges, ion with higher mobilities (Mg^{2+}, K^+) are replaced by ions with lower ones (Li^+, Na^+). Letting the throughput only be driven by electric forces leads to very low output concentrations. To increase the output, external pressure is applied leading to a higher velocity and increased fluid flow. However, this results in higher Mg^{2+}/ Li^+ ratios compared to a scenario without pressure. In a scenario Gong et al. simulated a pressure of 100Pa still resulted in a Li^+/Mg^{2+} ratio of 2810. An outstanding aspect of this method is the big difference between the output concentrations of Li^+ and Na^+ and K^+ due to the high mobility of the latter. Because there are no chemical reactions in the brine and because of the large diameter of the microchannel, the system is not at risk of clogging problems which is a big advantage.

Graphene oxide (GO) as well is an interesting material for Nanochannels because of its well-defined pores. Joshi and co-workers [30] created laminates on graphene oxide basis with nano-scale interlayers (≈13±1 Å) that only let ions that have smaller hydrated diameters than 9Å to pass through. These membranes fabricated from graphene sheet suspensions via vacuum filtration are extremely tight in dry state but serve as ion sieve in water solutions. Doing different measurements to receive permeation rates, the authors found out that positively and negatively charged ions move stoichiometrically through these membranes and no electric field is built up. They also found out that all small species exhibit similar velocities through the membrane which makes them not applicable for separation of target ions from other monovalent ions. However, a separation of ions with hydrated radius smaller than 4.5Å from bigger ions can be realized. The authors explain that the existence of nanochannels in graphene oxide is due to two regions inside the GO crystallites: oxidized zones and pristine carbon crystallite regions. The oxidized zones provide capillaries for the flow of water layers and the carbon regions act as spacer so that the oxides do not touch each other (big channels would be created) and do not get dissolved. Advantages of GO membranes are their easy fabrication and mechanical robustness. Abraham et al. [31] fabricated sophisticated GO membranes with interlayer spacings of 6.4Å to 9.8Å which exclude multivalent ions. A selective permeation between monovalent ions is achieved at an interlayer spacing of 9Å. The permeation rate of ions, however, decreases exponentially with the interlayer space, meaning that the selectivity is achieved at the expense of the permeation rate. Moreover, Lithium having the greatest hydrated radius of all monovalent cations has the lowest permeation rate compared to K^+ and Na^+ which would result in a Lithium rich feed which would have to be concentrated again.

Other research has also been done in creating highly selective Nanochannels that allow satisfying throughputs. Razmjou et al. explain that the structure and inner surface charges of the channel play indispensable roles in its functionality. [32] These properties and the membrane driving force need to be optimized in order to obtain a well working system. They created 2D nanofluidic vermiculite channels to control the ion movement and get more insight into the selective transport of Lithium over other monovalent cations in such 2D nanostructures. Vermiculite is layered and consist out of a Magnesium layer that is sandwiched between two aluminosilicate layers. Between the units of layers there is interspacing which contains cations to balance the negative charge of the layers. Vacuum filtration was used to obtain a free-standing membrane out of the nanosheets. The movement in this membrane was measured by linear sweep voltammetry (LSV) and it was found out that the smaller the ion the higher its conductivity. The selectivity of the membrane was calculated using the I-V curves of LSV by dividing the currents at 0.2V of two cation species. This resulted in ion selectivity ratios of 1.26 for Li^+/Na^+, 1.59 for Li^+/K^+ and 1.36 for Na^+/K^+. To approve these results, they did experiments with mixed ion solutions and measured the ion concentration in the permeate using ICP-MS which gave similar selectivities. They compared the conductivity with commercially available membranes and found similar conductivity at much better selectivity for the VCT membrane. They also found out that more Li^+ ions get extracted the higher the applied

potential is. This effect is stronger for brines with high Li^+ concentration. Doing MD simulation, the authors found out, that at an interlayer spacing of under 1nm the ions hop from one wall to the other when moving in the channel but jump forwards at only one wall when the layers size is about 1.2nm. Absolute advantages of this structure are its good thermal, chemical and mechanical stability, its high conductivity and its low costs of raw material (≈20USD/kg) and production.

Nanochannels can also be formed by Metal-organic Frameworks (MOFs). These materials have homogeneously structured porosities and are due to their structural diversity and thus vast functionalities, broadly applicable. Guo et al. [33] took advantage of this and constructed a membrane out of MOF HKUST-1 and sodium polystyrene sulfonate (PSS). Sulfonate groups are known to attract alkaline and alkaline-earth metal ions and MOFs have regular structured pores to enhance uniform movement. To obtain the MOF with intrinsic sulfonate groups, they coated a thin film of copper hydroxide nanostrands (CHNs, highly positively charged) with negatively charged PSS and dipped it into a H_3BTC solution. In this solution the nanostrands transform into the MOF HKUST-1 and the PSS is “trapped” in it. The sodium ions of the Polystyrene Sulfonate salt are replaced by the copper ions of the MOF. Zeta potential measurements approved that through the PSS the membrane gets more negatively charged which helps attract positively charged ions into the MOF-channels. However, PSS contents over 6.7wt% hinder the controlled movement of Li^+ ions due to cracks or voids in the membrane. Using this membrane, they received outstanding separation factors of 78 for Li^+/Na^+ and 99 for Li^+/K^+ out of conductivity ratios from single ion solution measurements. For binary ion mixture experiments they used ICP-MS which resulted in selectivities of 35 and 67 for Li^+/Na^+ and Li^+/K^+, respectively. Other advantages are the maintained stability after being immersed in water for two months, the high Lithium flux of 6.77 $molm^{-2}h^{-1}$ at a feed concentration of 0.5M LiCl and the low activation energy of 0.21 eV.

Zhang et al. [34] found two other forms of MOF, ZIF-8 and UiO-66, suitable for the Lithium separation application. Those metal organic frameworks possess uniform pores that consist out of angstrom-sized pore apertures and nanometer-sized cavities (Figure 8). The first one acts as ion selective filter and the second one enhances the fast transport of the ions that passed the pore window. They compare this structure to biological ion channels in cell membranes that regulate ion transportation. The preparation process of the ZIF-8 membrane is divided into the fabrication of two-dimensional ZIF-8/GO nanosheets, the spin coating of those onto an anodic aluminum oxide (AAO) resulting in a seeding layer and the interfacial growth of ZIF-8 on it. To make the seeding layer nanoporous, the membrane was etched by air plasma. The interfacial growth was carried out by a counter-diffusion method which limits crystal growth and hinders the formation of defects in the layer. The result is an ultrathin ZIF-8 layer of 446 ±74nm on an aluminum oxide support. Good results in a gas permeation test showed that the membrane had no large defects. After doing current-voltage measurements with the ZIF-8/GO/AAO membrane, the GO/AAO membrane and the AAO support only, the authors found out, that the selectivity is based on the ZIF-8 layer and other part do not play inevitable roles in the separation performance. The authors describe that the mechanism

underlying the separation is a dehydration/hydration process of the ions. In aqueous solutions, ions normally exist in hydrated form, meaning that there are shells of water molecules around them. If the pore is big enough, the ion will enter it with its hydration shells. If not, however, the ion has to leave some shells of water behind to enter the pore resulting in a (partial) dehydration of the ion. Moving through the ZIF-8 layer, ions have to undergo several dehydration-hydration processes. Only those ions can enter whose dehydrated radii are smaller than the pore aperture of the ZIF-8 structure. The transport is enhanced by weak interaction between the MOF and the target ions and water molecules. To verify their ideas, the authors did molecular dynamics (MD) simulations and found out that the mobility of Lithium ions is enhanced in the ZIF-8 structure compared with its mobility in bulk water. For Potassium ions, however, it is the other way around. Further approaches for the explanation of target ion movement in metal organic frameworks will be discussed later on. Doing I-V measurements with the ZIF-8/GO/AAO membrane the authors reached selectivity ratios of 2.2 and 1.4 for Li^+/K^+ and Li^+/Na^+, respectively. The membranes stability was tested measuring its conductance after three cycles, using SEM after the I-V measurements and measuring its selectivity in different basic pH values. Another advantage is the fast ion movement already at very low applied potential, resulting in ~105 ions/s for one pore at 20mV. The authors also tested another MOF structure, UiO-66 on PET support, resulting in selectivities of 1.6 and 1.2 for Li+/K+ and Li+/Na+, respectively. They assign the smaller selectivity values compared to the ZIF-8 membrane to the bigger pore aperture of UiO-66.

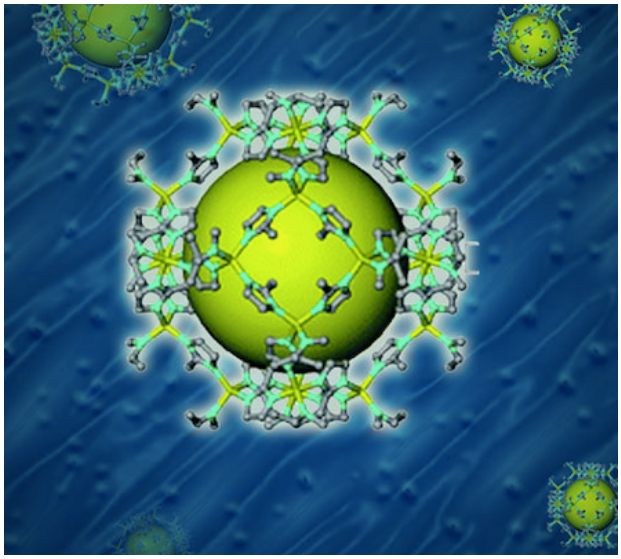

Figure 8: molecular structure of ZIF-8; tailored; designed by Environmental Molecular Sciences Laboratory (EMSL)

Lu and co-workers [35] pursue the same idea and create a membrane out of polymeric nanochannels with intrinsic UiO-66-$(COOH)_2$ structures. The ångström-sized MOF structures are placed only in the beginning of the pore to create an asymmetrical channel. This channel exhibits a sub-nanometer filter on top for selective ion sieving and a nanometer sized pore

underneath for fast and rectifying (only in one direction) transport of these ions. (Figure 9) The matrix membrane was produced by creating bullet-shaped nanochannels (NCs) in a PET membrane via an ion-track-etching method. This membrane was put in the middle of a cell with dispersed UiO-66-$(COOH)_2$ crystals on both sides of it. Applying potential of 2V enhanced the movement of the negatively charged crystals into the tip of the NCs, creating a seeding layer in it. The membrane with intrinsic seeding layer was then put in between a cell with ZrCl4 solution on one side and H_4BTEC solution on the other side to obtain interfacial growth via a counter-diffusion process. This process was facilitated by the seeds, however, also benzoic acid groups which are part of the PET served as ligands for the MOF structure ensuring no voids between the UiO-66-$(COOH)_2$ and the nanochannel. Doing I-V measurements with only PET-NCs, the authors found out that the preferential movement of cations is from tip to base which is due to the negative carboxylic groups on the NCs walls. The rectification ratios, meaning how many ions move in one direction compared to the other direction, for monovalent ions were much higher than the ones for divalent ions. To receive this ultrafast movement in only one direction an asymmetric structure of the pore is crucial. Using the modified UiO-66-$(COOH)_2$ in PET-NCs membrane the authors received highest conductance for K^+ followed by Na^+ and Li^+ leaving bivalent ions far behind. The higher conductivity of K^+ and Na^+ over Li^+ is due to the higher binding energy of Li^+ with the functional group -COOH. Binary ion permeation measurements resulted in selectivity ratios of 822.7, 336.7 and 197.6 for K^+/Mg^{2+}, Na^+/Mg^{2+} and Li^+/Mg^{2+}, respectively. The selectivity ratios between monovalent ions were so low that this structure is not applicable for target ion separation from brines with different alkali ions present. However, for brines with high Mg^{2+}/Li^+ ratios it could be used for concentration processes. The MOF structure is stable in chloride salt solutions also after being immersed in it for 10 days making it possible for continuous application.

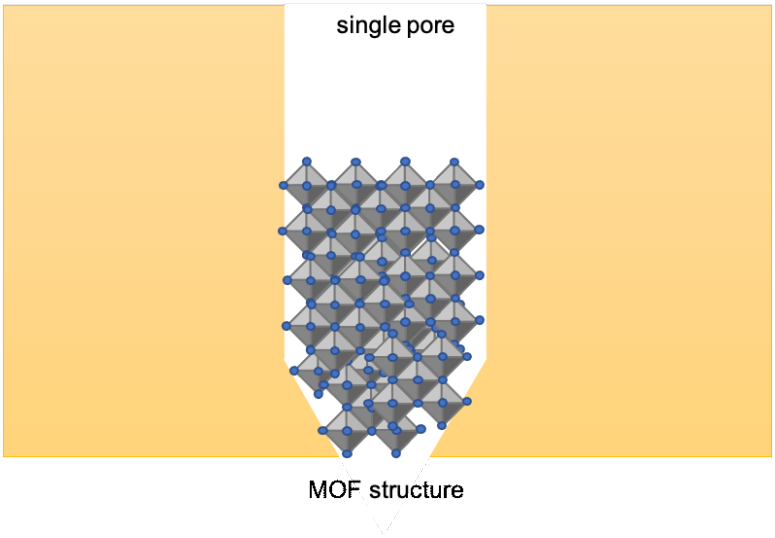

Figure 9: UiO-66-$(COOH)_2$ structures embedded in polymeric membrane; own image leaned on [35]

The ability of designing nanochannels capable of separating specific monovalent cations from brines with different species is highly dependent on the knowledge of why and how these ions

move in those channels and also whether there are factors that enhance or hinder their fast movement. Table 2 shows how selective different materials are and what aspects have to be considered at each of them.

Table 2: Performance properties of liquid membranes and Nanochannels

Material	Group	Selectivity factors			Aspects to consider	Source
		α_{Na}^{Li}	α_{K}^{Li}	α_{Mg}^{Li}		
Synthetic ionophores	Liquid membranes	0.664	3	5	Large transport of counter ions	[25]
Simulated microfluidic channel		~ 0.56	very high	2815	Co-existence of Na in permeate	[29]
Graphene oxide membranes	Nanochannels	-	-	-	Only separates small from large ions	[30], [31]
Vermiculite membrane	Subnanometer channels	1.26	1.59	α_{Ca}^{Li} ~ 10.5		[32]
MOF containing polystyrene sulfonate	Functionalized subnanochannels	35	67	1815	Needs functional groups	[33]
ZIF-8/GO/AAO membrane	(Sub)nanochannels	1.37	2.18	-	Stable only in basic conditions (7<pH<12)	[34]
UiO66/PET	(Sub)nanochannels	1.24	1.58	-	Larger window diameter than ZIF-8	[34]
ZIF-7/PET	(Sub)nanochannels	-	-	-	Superhydrophobic → no ion conductivity	[34]
PET Nanochannel containing	(Sub)nanochannels	-	-	197.6	Higher conductivity of K^+ and Na^+ over Li^+	[35]

UiO-66-$(COOH)_2$						

As can be seen, MOF structures exhibit very good selectivity properties. Ionophores often rather transport other monovalent ions over Li^+ which poses a problem in the desired application. Graphene oxides exhibit low selectivities considering monovalent ions with similar sizes and thus could be rather applied for different applications. The asymmetric structure of most metal organic frameworks, however, leads to selective and high ion flow in the pores which makes them very promising for separating Lithium out of brine. Chemical functionalization of those structures can cause even better performance. Thus, more insight into the framework chemistry and geometry of different MOF structures is highly needed. ZIF-7, for example, exhibits hydrophobic phenyl groups hindering polar liquids to pass through it. Although it has an even smaller pore aperture than ZIF-8 it is not applicable due to its chemistry.

Different phenomena trying to explain ion movement in nanochannels and how they can be implemented will be discussed in the following paragraphs.

3.5 Fundamentals of ion movement in nanochannels

In general, the attraction of target ions to specific nanopores and their transportation through them depends on several factors, which are the pore diameter, the chemistry and the morphology of the channel walls, the intensity of the driving force, and the size of the channel.

3.5.1 Influence of the diameter on ion movement

Depending on the separation target molecules, the diameter of the pore should not be too big to ensure its selectivity. The optimal pore diameter can be estimated by means of the Debye length which describes the thickness of the electrical double layer (EDL) that forms over charged surfaces (Figure 10). This double layer consists out of a stern layer where counter ions are fixed and a diffuse layer where the ions are not that tightly bond and therefore can move freely. Over the second layer the potential decays to zero. To hinder this decrease in potential, the double layers formed on both walls of a charged channel have to overlap and thus the diameter of the nanopore cannot be bigger than the double Debye length. In such an environment, counter ions predominantly exist (cations for a negatively charged surfaces). The reduction below double Debye length also leads to other phenomena such as internal/external ion enrichment, surface governed charge transportation, water stripping and current rectification. [36]

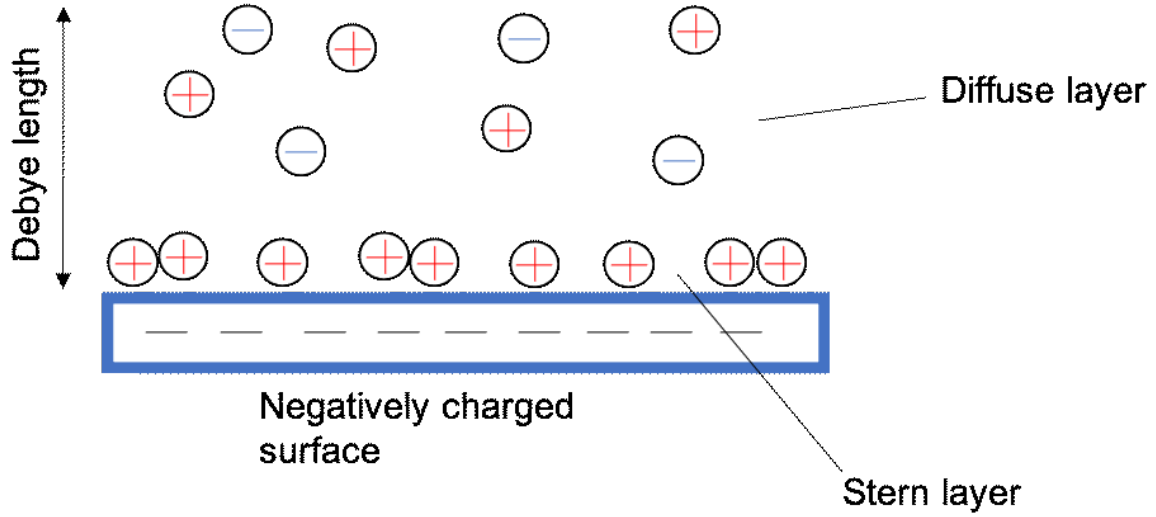

Figure 10:Formation of an electric double layer over a charged surface; based on [37]

The Debye screening length lays between 1 and 100 nm under actual conditions. [37] This length scale can be divided into three sections. In each of them different phenomena lead to a change of intermolecular forces in the solution which is confined into one length scale. If the solution enters a channel of a diameter between 1 and 2 nm the hydration forces between molecules in the solution and molecules of the solution and the wall of the channel change. This force is normally repulsive due to the hydration bonds that have to be broken. However, in a range of 1-2 nm it has an oscillating characteristic. In this scale also steric interactions influence the behavior of the molecule's flow. In channels with diameters up to 50 nm Van der Waals interactions can occur. These are due to dipoles that occur spontaneously because of changes in the charge distribution around molecules and atoms. In bigger channels, up to 100 nm in diameter, electrostatic interactions predominate. This means, that counter ions are attracted to the charged surface and co-ions are repelled. This underlines that in a length scale above 5 nm the ion flow can be described by continuum dynamics where electrostatic and partially van der Waals interactions predominate. In a channel with a pore diameter under 5 nm, however, the ion transport has to be described by stochastic and/or molecular dynamics. In continuum dynamics the most important equations are the Poisson-Nernst-Plank equation and the Stokes equation. Here, the Stern layer is expected to be held to the surface charges on the wall and thus has no contribution to the ionic current and plays no role in the calculations of the ion flow through the channel. The surface charge density is now consisting out of the channel's wall's charges and the Stern layer's charges. In most Nanochannels, the whole channel area is within the EDL, thus the solution only consists out of counter ions. Taking this into account, the type and concentration of the ions inside the channel can be governed by modifying the surface charges. If the channel dimension is larger than the Debye length, ion current control can only be achieved when the surface charge changes inside the channel from positive to negative. In that way a depletion or accumulation zone is created at the border.

In channels with diameters smaller than 5 nm, calculations cannot be done by the rules of continuum dynamics. As the time frame of an ion across a channel is larger than the typical time scale of molecular dynamics, this concept is not very suitable either. Stochastic dynamics, however, represent a way to calculate the conductance of an ion channel. [37] Stochastic means that there are parameters that have random fluctuations which, for example, can hinder the flow of ions. Models following stochastic dynamics are primary described by the Langevin equation of motion:

$$m_i\,\ddot{x}_i(t) = F_i\big(x_i(t)\big) - F_{i,frictional}\big(\dot{x}_i(t)\big) + R_i(t)$$

Where F_i describes the interaction between the particle and other particles. $F_{i,frictional}$ is the force on the particle due to the friction coming from the solvent when the particle moves through it. R_i describes the force on the particle that is exerted when it randomly interacts with solvent molecules. The frictional force is described as follows

$$F_{i,frictional} = \gamma_i * m_i * \dot{x}_i(t)$$

where γ_i is the collision frequency and m_i the particle's mass. Those two parameters can be combined to ξ_i, the friction coefficient. This coefficient is random which is caused by the random collisions of the particles. There are three situations that can be considered in such systems.

At one extreme, the integrated time period (integration time step) is much smaller than the velocity relaxation time. In this case the solvent does not affect the particles at all. At the other extreme, when the integration time step is much larger than the velocity relaxation time, the fluid is in a diffusive regime where the ion movement is weakened by the solvent. The third situation is in between the two extremes. To be able to proper describe one's situation in the calculation it is important to use the right approximations.

Although there is a problem with the time frame when using molecular dynamics for the calculation of ion transport through nanochannels, MD plays a role in the simulation of several processes. This is because ion movement in biological channels most likely happens via complex events where some ions move as a group and others as single ions. Thus, also MD have to be considered in an overall simulation.

Another interesting factor Razmjou et al. [36] indicated is that the movement mechanisms of ions inside the channel also depend on the channel's diameter. If it is below 1 nm, the ions hop from one channel wall to the other while passing the channel. If the diameter is above, movement is rather dominant on one surface.

In an early research, Razmjou and co-workers [6] indicated that especially when choosing the diameter of an ion-selective nanochannel it has to be considered that ions cannot move in the absence of water. Therefore, the size of the diameter should allow at least two to three layers of water molecules so that ions have a medium to flow in. However, it should not be much bigger than the hydrated diameter of the target ion to ensure its selectivity.

3.5.2 Effect of pore chemistry on the ion movement

The pore chemistry on the inside of the channel plays an important role for the movement of the ion inside it. Overall, for cation exchange membranes, the surface charge of the channel wall should be negative to only let cations move through it and exclude anions. This can be achieved by choosing the right functional groups on the wall. Their density has to be carefully chosen as too many functional groups (FG) per nm hinder a fast Li^+ movement through the channel as the activation energy a Li^+ ion needs to go from one FG to the next one increases. With too small density of FGs per nm, however, the transportation through the channel of ions via surface charges is not possible. This transportation is governed by the Grotthuss mechanism which says that protons hop from one water molecule to the next due to incoherent cleavage of hydrogen bonds. [38] Allocating this mechanism to the movement of Li^+ ions in nanochannels with functional groups, the transportation can be seen as Li^+ ions hopping from one functional group to the other. Selectivity in channels is obtained due to the little bonding affinity and activation energy Lithium exhibits in comparison to other monovalent ions. This allows the Li^+ ions to be faster transported through the channel because it can be more easily detached from functional groups than other ions. This is in accordance with a research of Sun et al. [39] who studied the effect of functional groups in GO membranes and found out that heavier metal ions interact stronger with oxygen atoms of functional groups than lighter metal ion.

Different functional groups have been tested with the goal of reaching high Li^+ conductivity and selectivity. Among others, sulfonate groups and carboxylic acid groups were tested recently. Lu et al. [35] tested PET nanochannels with deprotonated carboxylic groups and found out that there is Lithium selectivity towards Magnesium and Calcium. The separation of Lithium from Potassium and Sodium, however, remains a big challenge using these functional groups. Nafion membranes are typical applications of sulfonate groups. Though they allow fast ion movement, they have difficulties with selectivity due to a wide size distribution of their paths and incoherent free spaces. Guo et al. [33], however, incorporated sulfonate groups into a MOF structure taking advantage of their homogenous pore structure and the affinity of Li^+ to sulfonate groups. Razmjou et al. [32] created an exfoliated negatively charged vermiculite membrane out of Mg-based octahedral sheets between tetrahedral silicate sheets, where the silicate serves as the layer of functional groups. The implementation of functional groups in a material with nanoscale pores can be difficult and thus the morphology of the material plays a vital role.

3.5.3 Effect of the pore's morphology on ion movement

Morphology-wise there are two promising possibilities to create a nanochannel with a high permeation rate and selectivity. The first thing that comes to one's mind when creating a nanochannel that should be selective to very small ions is to decrease the diameter in a way that only those ions can pass it. The diameter of a dehydrated Li^+ ion is around 0.12nm. However, these ions are surrounded by layers of water molecules that are more or less tightly connected to the ion. When the diameter of the pore is much smaller than the diameter of the

hydrated ion (0.76 nm for Lithium [40]) , the permeation rate will decrease a lot due to the high dehydration energy barriers that have to be overcome to enter the channel. This problem can be addressed by breaking the symmetry of the pore. One way is to create channels that are inspired by biological protein nanochannels. Those natural channels selectively only let through certain alkali ions and are vital for the cellular equilibrium and neural signal transduction in everyone's body. Thus, they play an important role for every living being. Those pores consist of an ångström-sized filter (3-5 Å) and a nanometer-sized cavity of ~1.2 nm. A model of these channels is shown on the left side of Figure 11, the right side shows a biological ion-selective pore in a lipid bilayer.

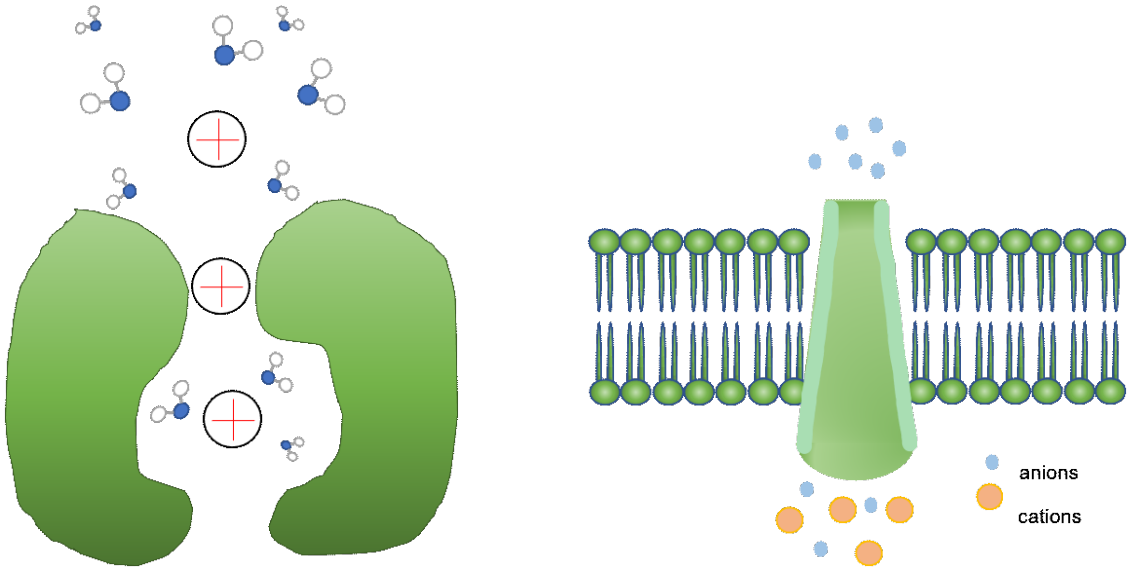

Figure 11: biological ion filter (left) and biological pore in lipid bilayer (right); based on [41]

The filter leads to the pore's selectivity and the cavity allows a high permeation rate. [34] Looking at this morphology, several research attempts have been done to mimic biological ion channels. Zhang et al. [34], for example, took advantage of the morphology of the MOF zeolitic imidazolate (ZIF) - 8 which exhibits an ångström-sized pore aperture and a nanometer-sized cavity. The results of their work were explained earlier. With such a pore structure, ions pass through several dehydration and rehydration processes. This lowers the dehydration energy barrier compared to when ions have to pass symmetric channels with diameters that are much smaller than the ion's diameter in hydrated state. Those channels can be non-charged.

Other asymmetric channel structures incorporate conical shaped pores. This structure strongly uses the **rectification effect**. This means that more ions will move in one direction of the pore than in the other direction, resulting in an asymmetric ion transportation and to be seen in asymmetric current-voltage (I-V) curves. These curves can be obtained by analysing the transport of ions through the membrane using linear sweep voltammetry (explanation see

chapter 3.8.1) where a voltage is applied between two electrodes that are submerged in an electrolyte and the current is obtained as response to the applied voltage. The rectification phenomenon is also used by biological pores that are embedded in lipid bilayers [41] (Figure 11, right side). A conical Nanochannel that exhibits rectification effects requires several characteristics. First, the tip cannot be bigger than the electrical double layer. Then, excess positive or negative charge has to be part of the inner wall of the channel. Last, interactions of ions with the channel walls have to be different meaning asymmetric on both ends of the channel (tip and base). Through these interactions, the internal potential in the channel changes which affects the direction of the ion flow.

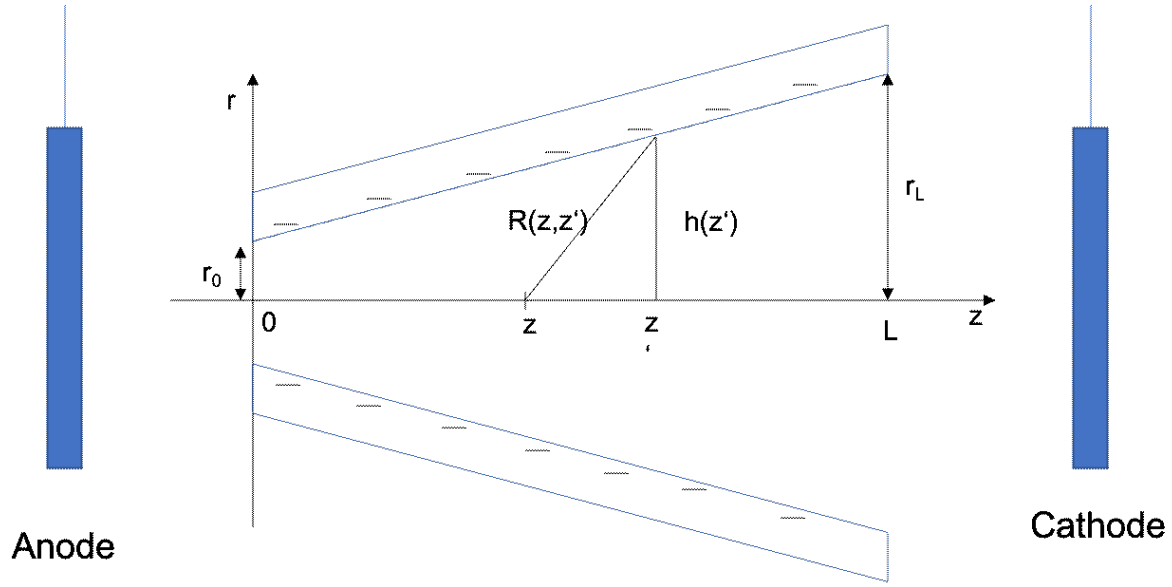

Figure 12: conical Nanochannel with external voltages; based on [42]

When the polarity of external voltages is negative, meaning that the cathode is located on the base side (see Figure 12), cations interact with the strong negative charges on the walls of the tip side and flow from tip to base to the cathode. However, when the anode is on the base and cathode on the tip side resulting in positive external voltages, an electrostatic trap is formed. This is because anions need to go from tip to base side in such a configuration but have difficulties entering the tip because it is so small that the electrical double layer overlaps and hinders anions to enter. Cation could move into the base side direction tip side but because electric neutrality in the channel has to be preserved and no anions can enter it, also the flow of cations is very limited. [43]

One model to describe this effect is called the ratchet model. [42] It is based on the fact that the interaction of ions on the tip (narrow opening facing the anode) and base (wider opening

facing the cathode) of the Nanochannel is asymmetric which determines the direction of the ion flow. The force on ions at any point z of the channel can be calculated using the following formula, in which the position z = 0 is at the tip of the channel:

$$F(z) = -2\pi\delta \int_0^L dz' \frac{z - z'}{R^3(z, z')} [1 + \lambda R(z, z')] e^{-\lambda R(z, z')}$$

Additional to the rectification effect due to the shape and inner charges of the channel the ion is driven by the external field resulting in an oscillating periodic force. If there were no external voltages, the cation would rest somewhere near the narrow end of the channel in its equilibrium position. With an external driving force, however, the force F(z) on the (cat)ion is high near the tip and decreases along the channel. It increases again near the base facing the cathode due to the power of attraction (see Figure 13). The strongly positive force on the left of the tip is due to the repulsive force of the anode. When the ion has overcome the energy barrier of the channel and reaches through the window, the force is highly negative, meaning attractive, due to the strong negative forces that are built by the inner surface charges. This power of attraction decreases along the channel because of the increase of the space between the channel walls. At the base of the channel, the negative force increases again due to the power of attraction of the cathode. This model especially describes the fundamental of asymmetric nanochannels that should separate cations from anions.

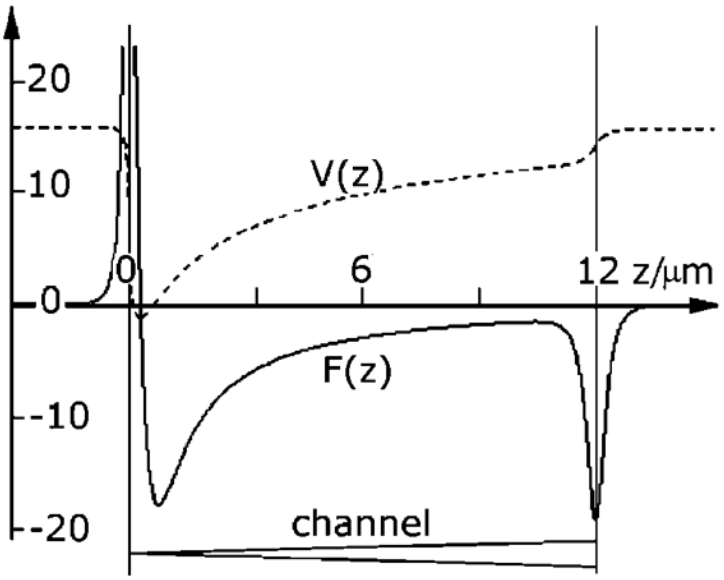

Figure 13: Force F(z) on a cation in a conical shaped channel with negative external voltages, copied from [42]

If cations should be separated from other cations depending on their hydrated/partly dehydrated size, however, another effect is more vital than the one explained by the ratchet

model. Recently, Razmjou et al. [6], explained the most vital reasons why asymmetry plays an important role for successful Lithium-ion separation. The main reason is that in conical channels hydrated Li^+ ions can gradually lose their hydration shells which lowers the energy barrier to enter the channel compared to cylindrical pores with a symmetric geometry. The base of the channel can be entered by hydrated bivalent and monovalent ions. As those ions move further in direction of the tip, they have to lose some of their hydration shells and bigger ions might not be able to move further. (Figure 14) The tip so narrow that only Lithium ions with a water shell in one plane can pass through. This gradually loosing of water shells demands much less energy as when hydrated ions have to strip all of their water shells at once and thus a higher permeability is reached. For this ion movement to happen, the cathode needs to be on the tip side of the channel. As said before, this leads to an electrostatic trap where the ion flow is very limited. With the right adjustments, however, this can lead to a good selectivity of Lithium compared to other monovalent cations.

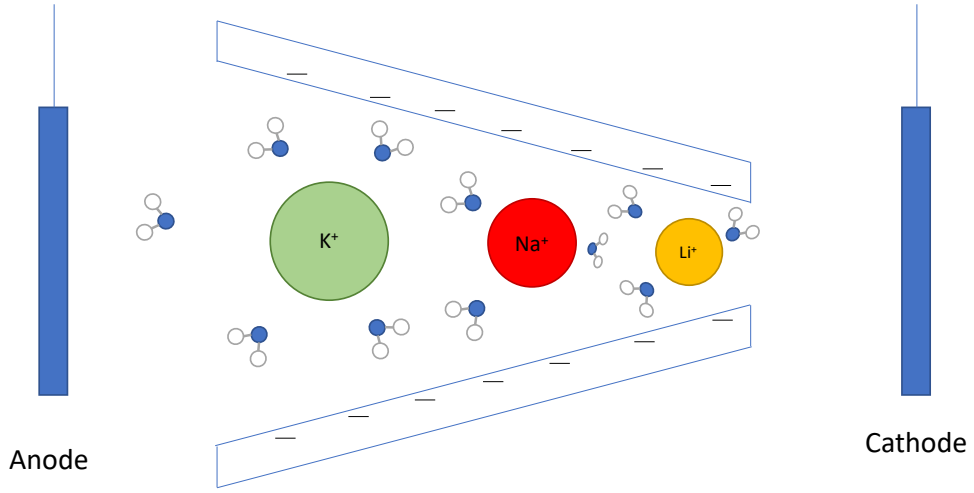

Figure 14: monovalent ions gradually losing their hydration shells in asymmetric nanochannel; based on [6]

3.5.4 Impact of the driving force on the ion movement

As said before, the driving force also plays a vital role in the transportation of Li^+ ions in nanochannels. Electrical potential as driving force can be represented by two ohmic regions on the tip and base side of the Nanochannel which act as the limiting regions. When the potential difference between those two regions is high enough, a phenomenon called “ion-enrichment and ion-depletion effect”[44] can be detected and seen in an asymmetric I-V curve. Ions are enriched at the cathode and depleted at the anode. This applies to both, anions and cations which may sound incorrect but will be explained in the following. If the surface charge of the nanochannel is, for example, negative, the electrical double layer is positively charged, meaning that there are more cations than anions in this area. If there is an overlapping of the double layers inside the nanochannel, the concentration of cations will be higher than that of

anions. The fluxes in the Nanochannel and outside of the Nanochannel can be calculated by the electric field strength, the cross-section, the electrophoretic mobility and the concentration of the ions. The flow of cations inside the nanochannel will be higher than outside of the channel. The flux, that brings cations from the bulk solution to the end of the nanochannel that's near the anode (tip side of the nanochannel) due to repulsion is smaller than the flux inside the Nanochannel that moves the cations to the base of the channel. This results in a depletion zone at the tip and at the same time to an enrichment zone at the base. The flow of anions in the nanochannel, however, will be lower than that outside of the channel. At the tip (near the anode), the flux that brings away the anions is higher than the flux inside the nanochannel that brings the anions to this position. This also results in a depletion zone at the nanochannel's tip. At the same time an enrichment of anions at the base of the nanochannel is created as anions are brought fast to this end of the nanochannel from outside due to the repulsion of the cathode but are only slowly transported in the inside of the nanochannel. This effect decreases when the buffer concentration increases because the double layer thickness decreases with increasing ionic strength of the solution. Also, enrichment and depletion will be much higher of the ions that are predominant inside the channel due to the electrical double layer overlap.

This depletion and enrichment effect results in concentration polarization and a non-linear I-V curve. Concentration polarization means that the ion concentration near the nanochannel is higher than that in the bulk. Non-linearity in the I-V curve is only received if the potential does not exceed the current operating limitation (V_{lim}). If the current is higher, I-V curves will become linear. Non-linearity is important for the membrane's selectivity. Pushing power density just before this limit, however, improves Li^+/Na^+ and Li^+/K^+ selectivity. Razmjou and co-workers explain in a recent work [6], that this could be due to the phase changes of water when confined in nanochannels. In such small confinements the phase of water changes into an ice-like phase which lowers the mobility of ions and therefore increase the selectivity of small ions that are still able to move. Pushing the power density as high as possible increases the small ions velocity which results in an even higher selectivity.

Another driving force for the transportation through channels is pressure. In the same work, Razmjou and co-workers [6] explain that applying pressure as driving force for Li-ion extraction could harm the membrane due to mechanical stress. Therefore, when thinking of an industrial scale up, electrical driven processes are a more promising method.

3.5.5 Ion movement in nanochannels with non-charged inner surface walls

The above mechanisms mostly apply to nanochannels with negative inner surface charges. However, it is also possible to selectively transport Lithium ions through channels with neutral inner walls. Then, the diameter of the pore has to be smaller than the diameter of hydrated Lithium, which is 0,764 nm. To enter the channel, Lithium ions have to lose some of their hydration shells. In doing so they are overcoming a certain dehydration energy barrier. This barrier has different values for different ions; thus, a selective ion transport is obtained. At this

point it is important to consider that from to dates point of research, ions can only be conducted in hydrated state.

The first to look at selective movement of ions in channels was George Eisenman in the 1960s. [45] Considering classic thermodynamics, selectivity comes from the relative free energy difference of ions in the channel compared to the bulk which is different for each type of ion. In his research, Eisenman found out that glass electrodes with different compositions exhibit different sequences regarding the binding of the five different alkali metal ions which are Li^+, Na^+, K^+, Rb^+ and Cs^+. By testing a lot of different electrode compositions, researchers found out that there exist 11 different sequences, called the “Eisenman sequences”. Eisenman undercuts his ideas by calculating the equilibrium binding of the ions to the glass and the energetic difference of the ion between binding to water and to the glass. He finds out that the more vital factor that determines the selectivity is the anionic field strength of the ion to the glass. He also remarks that ions that bind water molecules strongly to themselves need strong negative electrostatic potentials to dehydrate and then bind to those negative sites. This regards smaller ions, especially Lithium. Larger ions, however, bind water molecules less strongly. A high negative site rather binds the water molecules around it than the large ion itself. At weaker negative potential, Cesium, the largest alkali ion, would rather bind to the sites than smaller ions. Taking this to account, at highest anionic field strength the **sequence XI (Li^+>Na^+>K^+>Rb^+>Cs^+)** will be observed. At lowest anionic field strength, the sequence will be the other way around. Molecular dynamics simulation made it possible to reconstruct the different sequences for different anionic field strengths. They use the alchemical free energy perturbation (FEP) technique which helps to find free energies of several processes. But ion selectivity in a channel is not only based on thermodynamic equilibria as said before. Horn et al. [45] point out that also the different barriers in a channel the ion has to overcome when it passes it play vital roles in the channel’s selectivity. Also, these barriers may not have static energy levels and might fluctuate with time as well as the fact that other ions are present in the channel can affect the conduction of ions. The permeation of ions through the channel can be seen as a process of hopping from one barrier to the next. The authors point out that research has still to be done to be able to completely understand and explain selective processes in ion channels and that especially the mechanical robustness of these channels plays a challenging factor in latest research.

Oppositional to Eisenman’s idea that the anionic field strength of ions to binding sites are most important for selective flow, also selective channels without intrinsic charges exist. For those channels the diameter which cannot be bigger than the diameter of the hydrated ion plays a vital role. Adjusting the diameter, however, is critical and has to be done carefully. For some materials diameters that are too small can lead to a formation of monolayers of water molecules in the channels whereas two to three layers are essential for the transport of ions. [30] This is the case for graphene oxide laminar membranes with interspacing layers of lower than 0.7 nm.

A promising material with rapid transportation of Lithium was found by Choi et al. [46] in single walled carbon nanotubes. Those channels, however, are not yet embedded in a membrane-like structure which could pose problems in the future.

Thinking of the nanochannel's size, not only the diameter is important but also the length. Lithium ions show different acceleration-deceleration behaviors in nanochannel with different lengths. As can be seen in Figure 15 there is linear acceleration at the entry of the channel followed by a deceleration. How strong and where this deceleration happens depends on the length of the channel. This stands in accordance with a high force on the ion at the narrow end of the channel to be seen in Figure 13. This force leads to faster movement of the ion. Therefore, a decreasing force leads a deceleration of the ion movement. The increase in force on the wide end of the channel, however, is not in accordance with the velocity loss in Figure 15.

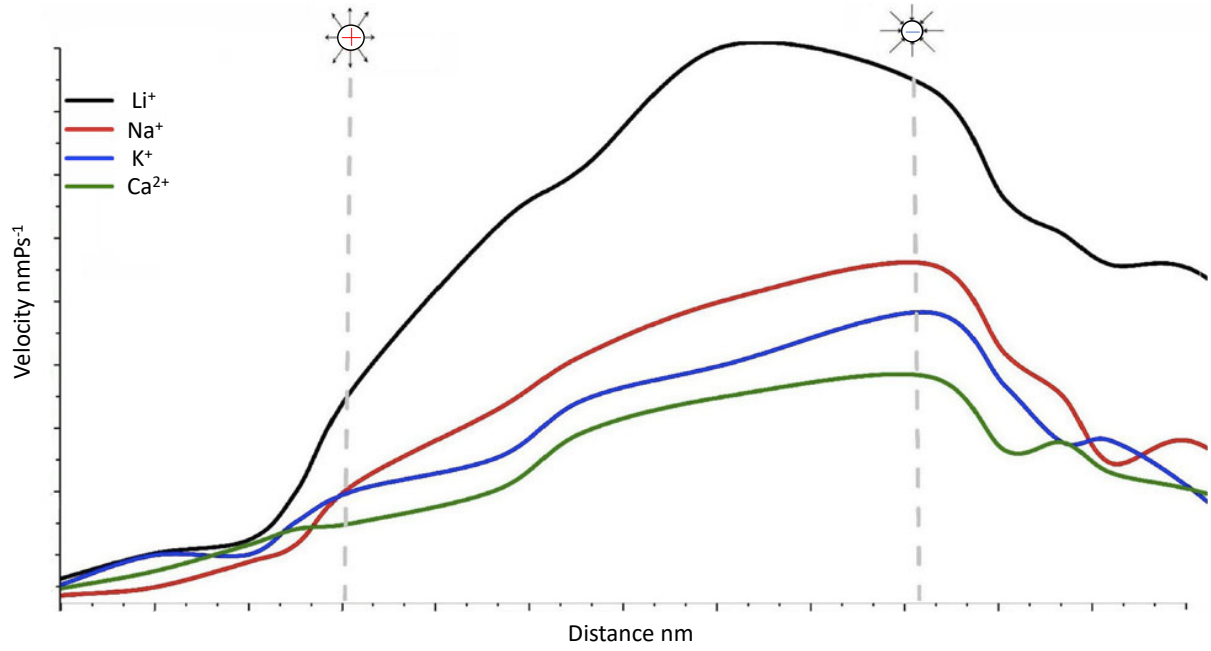

Figure 15: velocity profile of Li+, Na+, K+, and Ca2+ ions in 0.4 nm vermiculite nanochannel, copied from [32]

Razmjou et al. [36] point out another promising material for selective Lithium ion transport, namely Covalent/Metal organic frameworks (COF/MOF). Their well-structured pores with narrow size distribution make them especially interesting for such applications. Jung et al. [47], for example, fabricated lipid bilayers with intrinsic MOP-18 which showed a Li^+/K^+ selectivity of 1.7. Although this seems very promising, a poor rigidity of the material makes more research inevitable. Zhang et al. [34] fabricated thin MOF layers on anodic aluminum oxide support using the MOF structures ZiF-7, ZiF-8 and UiO-66. ZiF-7, that exhibits a pore aperture of 0.29nm did not show any Li-ion transport although dehydrated Li^+ exhibits a smaller

dehydrated diameter of 0.12 nm. The authors claimed that the lack of ion transport through this material is due to its superhydrophobicity which prevents water to pass through. Therefore, no ions can be transported. UiO-66 with a window size of 0.6nm showed a higher transport but lacked in Li^+ selectivity. ZiF-8, however, exhibiting a window of 0.34nm, shows Li^+ selectivity and conductivity. The authors claim that this selectivity is due to the partial dehydration of the ions, weak interactions between dehydrated ions, water molecules and the MOF structure and the size exclusion. They explain that dehydrated Li^+ ions in nanochannels have higher ionic mobility than other ions. This is in accordance with Wen et al. [48] saying that partially dehydrated Li^+ ions bind their hydration shells more tenaciously making them more mobile and thus faster. The possibility to enter the channel, meaning the size of the pore aperture, determines if the ion will lose some of their hydration shells or not. Recently, another metal organic framework membrane was fabricated by Liang et al.[49] using ZIF-8. They encapsulated sulfonated spiropyran (SSP) in the ZIF-8 crystals which exhibited up to three-digit selectivities for monovalent ions. Amongst others this work leads to the assumption that metal organic frameworks represent high potentials for selective ion transport and thus for Lithium recovery from brines in a sustainable way. Some of their uncontroversial advantages are their ordered and adjustable pore size, especially in the angstrom range, their narrow pore size distribution and their large specific surface area. Also, they can be modified in a lot of ways to exhibit special functionalities.

As said before, biomimicry plays a vital role in the construction of synthetic channels that selectively transport ions. Based on biological ion channels, morphologies like those in Figure 11 could be hold as examples to mimic. What if both of these morphologies could be combined? Meaning to benefit from the fact that a lot of metal organic frameworks exhibit angstrom-sized pore windows and nanometer-sized cavities, like in Figure 11 on the left, and combine them in a hierarchical structure resulting in a conical-like shape, like in Figure 11 on the right. This could be achieved by combining several layers of structures with different pore sizes. The fact that most metal organic frameworks have sufficient binding sites facilitates a combination of several MOF layers.

The combination of MOF and COF (covalent organic framework) structures was also recently used by Das et al. [50] who fabricated a 2D COF - 3D MOF composite membrane for high-flux gas separation with high selectivities. They created a thin layer of the 2D H2P-DHPh covalent organic framework on a 3D UiO-66 MOF layer. The 2D COF layer exhibits channels that are perpendicular to the membrane surface and therefore enhances fast gas transport. The binding units that build this layer are horizontally bond to each other but lack in strong bondings to polymeric or other substrates. This is where the 3D MOF layer is a good alternative. It's binding sites strongly bond the COF building units and also help them to grow in an ordered way. This results on one hand in an outstanding mechanical strength that cannot be obtained with different substrates and on the other hand in an ordered COF layer for fast gas transport. This shows that some different MOF or COF structures are very compatible and enhance each other's functionalities. In this example it is the mechanical strength that is increased by combining these two structures. Different to ion movement in membranes, gas is mostly

transported by the solution-diffusion mechanism. This means that the velocity of solution and diffusion play a more vital role than the diameter of the pore. The diffusion mechanism is strongly enhanced by the ordered form of the 2D COF structure whereas the 3D MOF layer helps to form this structure.

Elsaidi et al. [51] also used a dual layer MOF composite membrane to enhance gas separation. Their main goal, however, was to construct a membrane with a selective layer on top and a layer exhibiting a bigger pore size underneath for fast transport. This combination is especially interesting to enhance the well-known trade-off between selectivity and permeability. The authors created purely inorganic MOF composite membranes of SIFSIX3-Ni on SIFSIX-1-Cu and HKUST-1 and by doing so they increased their selectivities from 5.7 to 13.4 for HKUST-1 and from 2.3 to 7.4 for SIFSIX-1-Cu. The idea of having one layer which exhibits a small pore size to ensure good selectivity and another layer with bigger pores to control fast transport could be also interesting for Lithium-ion sieving. However, there has not yet been done a lot of research which is why an approach was done in this work. Which metal organic frameworks structures were used to fabricate a Lithium-selective membrane, why they were used, and their performance will be discussed in the next chapters.

3.6 Hierarchical structure of two-layered metal organic framework membrane with NF90 support

The goal of this research was to build a material with a hierarchical structure all throughout the pore to mimic biological ion channels. The first layer should be a material with big pores whereas on the top there should be the one with the smallest pore diameter to ensure selectivity. As basis, the commercial membrane NF90 was used. It is a thin film composite membrane consisting out of a polyester support web on the bottom, a microporous polysulfone film and a polyamide thin film of 0.2µm on top (Figure 16).

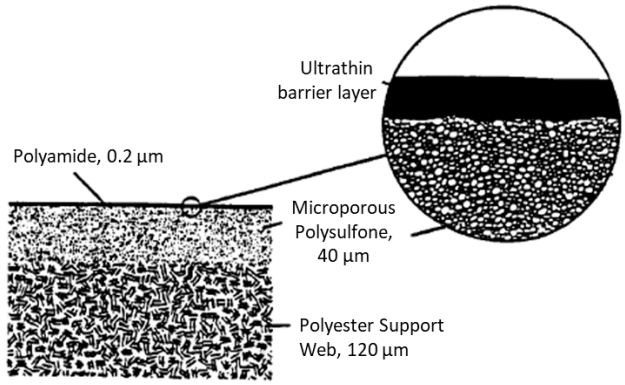

Figure 16: Hierarchical structure of an NF90 membrane; based on Tech Manual Excerpt ”FILMTEC Membranes” of DOW

The membrane is chemically resistant and exhibits free amines in the top layer as functional groups for an easy growth of other layers on top. On this basis a layer of the broadly researched zeolitic imidazolate 8 structure was grown using an in-situ method which will be explained later on. This structure, also called ZIF-8, is known for its thermal and chemical stability and is built out of Zn(II) and imidazolate linkers. It exhibits a pore aperture of 3.4Å and the diameter of the cavity inside the structure is 11.6Å. This shape ensures on one hand the effect of dehydration and rehydration. On the other hand, the small aperture enhances selectivity, and the big cavity leads to a high permeability. The topology of ZIF structures is based on Zeolite structures which consist of tetrahedral $Si(Al)O_4$ that are covalently bond by O atoms. The ZIF structure involves ZnN_4 tetrahedra that are bond by imidazolate (IM). The angle that arises in the M-IM-M form is similar to the one of Si-O-Si in Zeolites, which is close to 145°. Having this shape, it mimics the open framework of zeolites with many possibilities of tailoring. ZIF-8's porous structure is very symmetrical which broadens its application possibilities. This structure can be seen in Figure 17a. On the right picture the biggest cavity is represented by a yellow bubble which has a diameter of 11.6 Å for ZIF-8. The left and middle picture confirms that the structure is well ordered and that the pore size distribution should be narrow. Unlike other metal organic frameworks, ZIF structures also possess good chemical stability in water and alkaline solutions. [52]

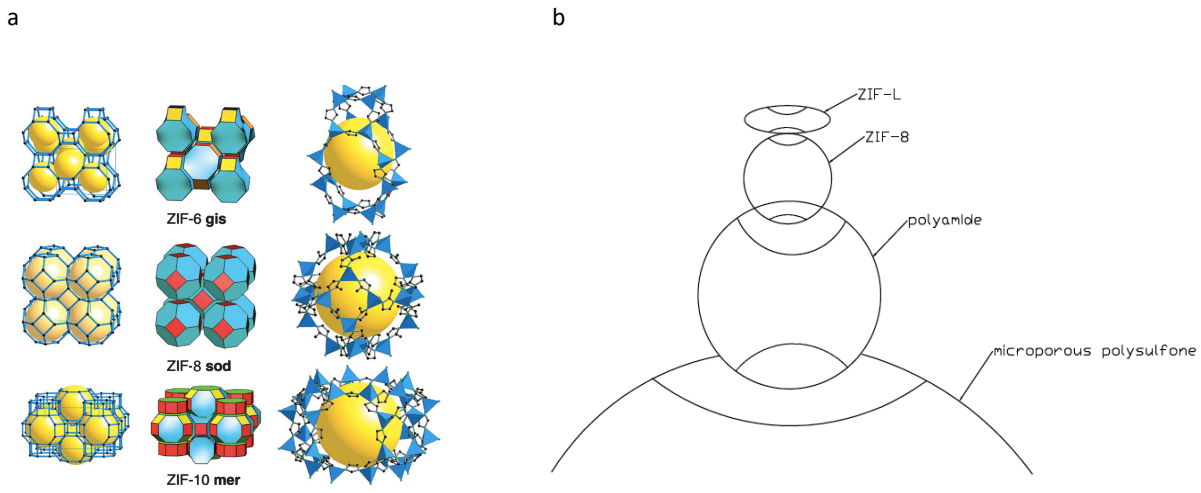

Figure 17: a. different ZIF structures with ZIF-8 in the middle. ZnN_4 tetrahedra are in blue (right picture) and are bond by IM molecules, the yellow sphere indicates the cavity; copied from [52] b. hierarchical structure of pore after growth of ZIF-8 and ZIF-L on NF90

To reach higher selectivity and to stay in a pyramid-shaped order, a layer with an even smaller cavity size was grown on top of the ZIF-8 layer. The structure this layer is formed of is called ZIF-L and exhibits a six-membered ring, like ZIF-8. This ring has an aperture of 3.4 Å and the structure has a cushion shaped cavity with dimensions of 9.4 Å x 7.0 Å x 5.3 Å which results in a cavity volume that is less than half of the one in ZIF-8. The result of putting a layer of this structure on top of the assembled membrane is a pore with a hierarchical shape to mimic biological ion channels. (Figure 17b) The structure of ZIF-L is anisotropic and can have two crystallographic orientations depending on the growing method. Like ZIF-8, ZIF-L consists out

of inorganic ZnN_4 tetrahedra that are bond by organic imidazolates. The crystals are two dimensional and leaf shaped. Part of this two-dimensional structure is a 6-membered ring which is known for the sodalite topology and can be found also in ZIF-8. The cushion shaped cavity is found between the layers of the 2D structures. As ZIF-L exhibits the same 6-membered ring as ZIF-8, the first layer of ZIF-L can perfectly form on the ZIF-8 layer. (Figure 18) The next layers of ZIF-L will grow on top of the first one and therefore a cushion shaped cavity will arise between the layers.

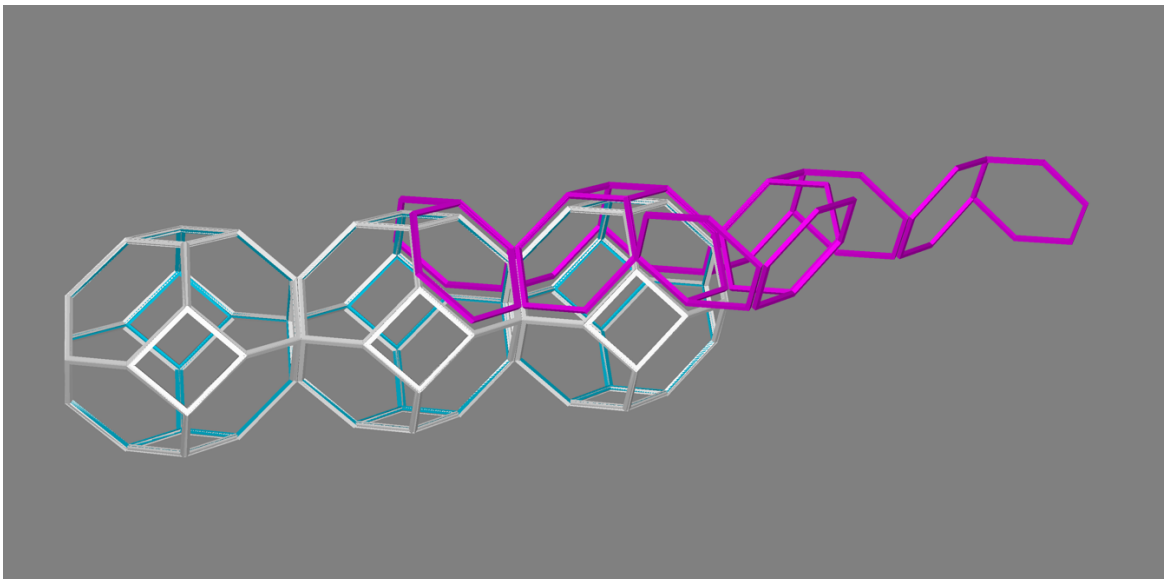

Figure 18: ZIF-L layer grown on top of ZIF-8; ZIF-8 layer in grey and blue and c-oriented ZIF-L layer in pink

Depending on the growing method, ZIF-L layers can be either c-orientated, where the leaf-shaped crystals are parallel to the support layer, or b-orientated, where they are orthogonal to it (Figure 19). Zhong et al. [53] found out that c-oriented layers on support membranes result in higher ideal selectivities for gas separation over b-oriented ones. They obtained a layer of the latter one by dipping alumina support in a seeding solution, letting it dry and then placing it in a beaker with the same solution. The first step placed seeds on the support where an oriented layer of vertical ZIF-L structures could grow on in the second step. For a c-oriented layer, the group prepared ZIF-L crystals by repeated centrifugation, dissolved these crystals in a PEI solution and vacuum filtered it on an alumina support. To obtain a continuous layer of these parallel ZIF-L structures, secondary growth was performed for a small period of time. The authors found out that randomly oriented seeds always lead to b-oriented ZIF-L layers. They explain it by the evolutionary selection model, also called van der Drift growth. The factor that is determining the crystallographic preferred orientation (CPO) is how fast the crystals are growing into its three dimensions. The dimension that is growing the fastest needs the most space. This is why the leaf shaped ZIF-L crystals either already grow perpendicular to the alumina support or eventually ‘stand up’ to obtain sufficient space to grow.

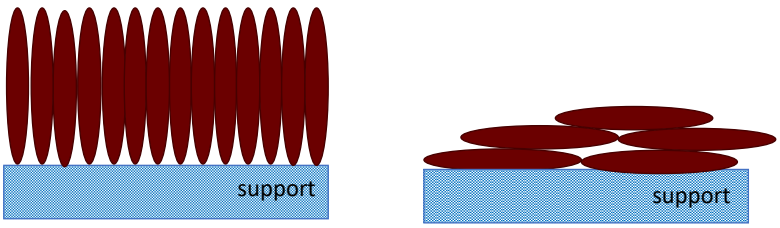

b-oriented c-oriented

Figure 19: ZIF-L layers with different crystallographic preferred orientations

3.7 Characterization

The successful growth of layers of metal organic frameworks can be determined by several characterization methods. In this work, a scanning electron microscope (SEM and SEM/EDS), X-ray diffraction (XRD) and a Fourier transform infrared spectrometer (FTIR) were used. Those methods will be shortly explained in the following.

3.7.1 Scanning electron microscope (SEM)

A scanning electron microscope produces images of samples by scanning its surface with a highly energetic beam of electrons in a raster scan. When electrons of the beam reach the sample, they excite it which leads secondary electrons to emit from the specimen and the electrons from the beam to be backscattered elastically. [54] Both, the low energy secondary electrons and the high energy back scattered electrons (BSE) produce the image. The intensity of those beams is characteristic for the part of the sample surface where the beam hit. The specimen also emits characteristic X-rays which provide information over its elemental composition. If the microscope includes X-ray detectors this information can be provided in different forms (chemical mapping, for example) which is called Energy Dispersive X-ray Spectroscopy (EDS). For sharp imaging the sample needs to be conductive which can be achieved by metallic coating. Also, there should be no moisture in the chamber. The beam hits the sample in a high vacuum. Figure 20 shows the way of an electron beam from the gun to the specimen. The electron beam that is produced by the electron gun is focused by magnetic lenses and directed on the specimen. Different detectors collect the secondary electrons and the backscattered ones and lead their information to a software for evaluation which gives the picture. Higher resolution of the images can be achieved by transmission electron microscopy (TEM) where transmitted electrons through the sample are looked at. For enhancement of the images SEM and TEM can be combined. By using this microscope, information about the morphology, meaning the shape and material distribution on the surface, the topography meaning quantitative measurements and the chemical composition can be revealed.

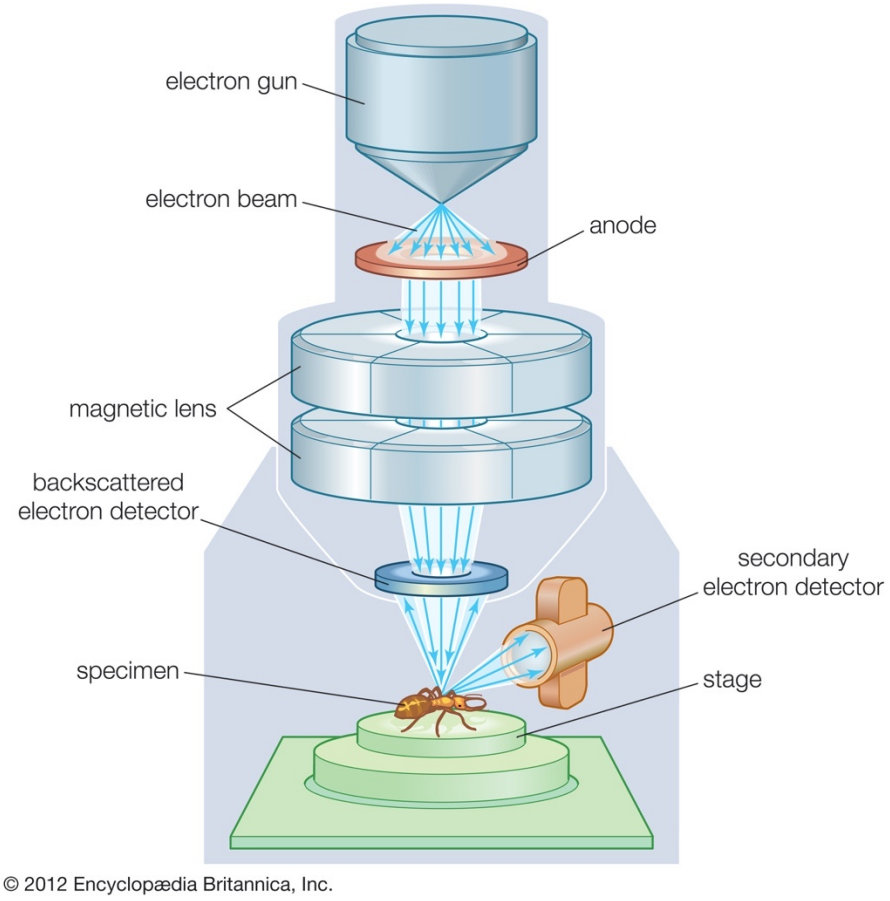

Figure 20: Operating mode of a scanning electron microscope [55]

3.7.2 X-Ray Diffraction

X-Ray diffraction is an analyzation technique that can provide information about the crystallographic structure and the chemical composition of a material. [56] A beam of X-ray hits the sample in different angles and gets scattered back. The intensity of the outcome gives a peak which is characteristic for the crystallographic structure of the material and is due to an interference of backscattered X-rays. The interference can be constructive or destructive resulting in an increase or decrease of the backscattered wave's amplitude. This phenomenon was first observed by physicist Bragg and his son. They found a relation between the X-ray beam's wavelength and the distance between atomic layers in crystals. Bragg's law is explained by the following formula:

$$n\lambda = 2d\ sin\Theta$$

Where λ describes the wavelength of the X-ray beam, n is an integer, d is the distance between the atomic layers in the crystal structure of the material and Θ is the angle at which the beam hits the sample. (Figure 21)

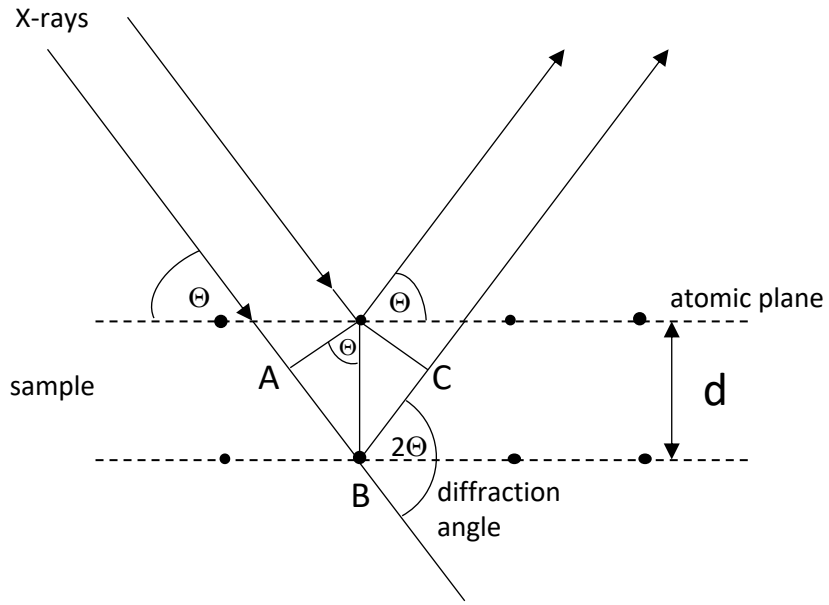

Figure 21: visualization of Bragg's law

Constructive interference only occurs when the distance AB+BC is a multiple of the X-ray's wavelength. As AB and BC have the same length, this condition can be described as follows:

$$n\lambda = 2AB$$

The distance AB can be expressed by the angle at which the beam hits the sample using trigonometry:

$$sin\Theta = \frac{AB}{d}$$

Combining those two formulas results in Bragg's law which describes interferences of rays that were scattered from a crystal which is called X-ray diffraction. When the incident beam hits the structure of the sample, it gets diffracted. All the diffracted beams that result from this interfere with each other and give a peak in the pattern that is characteristic for the angle of the incident beam and the crystallographic dimensions in the sample's plane. XRD can determine lattice constants using Braggs law and the right angle for the structure's plane. Each angle looks at a different plane in the crystal's structure. There are given XRD patterns (diffraction data) for a lot of crystallographic structures of different materials characterized by the International Center for Diffraction Data (ICDD). When comparing these patterns with a new pattern one can find the chemical composition of a new material. Each substance is characterized by its three strongest lines. Next to the peak's position, also the peak width and intensity are important for interpretation of patterns for example to find out grain size, phase composition and preferred orientation. As a typical XRD pattern consists out of peaks on different 2Θ

positions, the incident beam has to hit the sample in different angles. This is achieved by rotating the sample (or the X-ray tube) and the detector. (Figure 22).

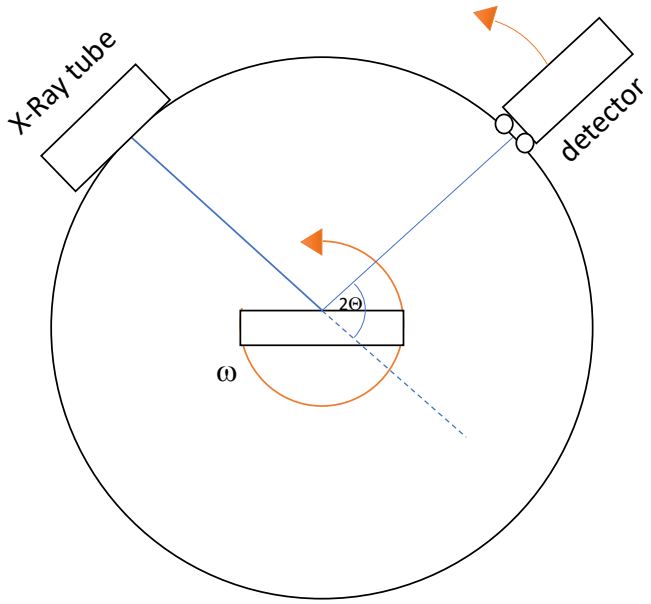

Figure 22: schematic of an X-ray diffraction, based on [57]

3.7.3 Fourier transform infrared spectroscopy

FTIR is a technique to identify a material's chemical composition especially its functional groups. [58] It is based on the fact that bonds in molecules can absorb light in the infrared range which results in a vibrance of the molecules. How much and at which wavelength the radiation gets absorbed, depends on the bonds between the molecules. The result of a characterization using FTIR is a spectrum where the level of absorption (absorbance) or the percentage of transmittance (%) is shown against the wavenumber (cm^{-1}). Transmittance and absorbance are mathematically proportional and can be converted by a FTIR software.

This characterization method only works for molecules that contain at least one dipole moment which makes this molecule "IR-active". When a particular radiation hits the bond, energy can be absorbed, and it starts back and forth oscillation. Every bond has its own natural vibrational frequency and can absorb radiation in the same frequency. This is why the percentage of the radiation (with a particular wavelength) which is let through the material (transmittance) or the absorbance is characteristic for the bonds that are present in this material. The absorbance is calculated by the following formula

$$A = \log \frac{I_0}{I}$$

Where I_0 stands for the intensity in the background spectrum and I for the intensity in the sample spectrum. When the radiation with a specific wavelength does not get absorbed, the intensity of the electromagnetic radiation in the background spectrum is the same as the one in the sample spectrum. I_0/I gets a value of 1 resulting in an absorbance of 0. Through Beer's

law, the absorbance is related to the concentration of a molecule in the sample which makes it possible to determine chemical compositions of samples.

When electromagnetic radiation in the right range hits material, electrons of this material will be excited and change their position from a lower energetic orbital to a higher one which is not occupied yet. This is called a transition. Infrared radiation does not contain enough energy to induce transitions in molecules, however, it can cause the bonds in molecules to vibrate in different ways, like mostly stretching and bending (Figure 23).

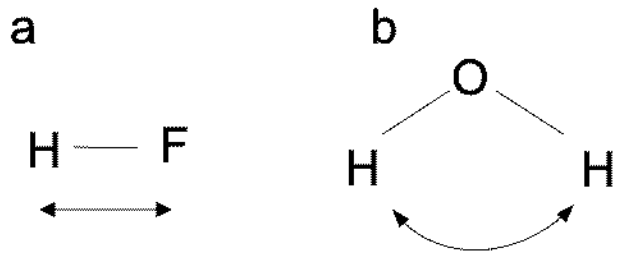

Figure 23: a. stretching vibration in a diatomic linear molecule, b. bending vibration in a triatomic molecule; based on [58]

As said before, only radiation that has the same frequency as the natural vibrational frequency of the molecule can be absorbed which increases the amplitude of the vibration in the molecule. Covalent bonds, which are the most common in organic molecules are always agitating at room temperature. If and how much of the radiation will get absorbed and therefore how strong the vibration will be depending on the polarity (strength of the dipole moment) of the molecule.

As each bond gets activated by different IR radiations, the sample has to be illuminated by a lot of radiations with different wavelengths. This tedious process was eased by the Fourier transform. Here, the sample gets hit by a burst of energy and each bond obtains its characteristic IR-radiation. Radiation in the range of 4000 – 600 cm^{-1} is typically used. These wavenumbers are directly related to the radiation's energy which makes interpretation easier than when wavelengths would be used. The result is an interferogram, a signal against time, which gets converted into an absorbance versus wavenumber spectrum by the Fourier transform algorithm.

An FTIR consists out of a light source, a Michelson interferometer, a sample chamber, a detector and an amplifier and computer (Figure 24).

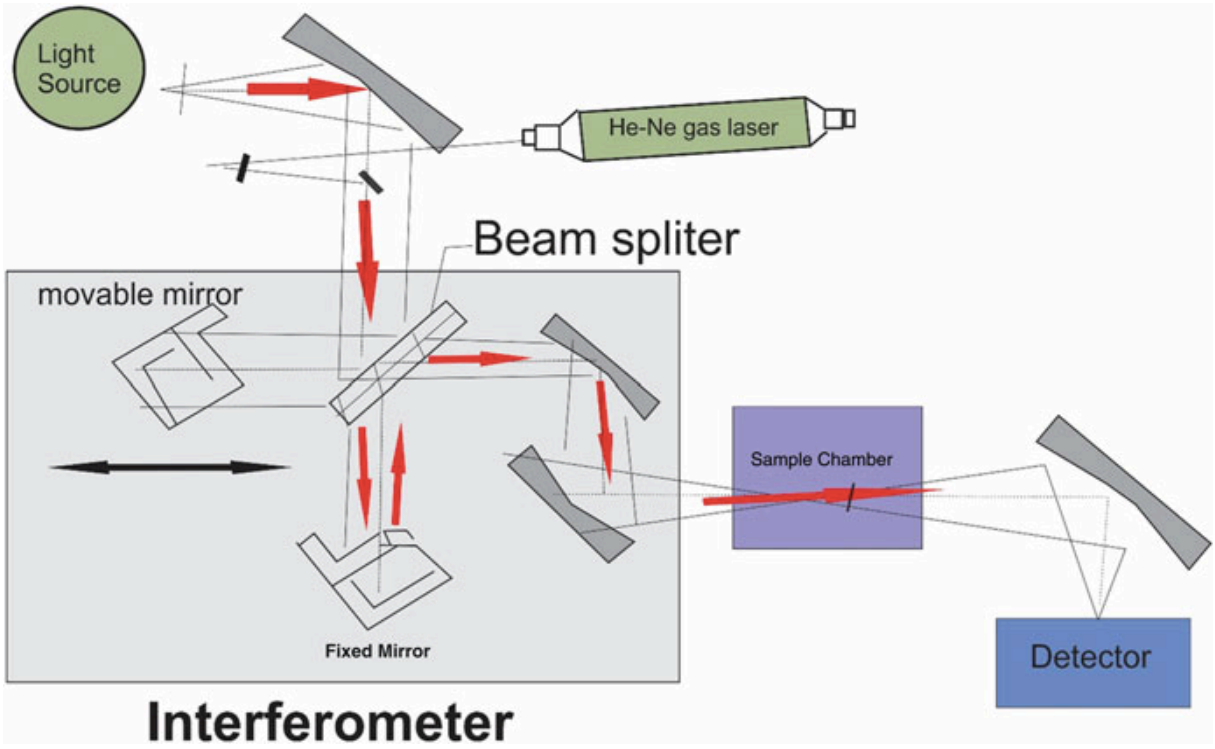

Figure 24: instrumentation of an FTIR; copied from [58]

Radiation from the light source passes through the interferometer, interacts with the sample and is afterwards detected. This analogue signal is amplified and converted into a digital one. This signal, which is called interferogram, is a signal of absorbance against optical path difference and is transformed into a wavenumber-spectrum using Fourier transformation. In the Michelson-Interferometer, the radiation gets split into two beams that are led to two mirrors and get recombined again at the splitter after reflexion at the mirrors. One mirror moves and creates different degrees of interference in the recombined beam that leaves the beam splitter for the sample chamber. The difference in the distance between beam splitter and the two mirrors is called optical path difference. As the mirror moves with a certain velocity, it is also possible to receive a signal against time. The way how interference works is explained in chapter 3.7.2. When the mirrors are at the same distance from the beam splitter, the signal will have its highest intensity due to constructive interference and is called centerburst. Moving one mirror will dim the light intensity due to the different phases of the beams. When the distance is at a multiple of the wavelength, the higher intensity will be gained back. This light intensity is measured and superposition of all the intensities from the different wave lengths results in the interferogram. Important to notice is that also an interferometer without a sample exhibits characteristic bands. Those are due to atmospheric molecules like water vapor or carbon dioxide. Therefore, it is indispensable to run a background spectrum when analysing using FTIR. The resulting spectrum only then includes the netto-absorbance that comes from the sample. Samples can be either prepared and placed into a cell or a holder or, more often, run in ATR (attenuated total reflection) mode. At this mode, the sample can be placed on the crystal without any preparation which eases the application. The beam from the interferometer

hits the crystal in an 45° angle and gets totally reflected due to the crystal's high refractive index (Figure 25).

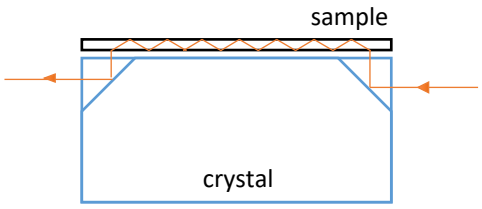

Figure 25: simplified mode of operation of an ATR crystal

The reflected beam reaches the crystal-sample interface and creates an evanescent wave that reaches to the sample and penetrates it. This wave is attenuated in those spectral regions where the sample absorbs energy. After some reflections this wave leaves the crystal for the detector.

3.8 Performance tests

As electrodialysis represents technically and economically a good method to extract Lithium out of brine [59], performance tests of the prepared membrane were done via linear sweep voltammetry and impedance measurements.

3.8.1 Linear sweep voltammetry (LSV)

LSV is a method to study electron transfer kinetics and transport properties of electrodialysis processes. It is executed by two electrodes that are submerged in an electrolyte. Depending on what is analysed, an electron transferring reaction could take place in the electrolyte. This could be $Fe^{3+} + e^- \rightarrow Fe^{2+}$. Through an electrochemical workstation, for example, a potential range is employed between the two electrodes. This means that the potential changes with time from a fixed low level to a fixed high level. A voltage scan rate can be defined which described how fast the potential changes and thus how fast the potential range is swept. The easiest way to describe electron transfer is by calculating the electrical current, which's definition is electron transfer. As voltage is bond to current via the ohmic law, the result of a LSV can be shown in a voltage – current plot. Out of this plot, the current of electrons at a special voltage can be defined. The flux of anions and cations is proportional to the current which makes this method meaningful for the analysis of ion flow through a membrane. The result of linear sweep voltammetry, the voltammogram, can have different forms depending on the rate of the reaction that is transferring the electrons, the reactivity of the reactants and the voltage scan rate. If the scan rate is low, the diffusion layer above the electrode will be much thicker than at high scan rate. A low scan rate therefore results in a smaller flux. If the reaction is fast compared to the scan rate, the equilibrium will always arise at the same voltage regardless of the scan rate. If the reaction kinetics are slow, however, the equilibrium will be only reached at higher voltages for slower scan rates. This is because here the current takes time to respond to the applied voltage.

In this work there was no reaction that needed to be analysed. The matter of analyzation was the transport of ions through a membrane. Thus, the membrane was separating two chambers containing the electrolyte and served as a resistance for the ion flow from one chamber to the other. Using electrochemical impedance spectroscopy, the resistance the membrane represents to the ion flow can be analysed.

4 Methods of fabrication, characterization and performance

The researched membrane that exhibits a hierarchical pore structure was fabricated by growing two ZIF layers using an in-situ growth method. For the application of this method, a PDMS mould was fabricated. A defect-free ZIF-8 layer is only possible due to the sufficient functional groups (free amines) the chosen base membrane exhibits. The layers of the membrane were characterized afterwards using scanning electron microscopy (SEM), X-ray diffraction (XRD) and Fourier Transform infrared spectroscopy (FTIR). Membranes with defect-free layers were then tested on their performance for Li-ion extraction using linear sweep voltammetry on an electrochemical workstation. To strengthen the performance findings, also an impedance measurement could have been done which is not the case in this work due to time limits induced by a worldwide pandemic that was in its beginnings while this work was done.

4.1 Materials

As base or support, the commercial membrane NF90 was used. Its properties are explained in chapter 3.6. Next to that, all used chemicals were purchased from Sigma-Aldrich and not further purified. Milli-Q water was used as buffer and produced by the Milli-Q IQ 7000 Ultrapure Lab Water System (Merck Millipore).

The used chemicals include:

- Zinc nitrate hexahydrate ($Zn(NO_3)_2*6H_2O$)
- 2-methylimidazole (HMIM, $CH_3C_3H_2N_2H$)
- Polydimethylsiloxane (PDMS)

4.2 Fabrication of PDMS mould

To create borders in between which the ZIF layers can grow, a PDMS template was fabricated. To do so, the Sylgard 184 silicone elastomer kit was used. Nine parts of silicone and one part of hardener were mixed and poured into a flat glass bowl. This was moved into a vacuum oven at room temperature to remove air bubbles. It was then left inside to oven for another 40 minutes at 78°C for hardening. After that, it could be moved out of the glass bowl using a cutter which also was used to cut openings into the mould to receive the borders for the in-situ growth. (Figure 26) The mould was then ready to be used. This mould has the advantage that it sticks to glass as well as to membrane pieces. It represents a practical way to grow different layers simultaneously without wasting time and space. The voids in the mould each have a volume of approximately 2.5ml.

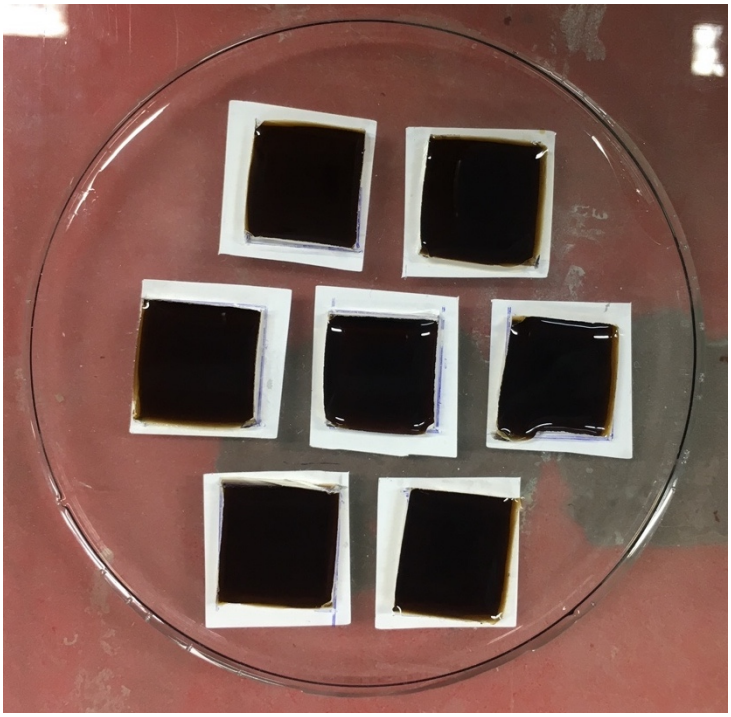

Figure 26: PDMS mould sticking on a glass plate with membrane underneath and black liquid in cut voids

4.3 Synthesis of ZIF-8 layer

For the ZIF-8 layer a precursor solution was prepared following a method done by Mohammad et al. [60]. To receive 2.5ml of the solution, 0.0068g of $Zn(NO_3)_2$*$6H_2O$ were mixed with 0.25ml of Milli-Q water and 0.1415g of HMIM were mixed with 2.25ml of water. When both the chemicals were completely dissolved, they were mixed together using a pipette and then transferred into a void of the PDMS mould on top of a sheet of an NF90 membrane. To enhance the dissolving process the measuring vials are put into a sonicator water bath which is activated for less than a second. After an exposure time of 30 minutes, the solution is removed from the template and the layer is washed with Milli-Q water using a pipette.

4.4 Synthesis of ZIF-L layer

Like the Zeolitic imidazolate 8, ZIF-L consists out of $Zn(NO_3)_2$*6H2O as metal ion and 2-Methylimidazole (HMIM) as ligand. To find the most appropriate ratio and concentration for an ion separation application, different recipes were found in literature and tested. The following table shows the recipes that were used in the synthesis experiments.

Table 3: Recipes for Zeolitic Imidazolate L

Nr	$Zn(NO_3)_2*6H_2O$		2-Methylimidazole		Ratio	Exposure time	Reference
	amount	concentration	amount	concentration	molar		
1	1mL	0.5M	10mL	0.8M	1:16	30mins	[61]
2	1mL	0.25M	10mL	0.4M	1:16	30mins /1h	
3	10mL	0.1M	20mL	0.4M	1:8	60min	[62]

The mixing procedure is the same as at the ZIF-8 layer. About 10% of the total Milli-Q water amount were used to dissolve the zinc nitrate hexahydrate and the rest to dissolve the HMIM. Before mixing and pipetting into the template, it is important that the ZIF-8 layer on NF90 is dry.

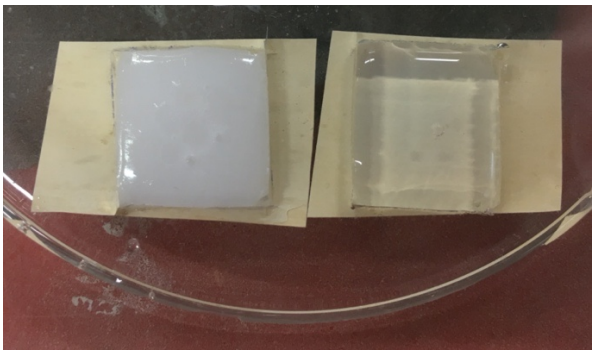

Figure 27: ZIF-L layers (recipe 1 and 2) on ZIF-8 layers on NF90 in PDMS template

As to be seen in Figure 27, the solution on the left side got turbid earlier than the one on the right side which can be linked to the higher concentration of the metal ion and ligand solution. It could be that in the left solution, crystals already form in the solution which would hinder a defect-free layer growth. Which of the recipes results in the best layer is to be seen in the results section.

4.5 Method to receive cross-section images

To be able to interpret performance results properly, it is also important to know how thick the two MOF layers on top of the NF90 membrane are. With this information it is possible to predict the influence the thickness of the membrane has to its performance. Therefore, a picture of the cross-section of the membrane is inevitable. To get a cross-section, an easy method was used. The prepared membrane was put into a bath of liquid nitrogen to freeze it and make it

brittle. The brittle membranes were either broken or cut and a cross-section was obtained. It is important to make the membrane brittle first to receive a sharp edge at the line of breakage. These specimens are then put onto a special arrangement (Figure 28) where they can be analysed in the scanning electron microscope.

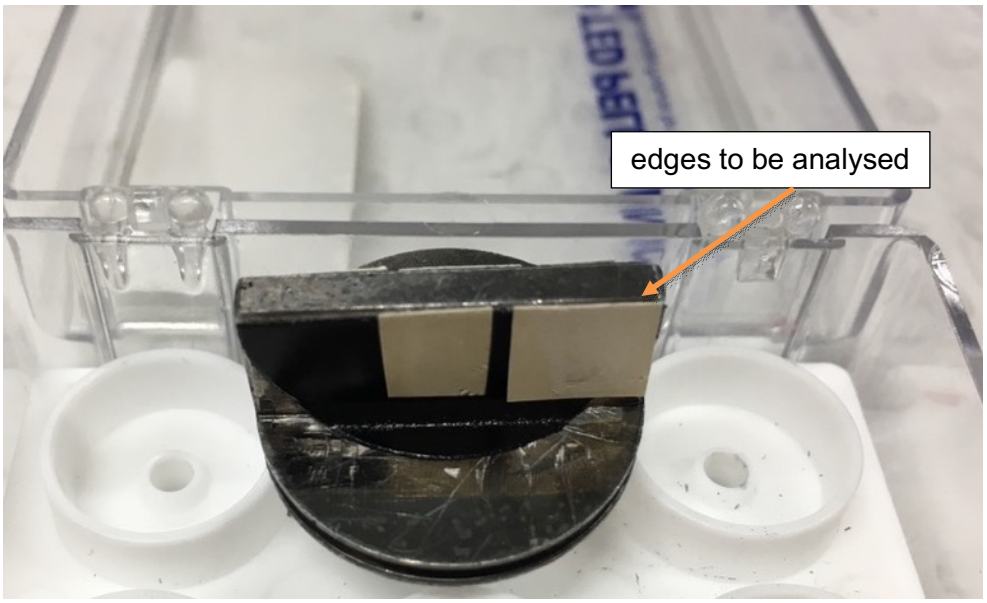

Figure 28: arrangement for cross-section analyzation

4.6 Characterization methods

To characterize the fabricated membranes concerning their morphology, chemical composition, the degree of defects and the thickness of the layers several methods were used. Their principle is explained in chapter 3.7 – in the following special probe preparation and how these methods were used will be explained.

4.6.1 Working with scanning electron microscope

Prior to characterization, the samples need to be sticked on a holder that is especially made for the SEM, like that in Figure 28. It is important to know the exact arrangement of the different samples also when the holder is turned. Therefore, if possible, different sizes of the samples should be cut out or a special arrangement should be chosen. After placement, the holder including the samples needs to get a metallic coating to make the whole specimen conductive which is important for sharp imaging. This was achieved by sputter coating a 10nm platinum layer under vacuum using the K575x Pt sputter coater. Then, the holder was put into the field-emission scanning electron microscope (FE-SEM) NanoSEM 230 and the sample was analysed at 5kV under vacuum. Pictures of the different samples were taken at a magnification of 5000, 10 000 and 40 000. FE-SEM is a special scanning electron microscope where the

electrons emit from a field emission gun and scan the sample in a raster pattern. A picture of where the sample holder including the sample is put into the SEM is shown next.

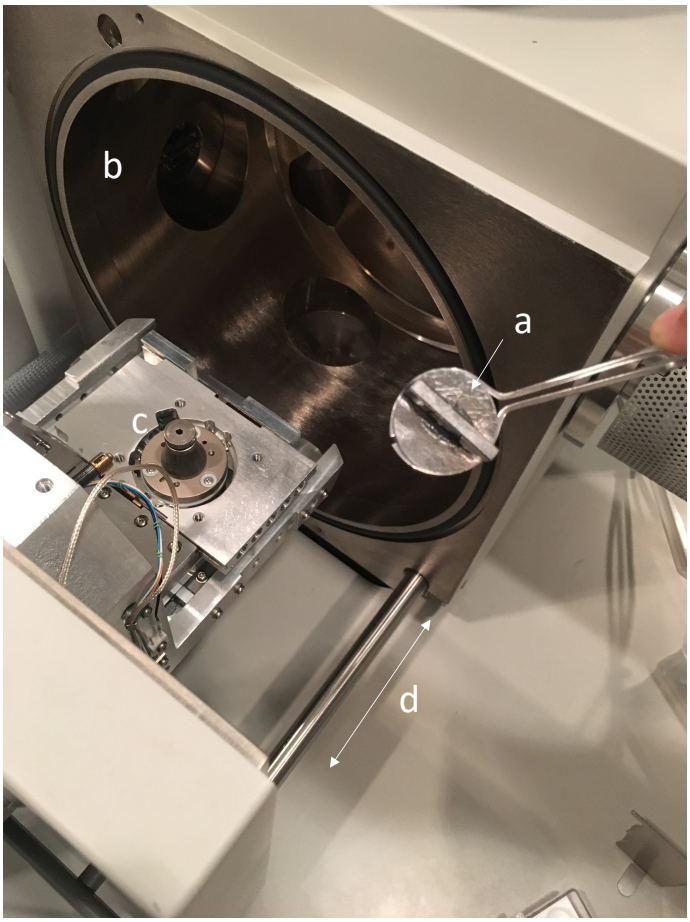

Figure 29: SEM sample chamber with a.) sample holder for cross-section analysations with sputter coated samples b.) vacuum chamber c.) stage for sample holder d.) mechanics to open and close the chamber

4.6.2 Working with X-Ray diffraction

To get crystallographic data from the ZIF8, the ZIFL and the ZIF8/ZIFL combination an XRD analyzation was done using Empyrean Thin-Film XRD Xpert Materials Research Diffractometer with 2 theta angles between 5 and 36° and a step size of 0.07 and 200 s per step. As the samples are not in a powdered state, sample preparation consists out of putting the samples as flat as possible on glass plates to receive a smooth and flat surface. For this step a two-sided sticky tape was used which might affected the received XRD pattern in a way of background scanning (discussed in chapter 5.1). Before starting the analyzation, a copper divergence slit is put in front of the X-ray source to vary the irradiated area in a way that it is never, meaning at no incident angle, bigger than the sample area. If it was bigger than the sample, it would lead to defects in the received pattern. Using a software, the scanning can now be started at the desired radian measure, step size and velocity.

4.6.3 Working with FT-IR

Fourier Transform Infrared spectroscopy was conducted to confirm the chemical composition of the layers in the fabricated membrane. The Alpha II FT-IR Spectrometer from Bruker was used in attenuated total reflection (ATR) mode for the analysis. In this mode, no sample preparation has to be done and therefore the membrane can be pressed on the ZnSe crystal for single reflection for wavenumbers between 400 and 4000 cm^{-1}.

4.7 Performance tests (ion current measurement)

To see if the fabricated membrane is selective to Lithium under specific voltage, linear sweep voltammetry (LSV) was conducted through it. For ions to pass through the channels in the membrane, those channels need to contain water which acts as a medium for the ion flow. As described in chapter 3.5.1 there should be two to three layers of water inside the channel for Lithium ions to be conducted. Therefore, the membrane was wetted by vacuum filtration using ethanol and Milli-Q water. The wetted membrane was then put into a container full of Milli-Q water for transportation. It was then placed into a permeation cell where it split two compartments. (Figure 30) Both of the compartments are filled with 40ml of the same ion solution using a pipette. The compartments were closed, and a silver/silver chloride (Ag/AgCl) electrode was put into the hole of the lid of each compartment.

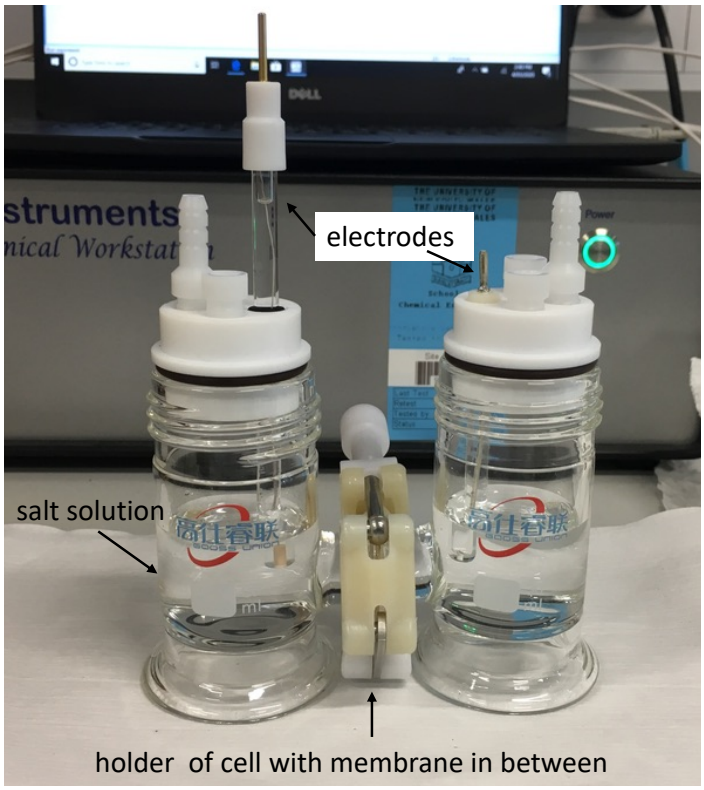

Figure 30: H-cell for performance test

The different salt solutions were:

- 1M LiCl
- 1M KCl
- 1M NaCl
- 1M $CaCl_2$
- 1 M $MgCl_2$

Then, cables of the electrical workstation were connected to the electrodes through which the potential was applied afterwards. Before the analysation the electrochemical technique LSV and a potential from -0.6 to 0.6V with a scanning rate of 0.001 V/s was chosen. After confirmation, the potential was applied between working electrode and counter electrode and the corresponding current was measured. To be sure that the instrument is correctly installed, the cables of the electrochemical workstation were connected to some known resistances and the result was compared to the one that is expected when calculating the current using Ohm's law. If that preliminary experiment turns out the expected way, the cables can be connected to the actual Ag/AgCl electrodes and the ion current measurement can be started. For this experiment, the electrochemical workstation CHI660e from CH instruments was used.

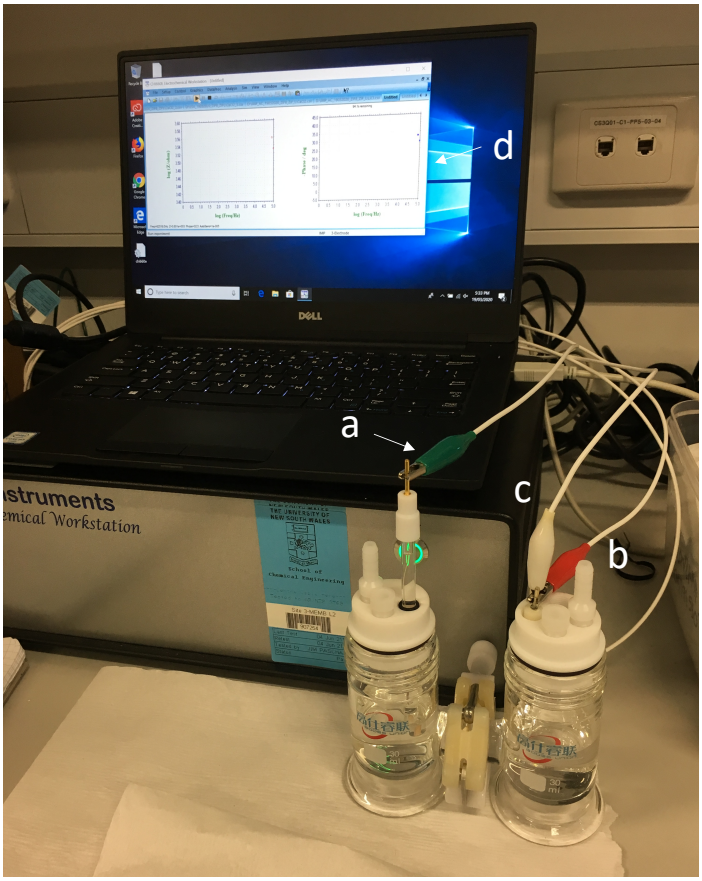

Figure 31: H-cell connected via a.) working electrode, b.) counter electrode and c.) reference electrode to electrochemical workstation which is connected to laptop showing d.) software for analysation

5 Results and Discussion

5.1 Surface characterization of the fabricated membrane

Scanning electron microscopy was used to ensure the ZIF-8 layers uniform structure and to select the most appropriate recipe for a ZIF-L layer that also has a uniform structure and no defects.

The recipe for ZIF–8 is well known among the research group of UNESCO Center for Membrane Science and Technology in which this work developed. Therefore, not a lot of characterisation was done regarding the ZIF-8 layer only as it is regarded as forming a continuous, flat layer with nearly no defects. This can be discovered in Figure 32 where, for a preliminary experiment, a ZIF-8 layer with encapsulated bio-functional molecules was grown onto a PP membrane. Polydopamine/Polyethyleneimine (PDA/PEI) served as an intermediate layer as PP does not exhibit enough functional groups for a continuous, flat MOF layer to grow on. Mohammad and co-workers [60] assured that the presence of a bio-functional molecule results in a rougher surface morphology than a layer without additional molecules. This being said leads to the assumption that later fabricated ZIF-8 layers, that were not regarded under SEM, have an even more uniform and flatter morphology than the one in Figure 32.

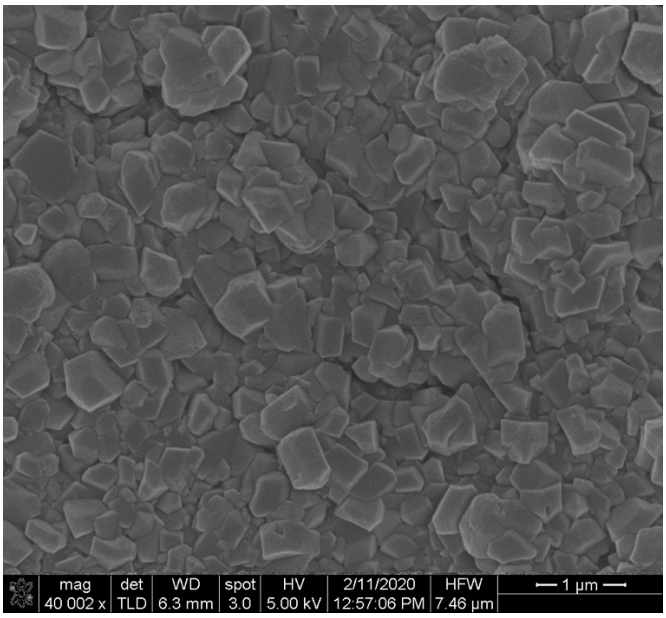

Figure 32: PP membrane with PDA layer and ZIF-8 layer on top

As described in chapter 4.4, three different recipes for the fabrication of ZIF-L layers were tried out to find the one that results in the most continuous and flattest layer with the smallest rate of defects. Also, we tried to think about aspects in the morphology that could enhance the separation of Lithium from other monovalent ions.

The first recipe (Table 3) exhibits a concentration of metal ions of 0.5mol/L and a concentration of ligands of 0.8mol/L. The molar ratio of metal ion to ligand is 1:16, which means that per one

mole of metal ions there is 16 moles of ligand molecules. Figure 33 shows a layer of ZIF-L where this recipe was used grown on a ZIF-8 layer on NF90. On the left (a.), it is clearly to be seen that the layer is very interconnected, nearly dense. This leads to the assumption that the layer on the bottom is c-oriented (see Figure 19 for crystallographic orientations) which results in very little possibilities of defects in the layer or holes. On the right, it is possible to recognize fully crystallized particles in leave- and floral-shape on top of the thin film. This makes the surface rough and inhomogeneous which is generally spoken not a wanted characteristic. However, if the layer is thicker, it could have a positive impact on the separation application.

a. b.

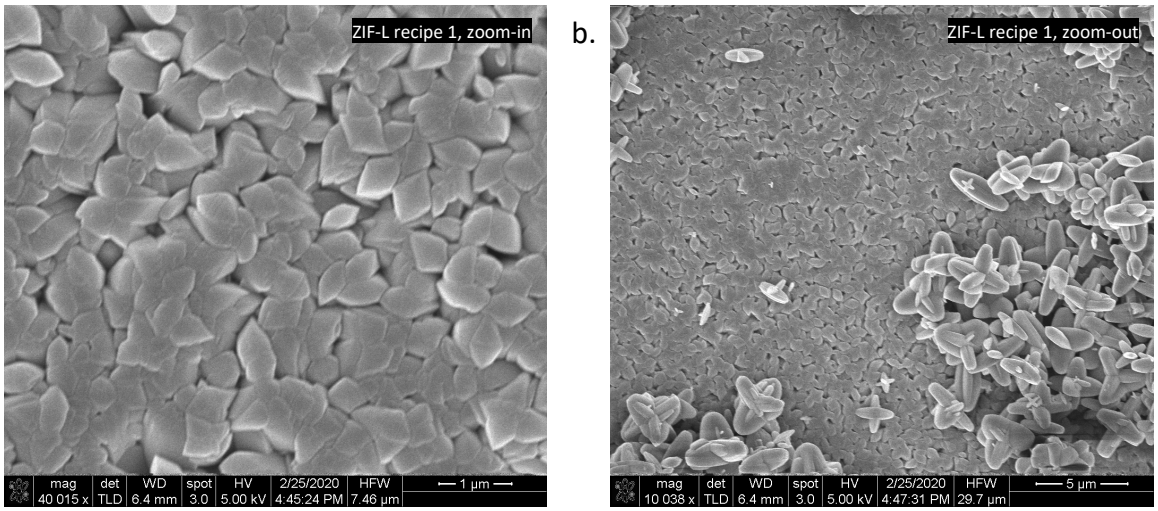

Figure 33: ZIF-L layer prepared from recipe 1 on top of ZIF-8 layer on NF90 support membrane; a. at magnification of 40 000, b. at magnification of 10 000

The second recipe was found by a member of the research group in which this work was developed and had the same amounts of solutions and half of the concentrations of recipe 1, meaning 0.25 mol/L and 0.4 mol/L for metal ions and ligands, respectively. Therefore, it also exhibits a molar ratio of 1:16. The results at a magnification of around 40 000 and 10 000 can be seen in Figure 34. Clearly, at these concentrations, the b-orientation is the crystallographic preferred one. Indeed, this leads to the thought that there could arise voids between the ZIF-L crystals in the layer more easily than at c-oriented layers, but as to be seen in a. the layer is very interconnected and it even seems like there are more layers on top of each other. In addition, this layer is totally homogenous throughout the surface, which can be seen in b. and which is an important characteristic for scale up purposes.

a. b.

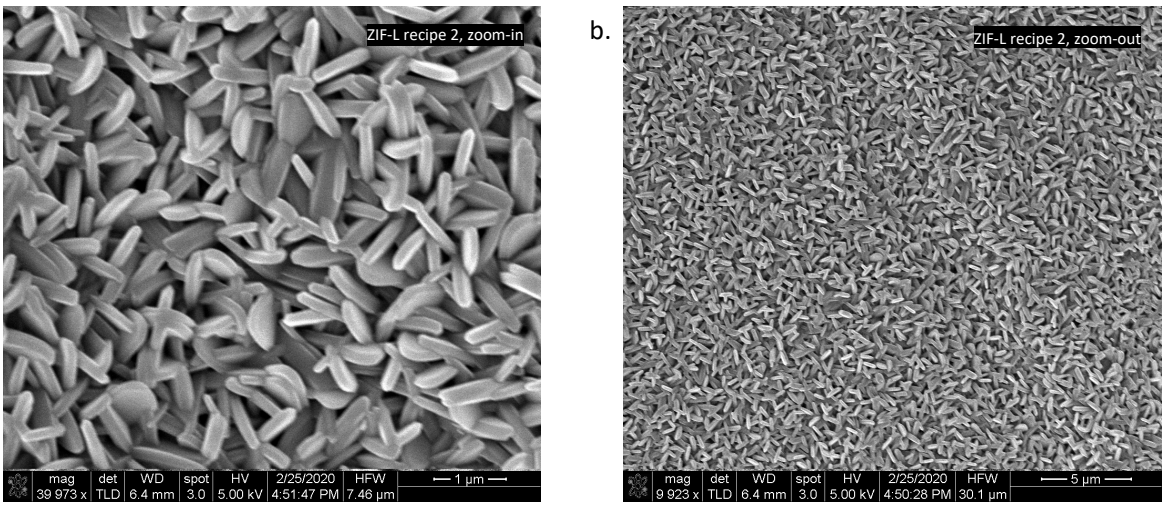

Figure 34: ZIF-L layer prepared from recipe 2 on top of ZIF-8 layer on NF90 support membrane; a. at magnification of 40 000, b. at magnification of 10 000

For the third recipe, the used solutions have a higher volume, but the ion concentration is lower. The molar ratio of metal ions to ligand molecules in the mixed precursor solution is 1:8. The exposure time was the double of recipe one and two, namely 60 minutes. This resulted in a layer that was not at all homogeneous (Figure 35) and had bigger ‘leaves’ of ZIF-L which is due to the higher exposure time of the precursor solution as stated in [62]. Also, there are parts that are not covered by the ZIF-L layer which leads to the assumption that instead of the growth of a layer of ZIF-L what might has happened is that some crystals were already built in the precursor solution and sedimented on the ZIF-8 layer. This results in an inhomogeneous surface which was not further investigated.

a. b.

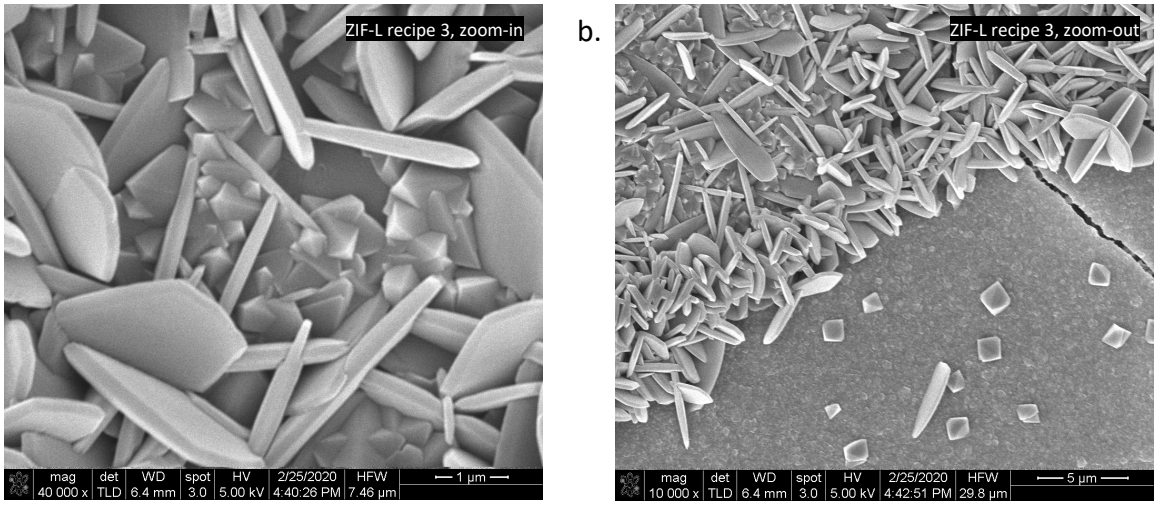

Figure 35: ZIF-L layer prepared from recipe 3 on top of ZIF-8 layer on NF90 support membrane; a. at magnification of 40 000, b. at magnification of 10 000

Looking at the results of all three recipes, it comes clear that an inhomogeneous layer with voids and areas where there are not both layer present, which is the case for recipe three, is

not appropriate for the application looked at in this work. The result of recipe one shows a very dense layer with no voids which is needed for a separation application. However, its inhomogeneous surface morphology due to crystals that might have grown already in the precursor solution, could lead to problems in scale up. Recipe two, however, shows results of a very intergrown, homogeneous and flat membrane, exhibiting important characteristics for application purposes. This is why it was chosen for further analysation.

The recipe that was chosen for further research exhibits a molar ratio of 1:16 with 0.25 mol/L and 0.4mol/L as concentrations for metal ions and ligands, respectively. The precursor solution stayed on the fabricated membrane for 30 minutes, was withdrawn using a pipette and afterwards washed with Milli-Q water.

As said before, to connect certain effects at the performance test to characteristics of the membrane, it is not only important to have an idea about the morphology and topology of the surface of the fabricated membrane, but also to know how thick all of the layers are that build up the membrane. To analyse the thickness and also the crystallographic orientation in the ZIF-L layer, a cross-section of the membrane was looked at under the scanning electron microscope. It was prepared as described in chapter 4.5. First, to get more insight into the structure of the commercial membrane NF90 and to find a characteristic that indicates where the top layer of NF90 ends, cross-section images of the commercial membrane only where taken. Figure 36 and Figure 37 show the results of this analysation where the hierarchical structure of NF90 can be clearly seen. The microporous polysulfone, which is on the right side of the picture, got bigger cavities than the polyamide layer that forms the last 0.2 µm of the membrane (in the middle of the picture). On the left image, it can be seen that from the edge of the cross-section (approximately in the middle of the picture) about 200 to 300nm to the right, the material is very dense and gets more porous in direction right edge of the image. This stands in accordance with the description of the commercial membrane in Figure 16, however, no sharp edge between those two layers is detectable.

a. b.

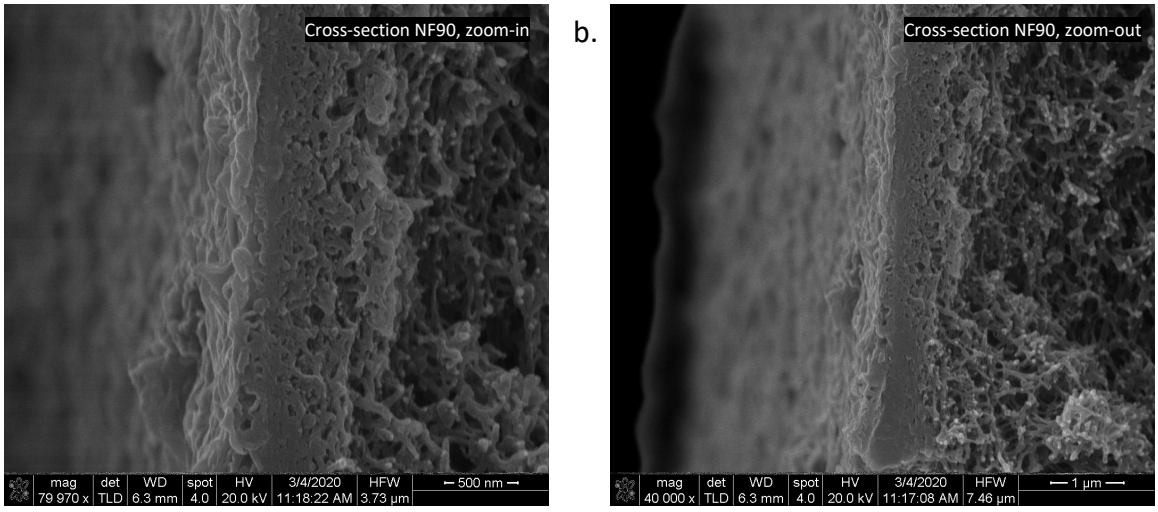

Figure 36: Cross-section images of top part of commercial membrane NF90 at a.) magnification of 80 000 and b.) magnification of 40 000

In Figure 37 also the polyester support web of the membrane which takes around 80% of the image can be seen. Clearly, this support which is on the base of the membrane got the biggest cavities which helps to build a hierarchical structure for an asymmetric pore.

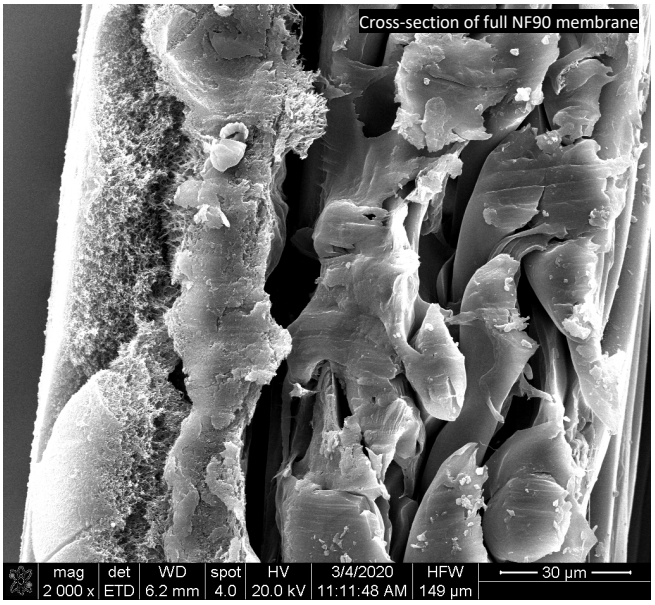

Figure 37: Cross-section image of commercial membrane NF90

After studying the support for the membrane, cross-sections of the membrane including a ZIF-8 layer and a ZIF-L layers were imaged. The ZIF-L layers that result from recipe one and two were analysed. Figure 38 shows the images of a membrane exhibiting a top layer that was fabricated from recipe one. Between the commercial membrane NF90 and the top layer, ZIF-L, there is a layer of ZIF-8. Both ZIF layers together exhibit a **thickness of 1.5 to 1.8 µm**. Although it is hard to distinct the exact border between the two layers, it is possible to identify a slight difference in shape of ZIF-L and ZIF-8. Clearly, both layers are very well interconnected.

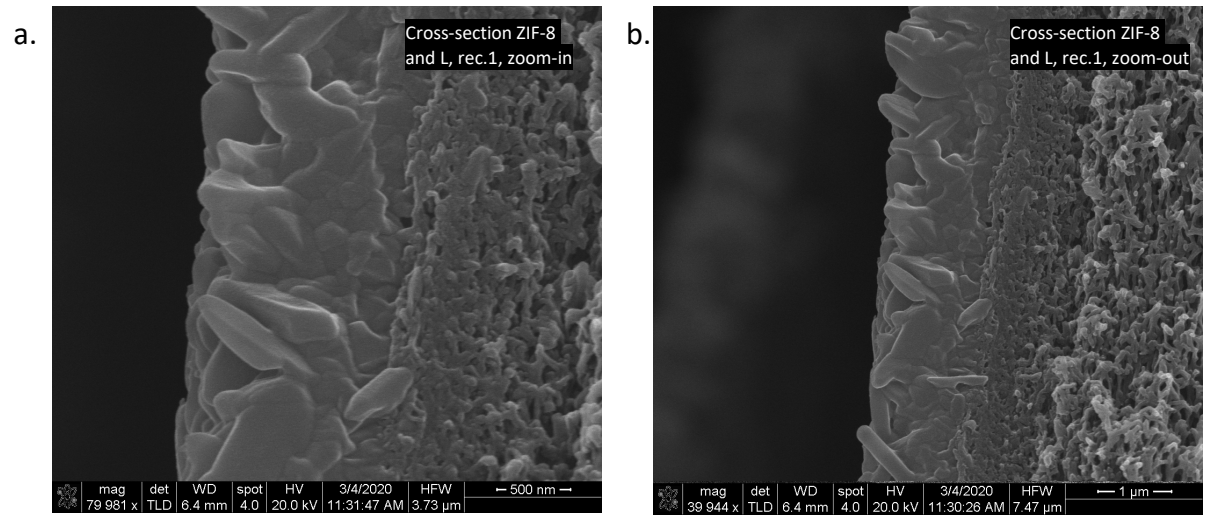

Figure 38: Cross-section images of top part of fabricated membrane using ZIF-L recipe 1 at a.) magnification of 80 000 and b.) magnification of 40 000

Figure 39 shows the fabricated membrane at a lower magnification where it is detectable that from the edge of the membrane (middle of the picture) to the right the density of the structure decreases whereas the pore size increases. This stands in agreement with the desired hierarchical structure of the asymmetric pore in the membrane.

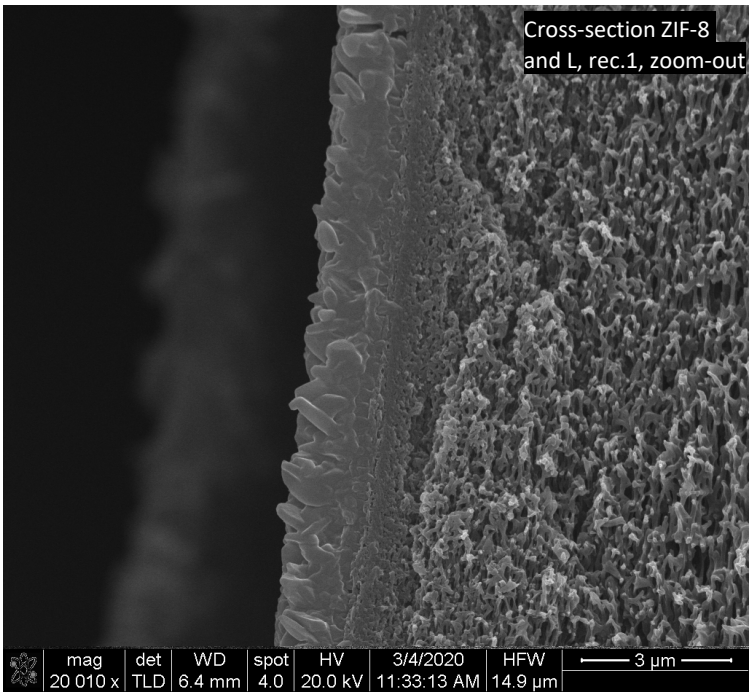

Figure 39: Cross-section image of fabricated membrane using ZIF-L recipe 1 at a magnification of 20 000

In comparison, at the results of the fabricated membrane using recipe two for the ZIF-L layer, a difference in the structure of ZIF-8 and ZIF-L crystals is not detectable which indicates that

the layers are very interconnected. (Figure 40) The ZIF layer containing ZIF-8 at the bottom and ZIF-L at the top is around **1.9µm thick** and it can be perceived that all ZIF-L molecules are homogeneously ordered perpendicular to the surface. This stands in accordance with the SEM picture that was taken in bird's eye view (Figure 34). Looking at the membrane at a lower magnification (Figure 41) indicates that the membrane has a homogeneous and flat surface which also confirms the hypothesis that was made at looking at the membrane in top view. The roughness that can be detected in the right half of the image can be attributed to problems at breaking/cutting the membrane under liquid nitrogen. However, also here, the hierarchical structure of the membrane from left to right in the image can be clearly identified. Combined with a homogeneous surface it seems promising for the ion separation application.

a.

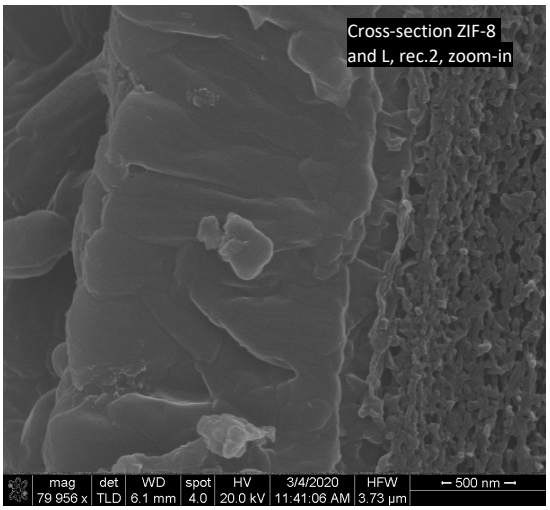

b.

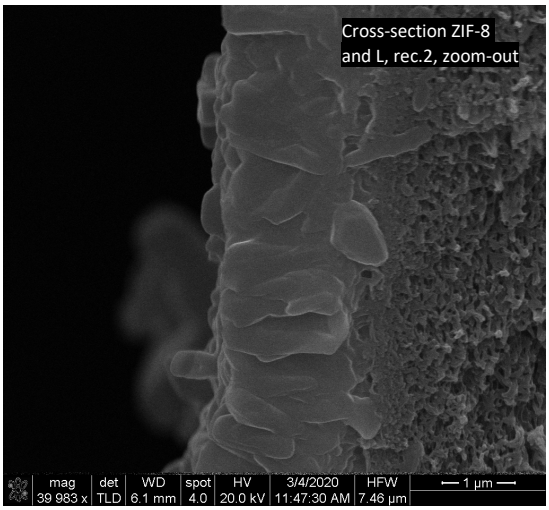

Figure 40: Cross-section images of top part of fabricated membrane using ZIF-L recipe 2 at a.) magnification of 80 000 and b.) magnification of 40 000

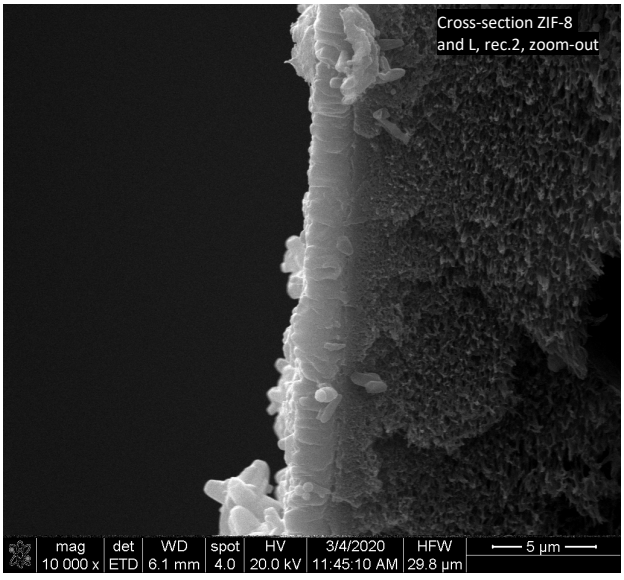

Figure 41: Cross-section image of fabricated membrane using ZIF-L recipe 2 at a magnification of 10 000

To assure the results that were received by the scanning electron microscope, analysations were also done using X-ray diffraction. This method can be used for crystallographic orientations analysation and chemical composition of a samples surface. Figure 42 shows XRD patterns of the support membrane only (blue), the membrane with a ZIF-8 and a ZIF-L layer using recipe one (red) and the membrane with a ZIF-8 and a ZIF-L layer using recipe two (green). Looking at the XRD pattern of Zhong et al. [53] confirms that the peaks between 10 and 12° and the peaks around 17° of the position are due to the ZIF-L on the top of the sample. They used the crystallographic preferred orientation (CPO) indexing method to determine the layers orientation and found out that the peak at around 11° represents the 020 plane which means that the ZIF-L crystals grow out of the plane, perpendicular to the surface. This stands in accordance with the assumption that the layer is mostly b-oriented. Recipe two got smaller peaks at the position between 10 and 12° which implicates the idea that the ZIF-L layer using this recipe is thinner. This could not be determined looking at the cross-section SEM images due to the high degree of intergrowth between the ZIF-8 and the ZIF-L layer. The peak at around 18° represents the 004 plane which means that also randomly oriented ZIF-L crystals exist in the layer. It could be that this is due to the little exposure time of the precursor solution on the membrane resulting in too little time for all the ZIF-L crystals to “stand up”.

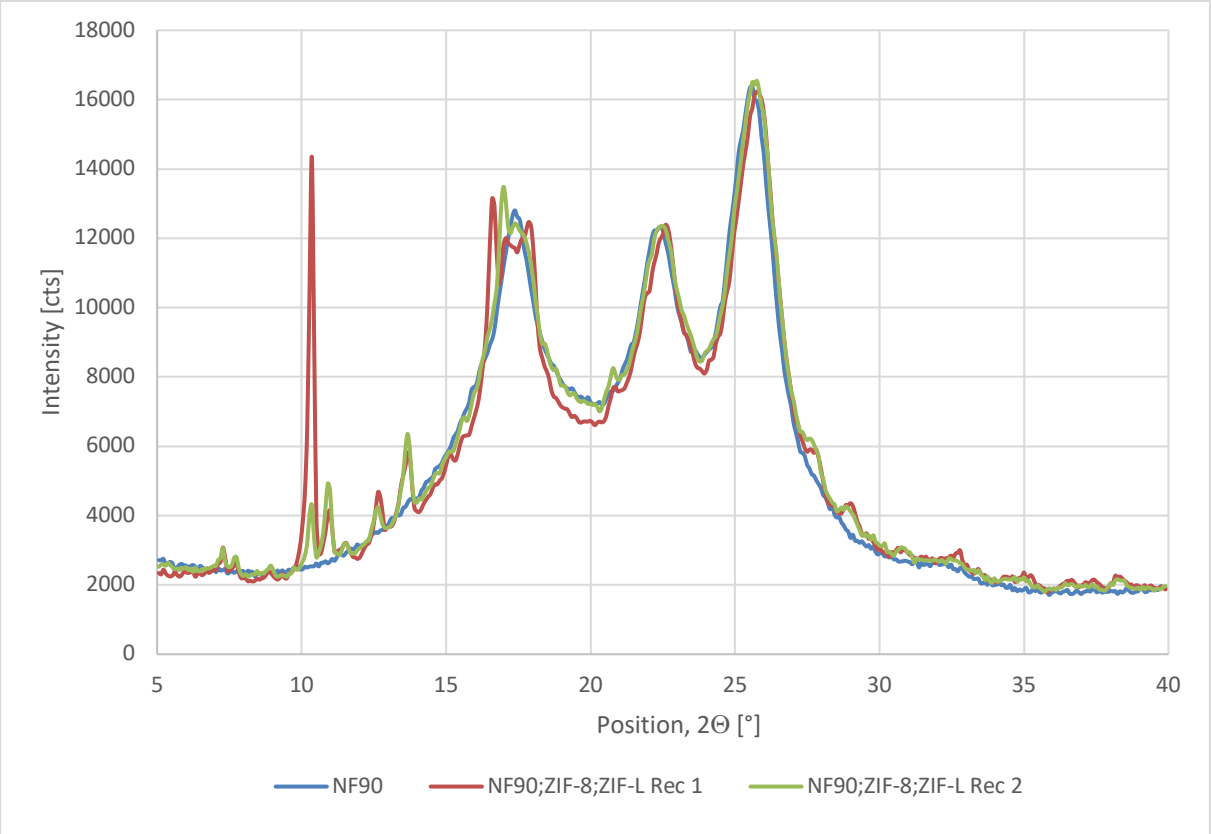

Figure 42: XRD patterns of fabricated membranes using recipe 1 and 2 for ZIF-L

Other peaks at positions lower than 20° are all due to the presence of ZIF-L on the surface, according to Zhong and co-workers [53]. Now that the highest peaks at the position of 10.3°

and around 17° could be allocated, the question to be addressed is where the peak at a position of 22.6° and 25.8° is coming from. Clearly, they do not come from a ZIF layer, as also the pattern of the NF90 only analyzation shows those peaks. It could be that the peak at 25.8 is due to the adhesive tape that was used to attach the samples on the glass plates. An XRD analyzation using only adhesive tape was done by another member of the research group and shows a peak at a position of 25.5°. However, the more promising explanation of those peaks in samples using recipe 1 and 2 is that the penetration is so deep that the X-rays get diffracted also by structures of NF90 which is underneath the ZIF-8 layer. Agboola et al.'s [63] work confirms that the peak at 22.6° and 25.8° is due to O12C96 and O18C36N18, respectively. Their NF90 pattern also got a peak around 17° which confirms the peak in the NF90 only pattern in Figure 42.

For further assurance of the chemical composition of the membrane, also FT-IR analysations were done with a sample containing ZIF-8 and ZIF-L. (Figure 43) As both of the layer consist of the same precursor solution and also exhibit some same bonds, it is possible to compare this result with a spectrum of ZIF-8 found in literature. Comparing this spectrum Liu et al.'s work [64], the absorption band at 3135cm^{-1} can be associated with a stretch in the C-H bond of the imidazole which functions as the ligand in both, ZIF-8 and ZIF-L. According to them the peak in absorption at 1579 cm^{-1} could be due to a stretch in the C=N double bond. They also observed bands in the region of 1100-1400 cm^{-1} which can be associated with a stretch in the C-N bond and the one at 420cm^{-1} to be ascribed to a stretch in the Zn-N bond. Therefore, the peaks in the spectrum confirm the presence of the bonds that are characteristic for ZIF-8.

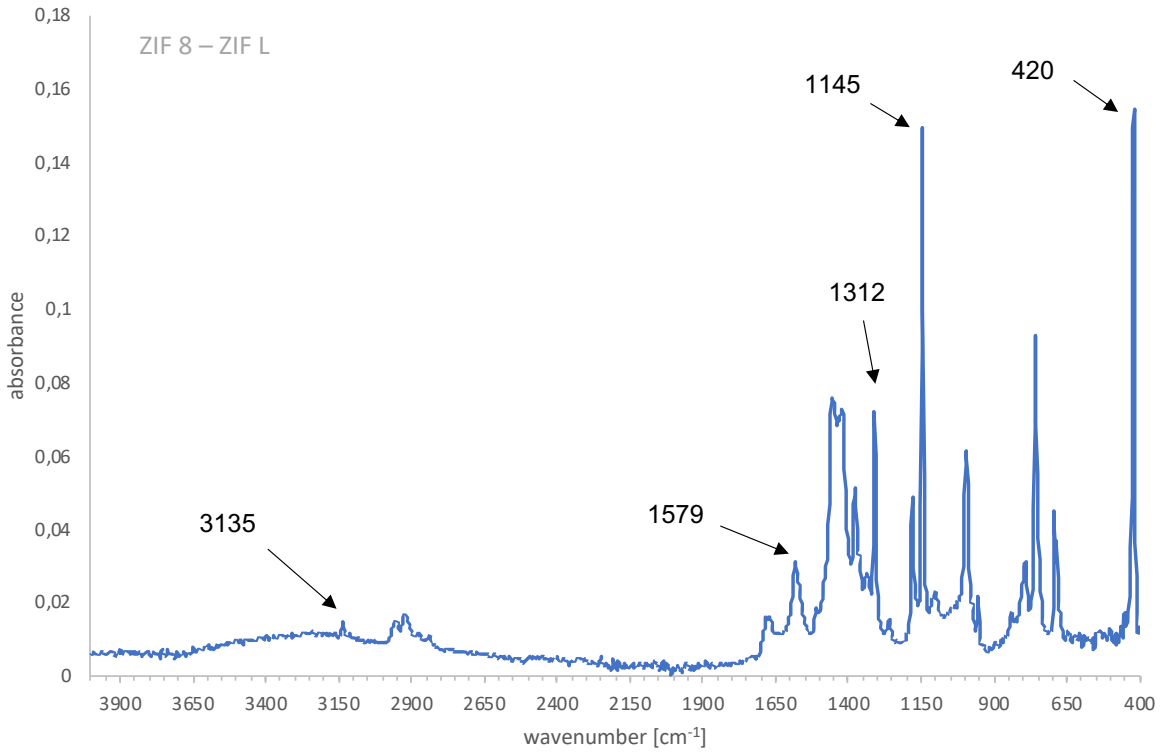

Figure 43: FTIR spectrum of sample with ZIF-8 and ZIF-L layer

5.2 Performance

The performance of the membrane, meaning its ability to separate Lithium ions from other present ions in salt or brine water was measured using linear sweep voltammetry. The membrane was deposited between the two compartments of an H-cell and the current through it was measured as described in chapter 4.7. Afterwards selectivities were calculated as the ratio of current:

$$S_{a/b} = \left|\frac{I_a}{I_b}\right| * \frac{z_a}{z_b}$$

Where I_a and I_b are the current at the same voltage for metal ion a and b and z_a and z_b are their ion valence. Here, it is important to notice that only at a low voltage range electrolysis of water is neglectable. This leads to the assumption that in this range every change in the IV curve is due to transport of cations. [32] As preliminary experiments, linear sweep voltammetry was done with no membrane at all, this was called a bulk experiment, and with the support

membrane (NF90) only. (Figure 44, Figure 45) Both graphs show very low current at the applied potentials.

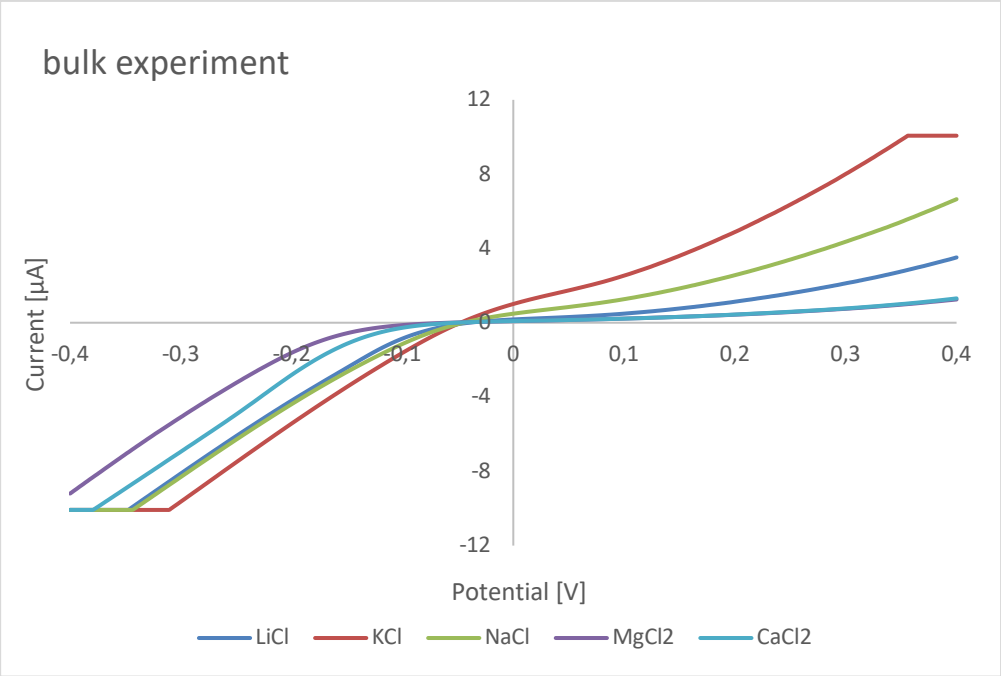

Figure 44: IV-curve from LSV experiment with no membrane

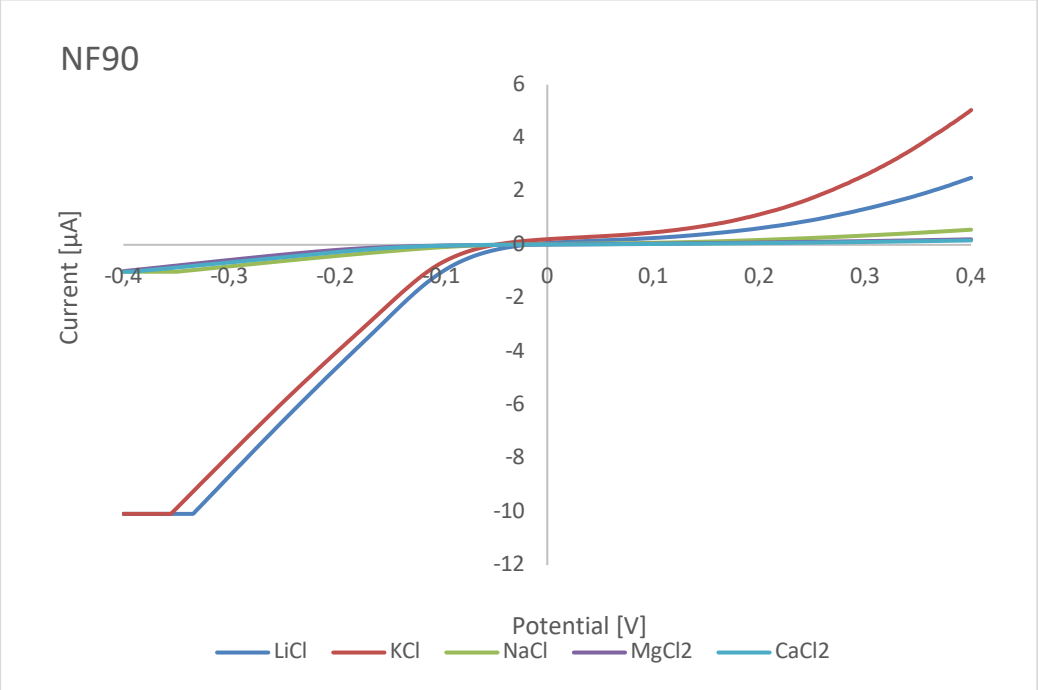

Figure 45: IV-curve from LCV experiment with support membrane (NF90) only

To be able to associate different results in the performance to the different layers this membrane was built of linear sweep voltammetry experiments were also done with a sample

containing NF90 as support and a ZIF-8 layer and with the final product containing NF90, ZIF-8 and ZIF-L. The membrane with a ZIF-8 layer on top resulted in selectivities of 3.59 for Li^+/K^+ and 1.26 for Li^+/Na^+ at a voltage of 0.2V. Monovalent/bivalent selectivities were above 2.2. The I-V curves are to be seen in Figure 46.

Interestingly, especially potassium but also sodium experiences a high increase in current at positive voltages. For potassium this high increase happens at potentials between 0.2 and 0.4V and the ascending slope is 129.2. This increase is notable compared to the ascending slope of Lithium in this area, which is quite linear throughout all measured voltages and reaches only 53.6. At voltages higher than 0.4, the potassium flow decreases to a slope of 91.4. Also, sodium experiences such an increase, however not at the same intensity and also in a different voltage area. For this metal ion the increase is rather between 0.1 and 0.3V and reaches an ascending slope of 69.1 which decreases after 0.3V to 67.5. Sabbagh et al. [65] explain that permselectivity in channels can be expressed by their electric resistance. If the channel is not selective the resistance stays the same at all voltages and currents can be easily calculated using Ohm's law resulting in linear I-V curves. If the channel is permselective, however, I-V curves will be only linear up to a limiting region (referred to voltage or current) in which ion concentration will be lower due to a depletion resulting from different properties of the nanochannel. This results again in a bigger resistance in this area due to the change of concentration polarization (CP) in the system. Above that area linearity in the I-V curve is gained back. Especially in this limiting region the channel exhibits its selective property. This non-linearity is an indicator for permselectivity of nanochannels and can be seen in Figure 46 for potassium and sodium. Yossifon et al. [66] also describe this phenomenon and name the different parts of an IV-curve of an ion-selective nanochannel the ohmic region, for the linear region before the limiting resistance region and the over-limiting region for the area after it. For potassium, in Figure 46, the ohmic region would be -0.6 to -0.1V, the limiting resistance region would be -0.1 to 0.4V and the over-limiting region would be above 0.4V where the current is linear again. Non-linearity is also visible at the I-V curves of the NF90/ZIF8/ZIFL membrane (Figure 47) especially for sodium and a bit for lithium. Here, however, possible defects in the top layer could have led to non-meaningful results.

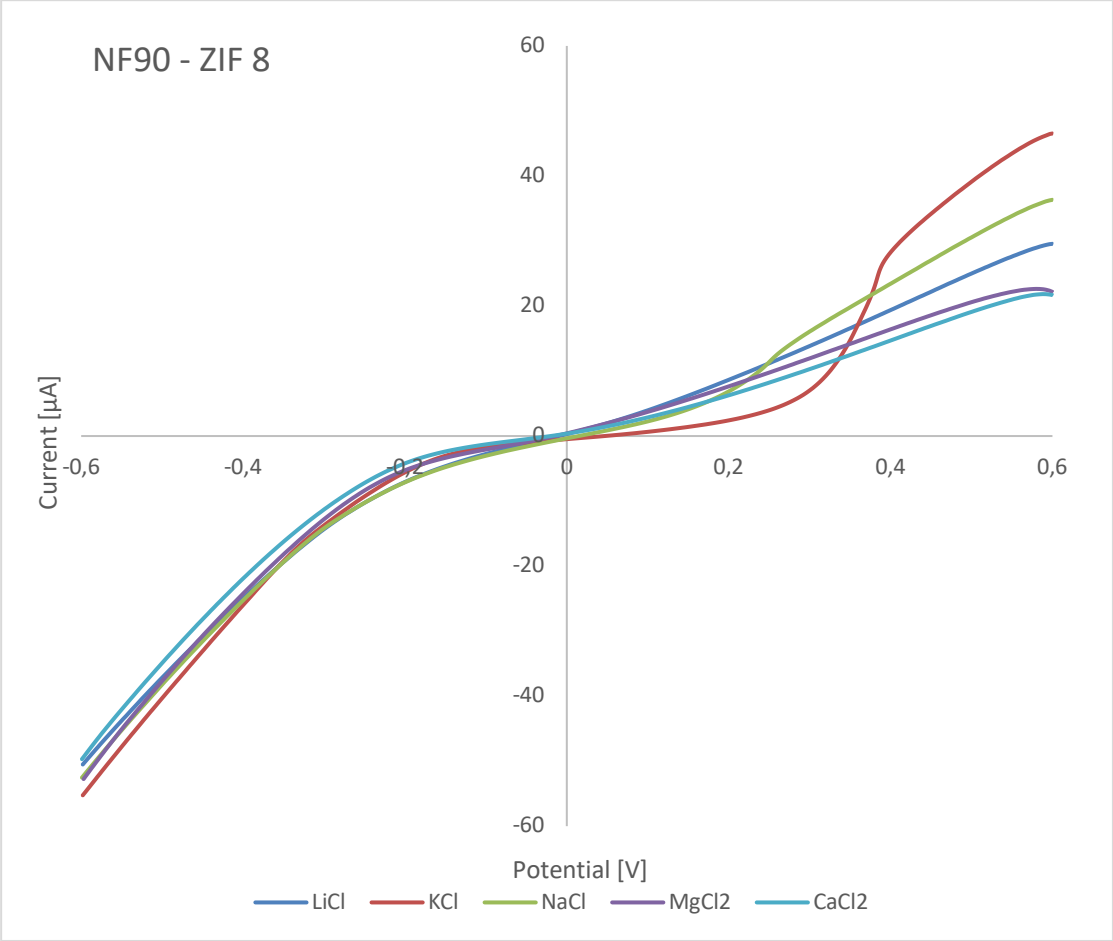

Figure 46: IV-curve from LSV experiment using NF90 membrane with ZIF-8 layer

Experiments with the final membrane resulted in selectivties of 1.52 and 1.09 at 0.3V for K^+/Li^+ and Na^+/Li^+, respectively. (Figure 47) Monovalent/bivalent selectivity was above 1.7. The abrupt current increase at positive voltages for potassium and sodium does not occur at the same intensity at this membrane setup.

The selectivities might seem low, especially compared to the results of the membrane containing only a ZIF-8 layer. However, currents are higher at the final membrane. As there is always a trade-off between selectivity and permeability, the lower selectivity does not mean that the final membrane is less appropriate for the application than the membrane consisting only of NF90 and ZIF-8. Why the final setup of the membrane leads to lower selectivities and what could be done to improve its selectivity will be discussed in the conclusion section. What can be said from this point of view is that it still is promising, however there has to be more experiments done to eliminate possible mistakes at the process of fabrication and measurement as a higher permeability and low selectivity could have been the result of missing linkers in the top layer. Also, it is important to notice that interpretations of the IV-curves from this stage are rather assumptions than facts. What is quite visible and leads to questions that should be researched in future progress is that monovalent-bivalent selectivity decreases but

permeability increases when MOF-layer were put on NF90 support which is the opposite than expected.

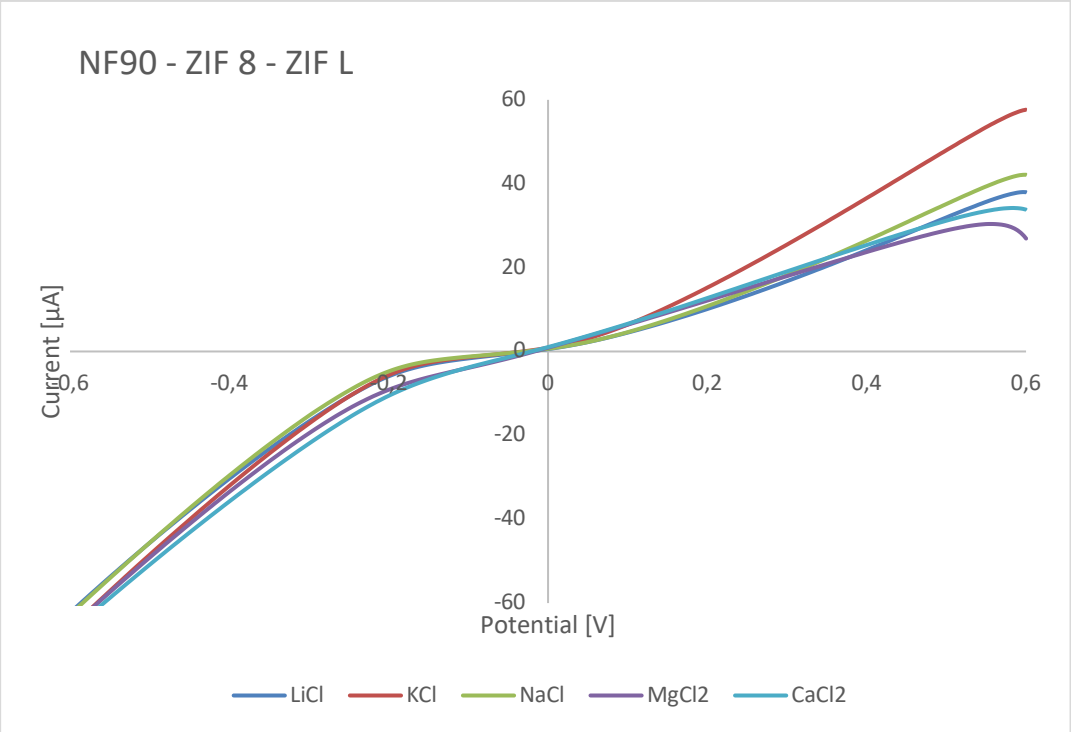

Figure 47: IV-curve from LSV experiment using NF90 membrane with ZIF-8 and ZIF-L layer

6 Conclusion

From literature we know that there are several approaches to the research question of finding a method to separate Lithium ions from other present ions in salt water or brines. Research of recent work especially in the field of using a membrane for separation has shown that Lithium-selective membranes can be classified into three groups.

Ion-exchange membranes, that exhibit vacant sites that only let target ions or smaller ones enter, are one big field of recent research. When those sites are occupied by target ions, they need to be stripped in a second process. Depending on the composition and concentrations of the feed, there are different materials that are most appropriate for separating Lithium ions. Although research shows highly promising results considering the capacities of those membranes, the process of separation consists out of two steps which complicates the application, especially for industrial scale.

Another field are liquid membranes where the transport of target ions is conducted via carriers. The membrane consists of a polymeric, porous matrix filled with an organic solution in which the carriers are inserted. The membrane is committed to the feed solution and the carriers absorb the target ions. The carriers are led into an acidic solution where the target ions are extracted. Crown ethers especially play a big role in liquid membranes as carriers. Drawbacks of liquid membranes could be the needed chemicals. To overcome challenges of ion-exchange and liquid membranes, an easy one-step process for separation is highly needed.

Nanochannels, that attract target ions and only let those pass through, are the third big field of research. As applying membranes exhibiting nanochannels for ion separation is an easy one-step process, they are the most promising. There are different materials those nanochannels can be made of and it is crucial for the performance of separation to investigate the nanochannels structure and surface chemistry. Promising materials for nanochannels exhibiting the right properties for a separation application are amongst others graphene oxide, vermiculite and metal organic frameworks (MOF). The goal is to improve the nanochannels properties in a way that the trade-off between selectivity and permeability is decreased resulting in a highly selective membrane with fast Lithium-ion throughput. To be able to create nanochannels with improved properties, first it is important to understand how Lithium ions can be attracted by nanochannels while other ions are not and what describes their movement in the channel. The properties that influence those mechanisms the most are the **pore diameter, the chemistry** and the **morphology** of the channel walls, the intensity of the **driving force** and the **length of the channel**. The diameter should be in the range of hydrated Lithium, not bigger to ensure the channels selectivity but also not smaller because Lithium ions need two to three layers of water inside a confinement to be able to move. The inside of the channel can be either charged or not charged. Charges on surfaces should be negative as positively charged target ions

get attracted and counter ions can get repelled more easily. Those charges are achieved by functionalising the inner walls of the channels with different functional groups (FG). Here it should be noted that the density of those FGs has to be chosen carefully. The morphology of the channel is another crucial property for successful separation. The most promising morphologies are leaned on biological protein channels that are important for nearly every living being and exhibit an asymmetrical structure. This leads to easier dehydration-rehydration processes of Lithium ions and therefore to better movement of target ions through the channel than at symmetric nanochannels. Mainly this is because the asymmetric channels allow the ions to lose their hydration shells gradually by moving from base to tip in conical channels which demands less energy as when the ion needs to strip all its water shells at once to fit in the symmetric channel. Also, asymmetry enhances the rectification effect meaning that ions will rather flow in one direction than in the other. As for the driving force, what is important to know is that an electrical potential should be preferred over pressure as the latter one could impact the mechanical stability of the membrane. The potential also has to be adjusted carefully and cannot exceed a current operating limitation (V_{lim}) which is important to maintain the membrane's selectivity. Also, an exceed of potential over 1.23V which is the potential for hydrogen gas formation should be carefully regarded as this leads to safety issues. Especially when using saline water, the formation of chlorine could pose a problem in a higher voltage range. Also, the length of the channel plays a vital role considering the velocity of ions inside nanochannels as the position where the ion accelerates and decelerates alters at different channel lengths.

Looking at all of the properties that have to be considered when designing a nanochannel capable of separating Lithium ions from other monovalent ions, the idea of creating a nanochannel with hierarchical structure to conform to asymmetry needs with a tip diameter that is smaller than hydrated Lithium ions and applying this channel to a potential driven set up, came to my supervisor's and my mind. We created a membrane that was built of different materials on top of each other beginning with a layer of the material with the biggest pores and ending with a highly structured material exhibiting pores in the ångström range whose apertures are lower than the hydrated diameter of Lithium (7.64Å). These highly structured pores can be achieved using metal organic frameworks (MOF). A hierarchical structured membrane was achieved by layer-by-layer-deposition of ZIF-8 and ZIF-L on an NF90 support membrane. Applying the fabricated membrane to an electrochemical workstation (CHI instruments) gave an idea of its selectivity and permeability for Lithium ions.

As announced in the previous chapter, the last results, meaning the results of linear sweep voltammetry to identify the flow of different ions through the fabricated membranes are not adamant and therefore, interpretation of this is not as meaningful as I would have wished for. More experiments would have had to be done for a satisfying interpretation of the performance for the described application of this material. These additional experiments could not have been done due to a worldwide pandemic that hit Australia as well as Austria

in March 2020, in the middle of the time frame in which the experimental part for this work was scheduled to be conducted. As laboratories closed and students from abroad were asked to leave the country, the experimental work was closed abruptly, and the idea of a literature-based work was born. However, there are interesting results, questions and conclusions from the analysations that we were able to be conducted in the time given.

First, when comparing results of preliminary experiments with the ones from the fabricated membranes, it comes clear that metal organic frameworks somehow enhance the ion flow much more, than commercial membranes, like NF90. This can be seen in ion currents around 10 times higher when using a membrane containing metal organic frameworks as an active layer. Permeation is even more enhanced when the active layer consisting of ZIF-L is placed on top of a ZIF-8 layer. As the used active layer has much smaller pores than the support membrane, this finding confirms that high selectivity and permeability has more sophisticated background than only separation due to size exclusion. Therefore, background of ion flow inside these channels has to be studied in future work. Table 4 shows selectivities of nanochannels for the separation of Lithium ions from saline waters found in literature contrasted to the selectivity results of this work.

Table 4: comparison of selectivity factors found in literature to the ones of this work

Material	**Selectivity factors**			**Source**
	α_{Na}^{Li}	α_{K}^{Li}	$\alpha_{bivalent}^{monovalent}$	
Vermiculite membrane	1.26	1.59	10.5	[32]
MOF containing polystyrene sulfonate	35	67	1815	[33]
ZIF-8/GO/AAO membrane	1.37	2.18	-	[34]
UiO66/PET	1.24	1.58	-	[34]
ZIF-8/NF90	1.26	3.59	2.2	this work
ZIF-l/ZIF-8/NF90	$\frac{1}{1.09}$	$\frac{1}{1.52}$	1.7	this work

To be able to enhance selectivity towards Lithium in the fabricated membrane, it is crucial to identify this background. Several studies, conducted by my supervisor, Amir Razmjou, try to explain the main parts of this background based on studies of nanochannels using

vermiculite as material. For this membrane set up especially, there has to be more experimental work done to identify its application possibility. There are several parts in the fabrication to be considered for future work. As permeability is already highly enhanced by the ZIF-L layer on top, the more important factor is selectivity. The reason for low selectivity could be that despite the ZIF-L layer looks homogeneous and defect-free from SEM analysations there are voids or interspaces where there is no ZIF-L structure present in the layer. This problem could be solved by using a different fabrication method to obtain c-oriented crystals instead of b-oriented ones resulting in lower possibilities of voids as ZIF-L crystals with this orientation exhibit more area in the plane parallel to the membrane. Another approach to reach a lower degree of defects in the layer would be a secondary growth of it. Also, a different analyzation method for the performance properties could help understand the background. A method could be electrochemical impedance spectroscopy (EIS) where the membrane resistance for different metal ions can be measured.

Resuming, this work gives insight into the possibilities of materials and systems for separating Lithium ions out of saline waters. Membranes containing metal organic frameworks have been further analysed and applied in an electrical potential driven system. The results are in the range of selectivity factors found in literature, however, to be able to interpret the results more meaningfully and get more specified insights into the background, more experimental work has to be done. For future progress, more insight into the background of the fabricated MOF structure and lithium-ion flow inside of it is desirable. With good results, lithium extraction of solutions coming from secondary resources should also be kept in mind.

7 Indices

7.1 Literature

[1] P. Meshram, B. Pandey, and T. Mankhand, "Extraction of lithium from primary and secondary sources by pre-treatment, leaching and separation: A comprehensive review," *Hydrometallurgy,* vol. 150, pp. 192-208, 2014.

[2] S. H. Windisch-Kern, A.; Ponak, C.; Raupenstrauch, H.;, "Pyrometallurgical Lithium-Ion-Battery Recycling: Approach to Limiting Lithium Slagging with the InduRed Reactor Concept," *Processes* vol. 9, 02.01.2021 2021.

[3] P. K. Choubey, K.-S. Chung, M.-s. Kim, J.-c. Lee, and R. R. Srivastava, "Advance review on the exploitation of the prominent energy-storage element Lithium. Part II: From sea water and spent lithium ion batteries (LIBs)," *Minerals Engineering,* vol. 110, pp. 104-121, 2017.

[4] C. Grosjean, P. H. Miranda, M. Perrin, and P. Poggi, "Assessment of world lithium resources and consequences of their geographic distribution on the expected development of the electric vehicle industry," *Renewable and Sustainable Energy Reviews,* vol. 16, no. 3, pp. 1735-1744, 2012.

[5] P. J. COLLINGS, "LITHIUM AND LITHIUM COMPOUNDS," *Kirk-Othmer Encyclopedia of Chemical Technology, Volume 15,* vol. 13, p. 120, 2005.

[6] A. Razmjou *et al.*, "Effect of chemistry and geometry of GO nanochannels on the Li ion selectivity and recovery," *Desalination,* vol. 496, p. 114729, 2020.

[7] "Energy storage plays a crucial part of our everyday lives." https://www.gelest.com/applications/batteries/ (accessed 24.01.2021.

[8] J. Moore and B. Shabani, "A critical study of stationary energy storage policies in Australia in an international context: the role of hydrogen and battery technologies," *Energies,* vol. 9, no. 9, p. 674, 2016.

[9] L. Ge *et al.*, "Monovalent cation perm-selective membranes (MCPMs): New developments and perspectives," *Chinese Journal of Chemical Engineering,* Review vol. 25, 2017.

[10] W. Li, C. Shi, A. Zhou, X. He, Y. Sun, and J. Zhang, "A positively charged composite nanofiltration membrane modified by EDTA for LiCl/MgCl2 separation," *Separation and Purification Technology,* vol. 186, 25.05.2017 2017.

[11] H.-Z. Zhang, Z.-L. Xu, H. Ding, and Y.-J. Tang, "Positively charged capillary nanofiltration membrane with high rejection for Mg2+ and Ca2+ and good separation for Mg2+ and Li+," *Desalination,* vol. 420, 13.07.2017 2017.

[12] X. Xu *et al.*, "Extraction of lithium with functionalized lithium ion-sieves," *Progress in Materials Sciece* vol. 84, 18.09.2016 2016.

[13] C. P. Lawagon *et al.*, "Adsorptive Li+ mining from liquid resources by H2TiO3: Equilibrium, kinetics, thermodynamics, and mechanisms," *Journal of Industrial and Engineering Chemistry,* vol. 35, 18.01.2016 2016.

[14] H.-J. Honga *et al.*, "Highly porous and surface-expanded spinel hydrogen manganese oxide (HMO)/Al2O3 composite for effective lithium (Li) recovery from seawater," *Chemical Engineering Journal,* vol. 337, 26.11.2017 2017.

[15] M. J. Park *et al.*, "Recyclable composite nanofiber adsorbent for Li+ recovery from seawater desalination retentate," *Chemical Engineering Journal,* vol. 254, 21.05.2014 2014.

[16] J.-L. Xiao, S.-Y. Sun, X. Song, P. Li, and J.-G. Yu, "Lithium ion recovery from brine using granulated polyacrylamide–MnO2 ion-sieve," *Chemical Engineering Journal,* vol. 279, 23.05.2015 2015.

[17] M.-Y. Zhaoa *et al.*, "Study on lithium extraction from brines based on LiMn2O4/Li1-xMn2O4 by electrochemical method," *Electrochimica Acta* vol. 252, 30.08.2017 2017.

[18] C. P. Lawagon, G. M. Nisola, R. A. I. Cuevas, H. Kim, S.-P. Lee, and W.-J. Chung, "Li1−xNi0.33Co1/3Mn1/3O2/Ag for electrochemical lithium recovery from brine," *Chemical Engineering Journal,* vol. 348, 5.05.2018 2018.

[19] M. Kazemabad, A. Verliefdea, E. R. Cornelissen, and A. D'Haesea, "Crown ether containing polyelectrolyte multilayer membranes for lithium recovery," *Journal of Membrane Science,* vol. 595, 29.08.2019 2020.

[20] J. Lu, Y. Qin, Y. Wu, M. Meng, Y. Yan, and C. Li, "Recent advances in ion-imprinted membranes: separation and detection via ion-selective recognition," *Water Research & Technology* vol. 5, 16.08.2019 2019.

[21] S. A. Piletsky *et al.*, "A Biomimetic Receptor System for Sialic Acid Based on Molecular Imprinting," *Analytical letter* vol. 29(2), 06.10.1995 1996.

[22] J. Lu *et al.*, "Multilayered ion-imprinted membranes with high selectivity towards Li+ based on the synergistic effect of 12-crown-4 and polyether sulfone," *Applied Surface Science,* vol. 427, 1.08.2017 2018.

[23] D. Sun, Y. Zhu, M. Meng, Y. Qiao, Y. Yan, and C. Li, "Fabrication of highly selective ion imprinted macroporous membranes with crown ether for targeted separation of lithium ion," *Separation and Purification Technology,* vol. 175, 9.11.2016 2017.

[24] Y. Wang, J. Xu, D. Yang, T. Zhang, F. Qiu, and J. Pan, "Calix[4]arenes functionalized dual-imprinted mesoporous film for the simultaneous selective recovery of lithium and rubidium," *Applied Organometallic Chemistry,* vol. 32, 2018.

[25] J. Tomar, A. Awasthy, and U. Sharma, "Synthetic ionophores for the separation of Li+, Na+, K+, Ca2+, Mg2+ metal ions using liquid membrane technology," *Desalination,* vol. 232, 15.01.2008 2008.

[26] H. Gohil, S. Chatterjee, S. Yadav, E. Suresh, and A. R. Paital, "An Ionophore for High Lithium Loading and Selective Capture from Brine," *Inorganic Chemistry,* vol. 58, 15.05.2019 2019.

[27] I. Yilmaz *et al.*, "Potentiometric Selectivities of Ionophore-Doped Ion-Selective Membranes: Concurrent Presence of Primary Ion or Interfering Ion Complexes of Multiple Stoichiometries," *analytical chemistry,* vol. 91, 4.01.2019 2019.

[28] S. Tas, B. Zoetebier, M. A. Hempenius, G. J. Vancsob, and K. Nijmeijer, "Monovalent cation selective crown ether containing poly(arylene ether ketone)/SPEEK blend membranes," *RSC Advances,* vol. 6, 27.05.2016 2016.

[29] L. Gong, W. Ouyangb, Z. Lia, and J. Hana, "Direct numerical simulation of continuous lithium extraction from high Mg2+/Li+ ratio brines using microfluidic channels with ion concentration polarization," *Journal of Membrane Science,* 30.03.2018 vol. 556, 29.03.2018 2018.

[30] R. Joshi *et al.*, "Precise and ultrafast molecular sieving through graphene oxide membranes," *science,* vol. 343, no. 6172, pp. 752-754, 2014.

[31] J. Abraham *et al.*, "Tunable sieving of ions using graphene oxide membranes," *Nature nanotechnology,* vol. 12, no. 6, p. 546, 2017.

[32] A. Razmjou *et al.*, "Lithium ion-selective membrane with 2D subnanometer channels," *Water Research* vol. 159, 5.05.2019 2019.

[33] Y. Guo, Y. Ying, Y. Mao, X. Peng, and B. Chen, "Polystyrene Sulfonate Threaded through a Metal–Organic Framework Membrane for Fast and Selective Lithium-Ion Separation," *Angewandte Chemie Communications,* vol. 55, 31.10.2019 2016.

[34] H. Zhang *et al.*, "Ultrafast selective transport of alkali metal ions in metal organic frameworks with subnanometer pores," *Science advances,* vol. 4, no. 2, p. eaaq0066, 2018.

[35] J. Lu *et al.*, "Efficient metal ion sieving in rectifying subnanochannels enabled by metal–organic frameworks," *Nature materials,* pp. 1-8, 2020.

[36] A. Razmjou, M. Asadnia, E. Hosseini, A. H. Korayem, and V. Chen, "Design principles of ion selective nanostructured membranes for the extraction of lithium ions," *Nature Communications,* vol. 10, no. 1, pp. 1-15, 2019.

[37] H. Daiguji, "Ion transport in nanofluidic channels," *Chemical Society Reviews,* vol. 39, March 2010 2010.
[38] N. Agmon, "The grotthuss mechanism," *Chemical Physics Letters,* vol. 244, no. 5-6, pp. 456-462, 1995.
[39] P. Sun *et al.*, "Selective ion penetration of graphene oxide membranes," *ACS nano,* vol. 7, no. 1, pp. 428-437, 2013.
[40] E. Nightingale Jr, "Phenomenological theory of ion solvation. Effective radii of hydrated ions," *The Journal of Physical Chemistry,* vol. 63, no. 9, pp. 1381-1387, 1959.
[41] K. Xiao, L. Wen, and L. Jiang, "Biomimetic solid-state nanochannels: from fundamental research to practical applications," *Small,* vol. 12, no. 21, pp. 2810-2831, 2016.
[42] Z. Siwy and A. Fuliński, "Fabrication of a synthetic nanopore ion pump," *Physical Review Letters,* vol. 89, no. 19, p. 198103, 2002.
[43] C. Wang, F. F. Liu, Z. Tan, Y. M. Chen, W. C. Hu, and X. H. Xia, "Fabrication of Bio-Inspired 2D MOFs/PAA Hybrid Membrane for Asymmetric Ion Transport," *Advanced Functional Materials,* vol. 30, no. 9, p. 1908804, 2020.
[44] Q. Pu, J. Yun, H. Temkin, and S. Liu, "Ion-enrichment and ion-depletion effect of nanochannel structures," *Nano letters,* vol. 4, no. 6, pp. 1099-1103, 2004.
[45] R. Horn, B. Roux, and J. Åqvist, "Permeation redux: thermodynamics and kinetics of ion movement through potassium channels," *Biophysical Journal,* vol. 106, no. 9, pp. 1859-1863, 2014.
[46] W. Choi, Z. W. Ulissi, S. F. Shimizu, D. O. Bellisario, M. D. Ellison, and M. S. Strano, "Diameter-dependent ion transport through the interior of isolated single-walled carbon nanotubes," *Nature communications,* vol. 4, no. 1, pp. 1-8, 2013.
[47] M. Jung, H. Kim, K. Baek, and K. Kim, "Synthetic ion channel based on metal–organic polyhedra," *Angewandte Chemie International Edition,* vol. 47, no. 31, pp. 5755-5757, 2008.
[48] Q. Wen *et al.*, "Highly selective ionic transport through subnanometer pores in polymer films," *Advanced Functional Materials,* vol. 26, no. 32, pp. 5796-5803, 2016.
[49] H.-Q. Liang, Y. Guo, X. Peng, and B. Chen, "Light-gated cation-selective transport in metal–organic framework membranes," *Journal of Materials Chemistry A,* 2020.
[50] S. Das, T. Ben, S. Qiu, and V. Valtchev, "Two-Dimensional COF–Three-Dimensional MOF Dual-Layer Membranes with Unprecedentedly High H2/CO2 Selectivity and Ultrahigh Gas Permeabilities," *ACS Applied Materials & Interfaces,* 2020.
[51] S. K. Elsaidi, S. R. Venna, M. H. Mohamed, M. J. Gipple, and D. P. Hopkinson, "Dual-Layer MOF Composite Membranes with Tuned Interface Interaction for Postcombustion Carbon Dioxide Separation," *Cell Reports Physical Science,* vol. 1, no. 5, p. 100059, 2020.
[52] K. S. Park *et al.*, "Exceptional chemical and thermal stability of zeolitic imidazolate frameworks," *Proceedings of the National Academy of Sciences,* vol. 103, no. 27, pp. 10186-10191, 2006.
[53] Z. Zhong *et al.*, "Oriented two-dimensional zeolitic imidazolate framework-L membranes and their gas permeation properties," in *Journal of Materials Chemistry A* vol. 3, ed, 2015, pp. 15715-15722.
[54] Y. Yan, "Tribology and tribo-corrosion testing and analysis of metallic biomaterials," in *Metals for Biomedical Devices*: Elsevier, 2010, pp. 178-201.
[55] E. Britannica, "Scanning electron microscope," ed.
[56] J. Epp, "X-ray diffraction (XRD) techniques for materials characterization," in *Materials characterization using nondestructive evaluation (NDE) methods*: Elsevier, 2016, pp. 81-124.
[57] S. A. Speakman. C. f. M. S. a. E. a. MIT. Introduction to X-Ray Powder Diffraction Data Analysis.
[58] S. K. Sharma, D. S. Verma, L. U. Khan, S. Kumar, and S. B. Khan, *Handbook of Materials Characterization*. Springer, 2018.

[59] X.-Y. Nie, S.-Y. Sun, Z. Sun, X. Song, and J.-G. Yu, "Ion-fractionation of lithium ions from magnesium ions by electrodialysis using monovalent selective ion-exchange membranes," *Desalination,* vol. 403, pp. 128-135, 2017.

[60] M. Mohammad, A. Razmjou, K. Liang, M. Asadnia, and V. Chen, "Metal–organic-framework-based enzymatic microfluidic biosensor via surface patterning and biomineralization," *ACS applied materials & interfaces,* vol. 11, no. 2, pp. 1807-1820, 2018.

[61] S. Gao *et al.*, "Improving the Acidic Stability of Zeolitic Imidazolate Frameworks by Biofunctional Molecules," in *Chem* vol. 5, ed: Elsevier Inc., 2019, pp. 1597-1608.

[62] S. Yuan *et al.*, "Structure architecture of micro/nanoscale ZIF-L on a 3D printed membrane for a superhydrophobic and underwater superoleophobic surface," in *Journal of Materials Chemistry A* vol. 7, ed, 2019, pp. 2723-2729.

[63] O. Agboola, T. Mokrani, and R. Sadiku, "Porous and fractal analysis on the permeability of nanofiltration membranes for the removal of metal ions," *Journal of materials science,* vol. 51, no. 5, pp. 2499-2511, 2016.

[64] J. Liu *et al.*, "NiO-PTA supported on ZIF-8 as a highly effective catalyst for hydrocracking of Jatropha oil," *Scientific reports,* vol. 6, p. 23667, 2016.

[65] B. Sabbagh, E. Stolovicki, S. Park, D. A. Weitz, and G. Yossifon, "Tunable Nanochannels Connected in Series for Dynamic Control of Multiple Concentration-Polarization Layers and Preconcentrated Molecule Plugs," *Nano Letters,* vol. 20, no. 12, pp. 8524-8533, 2020.

[66] G. Yossifon, P. Mushenheim, Y.-C. Chang, and H.-C. Chang, "Nonlinear current-voltage characteristics of nanochannels," *Physical Review E,* vol. 79, no. 4, p. 046305, 2009.

7.2 Abbreviations

LIB	Lithium-ion battery
MOF	Metal organic framework
LIS	Lithium-ion sieve
IIM	Ion-imprinted membrane
ISE	Ion-selective electrode
PEI	Polyethyleneimine
(I)CP	(Ion) concentration polarization
GO	Graphene Oxide
LSV	Linear sweep voltammetry
I-V	Current-Voltage
MD	Molecular Dynamics
PSS	Polystyrene sulfonate
CHN	Copper hydroxide nanostrands
AAO	Anodic aluminium oxide
ZIF-8	Zeolitic imidazolate 8
ZIF-7	Zeolitic imidazolate 7
ZIF-L	Zeolitic imidazolate L
UiO-66	Universitetet i Oslo 66 (metal organic framework structure)
PET	Polyethylene terephthalate
NC	Nanochannel
EDL	Electrical double layer
FG	Functional group
V_{lim}	Current operating limitation
COF	Covalent organic framework
IM	Imidazolate
Å	Ångström (1Å = 10^{-10}m)
ATR	Attenuated total reflection
HMIM	2-methylimidazole
PDMS	Polydimethylsiloxane

7.3 Tables

7.4 Figures